# Electrodeposition of Alloys from Deep Eutectic Solvents

Thesis submitted for the degree of

Doctor of Philosophy

At the University of Leicester

By

Abubakr Alhaji

Department of Chemistry

University of Leicester

September 2011

**University of Leicester**

**Abstract**

Thin films of copper alloys are of interest for electronic applications. These are routinely produced by electrodeposition using aqueous solutions. The solvent strongly affects composition and morphology of the deposit which consequently affects the electrical and mechanical properties. The novelty of this thesis is that copper alloys are deposited from Deep Eutectic Solvents, DESs, which are forms of ionic liquids. The work shows that novel morphologies and compositions can be obtained using this approach.

The electrodeposition of copper alloys is described from a solution of the metal salts in choline chloride based ionic liquids using urea and ethylene glycol as hydrogen bond donors. The thesis is split into three sections focussing on Cu alloys with Ag, Sn and P. These were chosen for their different phase behaviour. It is shown that the composition and morphology can be varied by altering the deposition potential and copper ion concentration of the plating bath. A variety of analytical techniques have been used to probe the deposition of these alloys. Although many of these are relatively standard for such studies this project uses an electrochemical quartz crystal microbalance (EQCM) for the first time to determine alloy composition in real time. From this data, the two systems Cu-Ag and Cu-Sn are shown to be close to 100% current efficiency, but the Cu-P does not fellow this trend. Analysis of the chronoamperometric transient behaviour during electrodeposition suggests that pure copper electrodeposition proceeds via three-dimensional instantaneous nucleation with diffusion-controlled growth. However, the deposition of most alloys does not fit either progressive or instantaneous nucleation models well. The alloy phases formed during deposition were analysed using X-ray diffraction and the surface morphologies and the compositions of the electrodeposited Cu alloys were analysed using SEM/EDAX.

Thin films of Cu and Cu-P were electroformed onto Ti substrates and then peeled off. The mechanical properties of these films were tested and it was found that the incorporation of phosphorous was found to have a significant effect on the stress-strain curves. The final part of this study involved the dissolution of copper using cyclic voltammetry and EQCM and it was shown that diffusion of the chloride ligand to the electrode limits the rate of the anodic process.

**Acknowledgements**

It is a pleasure to thank the many people who made this thesis possible.

*Abubakr*

# TABLE OF CONTENTS

**CHAPTER 6**

**Conclusions and Future Work**

**Appendix**

**Chapter 1: Introduction**

**Introduction**

Ionic liquids (ILs) are ionic materials that have a melting point below 100 °C. These compounds have large non-symmetric ions with low lattice energy and hence low melting points. Ionic liquids are interesting for electrochemistry because they are good solvents for both organic and inorganic compounds but they can also be made to be immiscible with many organic solvents.

Ionic liquids are in general not volatile, can be liquid at room temperature and used with high vacuum systems.[1] They also present an alternative to environmentally hazardous processes such as the use of cyanide for the electrodeposition of silver or use of chromic acid for chromium deposition. In general the cation controls the physical properties of the salt whereas the anion has a greater effect upon the stability and chemical reactivity.

## 1.1 A brief history

Walden is generally credited with preparing the first ionic liquid,[2] ethylammonium nitrate ($C_2H_5N^+H_3NO_3^-$) which has a melting point of 12 °C. This compound is highly reactive and this is why it has not been widely used. Hurley and Weir[3] prepared an ionic liquid by mixing and warming 1-ethylpyridinium chloride with aluminium chloride .

Osteryoung *et al.*[4, 5] and Hussey *et al.*[6, 7, 8] in 1970s and 1980s also worked on organic chloride–aluminium chloride ambient temperature ionic liquids and were the first to produce a major review of room temperature ionic liquids.[9] The first generation of ionic liquids were prepared using $AlCl_3$ but these had limitations due to their reactivity with water. In 1992, Wilkes and Zaworotko[10] reported the first air and moisture stable ionic liquids based on the 1-ethyl-3 methylimidazolium cation with either tetrafluoroborate or hexafluorophosphate as anions.

There has been an increase in the number of publications on ionic liquids in various fields including extraction/ separation, electrodeposition and electrochemical analysis etc, during the last decade.[11] For a comprehensive review of ionic liquids and their use in synthesis the books by Welton and Wasserscheid are recommended.[12, 13]

Wasserscheid[13] focused on the preparation and characterization of ionic liquids for use in the biphasic catalysis. On the other hand, the synthesis of new air and water stable ionic liquids at room temperature was demonstrated by MacFarlane.[14] In the last 10 years the wide application of ionic liquids has been made in the field of air and water stable and today around 300 types of different ionic liquids are commercially available. It is clear from an

electrochemical point of view these ionic liquids are particularly interesting due to their wide potential windows. Ohno focused his work on the synthesis of a series of polymerizable ionic liquids and their polymerization to prepare a new type of ion conductive polymers.[15] The polymer electrolytes that were prepared were made from mixing nitrite rubber [poly(acrylonitrile-cobutadiene) rubber] with the ionic liquid *N*-ethylimidazolium bis(trifluoromethanesulfonyl)imide and these were found to have a high ionic conductivity and good elasticity.

In fact, hundreds of ionic liquids have been reported with wide liquid temperatures, and one that remains liquid down to - 96 $^{o}$C is known.[16] The most commonly used ILs are non-haloaluminates with discrete anions such as $BF_4^-$, $PF_6^-$ and $(F_3CSO_2)_2N^-$, as they have superior physicochemical properties and are relatively water stable. In addition they have a wide range of fluidity, negligible vapour pressure even at elevated temperatures, high conductivities (up to 0.1 S/cm),[17] excellent chemical and thermal stability, and high heat capacity. Compared with commonly used organic compounds, they have lower toxicity and are non-flammable. Furthermore, variation of the anions or the length of the alkyl groups allows fine tuning of the physicochemical properties of ILs, such as viscosity, conductivity, solvation, catalytic activity and melting points, etc. Hence, ILs can be specifically designed for different applications.[18, 19] The application of ILs for electrochemical studies started in the beginning of the 1980s on pyridinium-based[20] and imidazolium-based[6] ILs. They have been described as ''green solvents'' due to their low vapour pressure but they are not inherently green.

Abbott has recently designed a range of stable, non-volatile ionic liquids, which are fluid at room temperature and with low eco-toxicity. These ionic compounds are can be economically produced on the multi-tonne scale. Most are based on choline chloride (vitamin B4), with hydrogen bond donors such as urea and glycerol and these have been applied to large scale industrial processes.[21]

## 1.2 Nomenclature

*Common cations:*
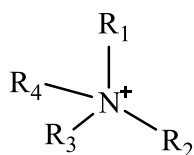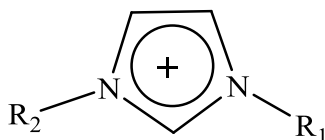


Ammonium       Imidazolium       Pyrrolidium
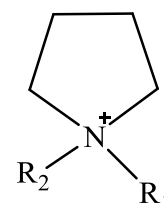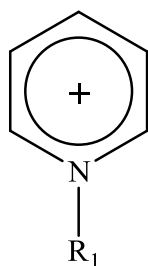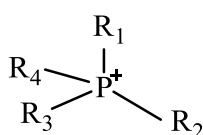
Pyridinium       Phosphonium       Guanidinium
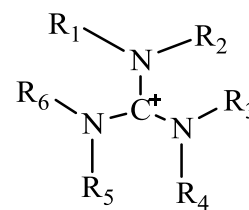
*Common anions:*

Chloride: $Cl^-$

Methylsulfate: $CH_3OSO_3^-$

Triflate: $CF_3SO_3^-$

Trifluoroacetate: $CF_3CO_2^-$

Hexafluorophosphate: $PF_6^-$

Tetrafluoroborate: $BF_4^-$

Bis(trifluoromethanesulfonyl)imide: $N(CF_3SO_2)_2^-$

Dicyanamide: $N(CN)_2^-$

*Table 1.1 Most common cations and anions used in ionic liquids*

Ionic liquids are defined as fluid semiorganic salts composed entirely of organic cations and organic or inorganic anions at or near ambient temperature. The most common cations in use are those containing alkylpyridinium, alkylimidazolium, alkylphosphonium, alkylammonium and alkylguanidinium, which can combine with anions such as chloride, tetrafluoroborate, methylsulfate, etc, to constitute a series of low melting ILs, as shown in **Table 1.1.** Generally, the various anions dominate the degree of miscibility of ILs in water. ILs are generally obtained by metathesis, starting from the pioneer chloride salts. In addition, cations will be adsorbed at the electrode surface at the deposition potential and hence the structure of the double layer is cation dependent, which affects the conductivity and viscosity of the ionic

fluids. Although phosphonium [22, 23] and sulfonium [24] based ionic liquids have been described, the majority of systems used for metal coating have been based on nitrogen-based cations. The other important role that the cation probably plays in electrodeposition is in controlling the structure and the Helmholtz layer thickness.[25] On the other hand, the anion can affect the coordination geometry around the metal ion on the metal deposition, which in turn affects the reduction potential, reduction current and nucleation, and also affects the conductivity and viscosity of the ionic liquids. The anion also affects the dissociation of the anode when a soluble anode is used. The anion can alter the speciation and hence the redox potential and this is currently the topic of a study by Abbott *et al*.[26]

## 1.3 Synthesis of ionic liquids

The synthesis of ionic liquids usually begins with the quaternisation of an imidazole or amine, to produce the cationic component.[6] This quaternisation of the ammonium salt is carried out using an alkylating agent such as alkyl halides.[27, 28] It is however not always possible to form the desired anion directly by this process, hence an additional step is required. Two possible steps for forming the anionic component are shown in **Reaction 1.1**. Eutectic based liquids can be formed starting from an ammonium halide $[R'R_3N]^+X^-$, for example, and reacting it with a Lewis acid, $MX_y$, leading to an ionic liquid that is of the form $[R`R_3N]^+[MX_{y+1}]^-$.[28] In this step all of the anionic species are observed in equilibrium. The ratio of species present depends upon the ratio of the two components, in this case $[R`R_3N]^+X^-$ and $MX_y$.
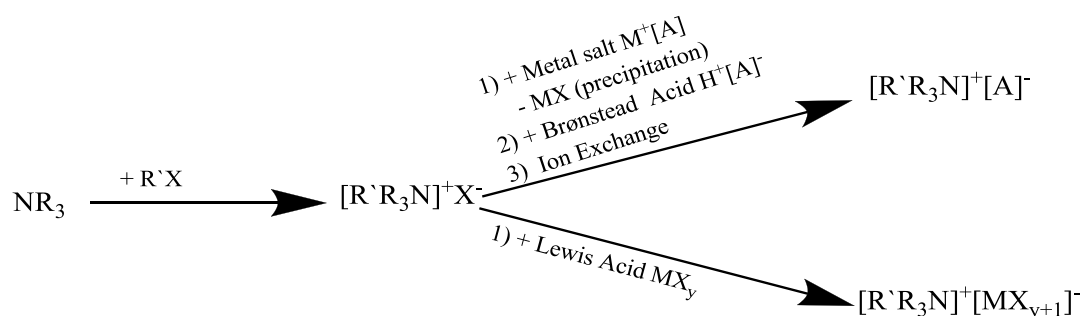


**Reaction 1.1** *Synthesis paths for the preparation of ionic liquids exemplified for quaternary ammonium salt*

A good example of this is displayed by the chloroaluminate melts. As the ratio of chloride to AlCl$_3$ ratio changes, so does the anionic species. When the mixture ratio is 1:1 [EMIM]Cl: AlCl$_3$ the predominant anionic species observed is AlCl$_4^-$.

When the molar fraction of AlCl$_3$ is at X(AlCl$_3$) > 0.5 the chloroaluminate anions become multi-nuclear. The various species formed can be seen in the below equations.[28]

$$[R`R_3N]^+Cl^- \quad + \quad AlCl_3 \quad \rightleftharpoons \quad [R`R_3N]^+[AlCl_4]^- \quad\quad (1.1)$$

$$[R`R_3N]^+[AlCl_4]^- \quad + \quad AlCl_3 \quad \rightleftharpoons \quad [R`R_3N]^+[Al_2Cl_7]^- \quad\quad (1.2)$$

$$[R`R_3N]^+[Al_2Cl_7]^- \quad + \quad AlCl_3 \quad \rightleftharpoons \quad [R`R_3N]^+[Al_3Cl_{10}]^- \quad\quad (1.3)$$
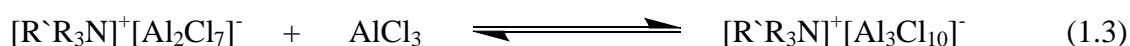
Although chloroaluminates are perhaps the best know ionic liquids that are formed by the use of a Lewis acid, they are not the only ionic liquids formed this way. Ionic liquids containing SnCl$_2$, CuCl$_2$, BCl$_3$ etc. as the Lewis acid have also been reported.[28]

It is also possible to change the anion by the addition of a metal salt M$^+$[A]$^-$ or by displacing it with a strong acid H$^+$[A]$^-$. These anion exchange methods, however, tend to result in impurities from residual halide species. These halide ions may interact with solute materials and so it is important to remove them. Unlike conventional solvents, purification cannot occur by distillation, so therefore an anion exchange resin must be used.[28]

## 1.4 Deep eutectic based ionic liquids

In the 1950s the first studies were carried out on ionic liquids and lower melting point eutectics were developed (ethylpyridinum chloride/ AlCl$_3$ mixtures).[3] Osteryoung researched use of  the N-buthylpyridinium cation [4] and Hussey [6] explored 1-ethyl-3-methyl-imidazolium as a cation. Around 40 years later Abbott et al.[21, 29] and Sun et al.[30, 31] studied the mixtures of zinc halides and quaternary ammonium halides. This has lead to use of other salts and organic compounds to form eutectic mixtures with quaternary ammonium salts. These liquids can all be described by the general formula R$^1$R$^2$R$^3$R$^4$N$^+$X$^-$·zY, where the anion X$^-$ is generally a halide (often Cl$^-$), R$^1$R$^2$R$^3$R$^4$N$^+$ a quaternary ammonium salt and Y is a complexing agent, where z is the number of molecules required. Depending on the complexing agent, Y can be divided in to three eutectic types:

Eutectic Type I        Y= $MCl_x$,               M = Zn, Sn, Fe, Al, Ga, Ge, In.

Eutectic Type II      Y= $MCl_x.yH_2O$,      M = Cr, Co, Cu, Ni, Fe.

Eutectic Type III     Y= RZ,              Z = $CONH_2$, COOH, OH.

Generally, the only $cat^+$ species studied have been based on pyridinium, imidazolium and quaternary ammonium moieties. Type I eutectics have relatively high viscosities and freezing points and relatively low conductivities when compared to those with discrete anions. The advantages for these types of ionic liquids are the ease of manufacture (they are simply mixed together at 80 $^\circ$C) and (with the exception of the haloaluminates) their water insensitivity, which is very important for the electrochemistry of metals. The relative proportion of anionic species depends on the ionic liquid composition. The anionic species have been identified in some of the eutectic such as Al,[32] Sn,[29] Zn,[29] Cr,[33] and urea.[34] In some studies they have also quantified the proportion of the anionic species present. They are also clearly useful for electroplating if the metal of interest falls in the category defined above under Type I and II, as the metal ion concentration can be as high as 10 mol dm$^{-3}$.

## 1.4.1 Type I Eutectics

The anhydrous metal halide-substituted quaternary ammonium salt mixtures are used in type I deep eutectic solvent ( DES). In this area the most investigated systems are those containing $ZnCl_2$, $SnCl_2$ and $FeCl_3$[29] all with a variety of quaternary ammonium salts. The three metal halides, when mixed with choline chloride (ChCl) in a 1:2 ratio, all form metal complexes that have freezing points below 100 °C. In fact, the term *deep eutectic solvents* arises from the fact that the melting point of the eutectic formed when the two components (A+B) are mixed together in the correct ratio is significantly lower than that of a theoretical ideal mixture. The eutectic point of a mixture (A+B), as shown in **Figure 1.1**, is the molar ratio of two compounds which affords the lowest melting point. The phase diagram of the metal chloride salts with ChCl clearly showed that Lewis basic ionic liquids could not be formed with tin and zinc, and this was related to the high charge density of the $MCl_3^-$ anion, which is similar to the result for aluminium chloride. As a result, it was found that the concentration of the $Zn_2Cl_5^-$ species varied with the composition of the ionic liquid.[21, 34-41] As the molar ratio of $ZnCl_2$ increases to more than half percent, several Lewis acidic chlorozincate clusters ($ZnCl_3^-$, $Zn_2Cl_5^-$, and $Zn_3Cl_7^-$) will be formed. Similar trends were observed for ionic liquids containing $SnCl_2$.[29]
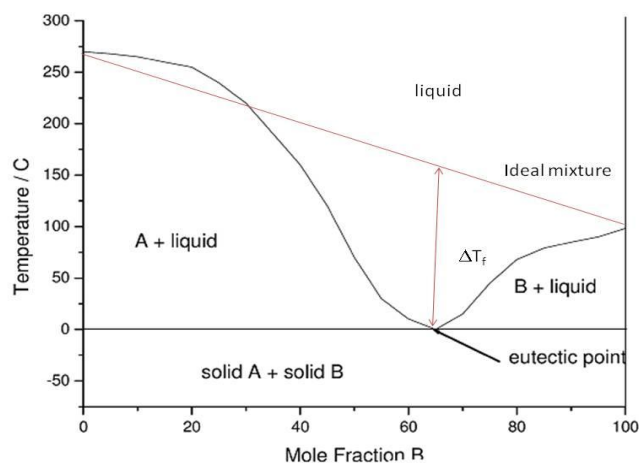
**Figure 1.1** *Schematic representation of a eutectic point on a two-component phase diagram.*
*Figure taken from ref.* [14]

The depression of freezing point compared to that in an ideal solution $\Delta T_f$ is related to the interaction between A and B. The larger the interaction the larger will be $\Delta T_f$. The interactions between different metal halides and the halide anion from the quaternary ammonium salt will, however, be relatively similar and so to get the freezing point to be at around room temperature the melting points of A and B will have to be relatively low. Analysing the metal salts which form DESs it occurs mostly with metal halides which have a low melting point. The same is true of the quaternary ammonium salts where it is the less symmetrical cations which have a lower melting point and therefore lead to lower melting point eutectics.

In the eutectic mixture a variety of halometallate species form and (Fast Atom Bombardment) FAB-Mass spectra suggests that most species are singly charged anionic species. Extended x-ray absorption fine structure (EXAFS) spectroscopy, however, shows that $ZnCl_2$ and $CuCl_2$ form $ZnCl_4^{2-}$ and $CuCl_4^{2-}$ although these could be the dimers $Zn_2Cl_6^{2-}$ and $Cu_2Cl_6^{2-}$ [42, 43] This difference is also observed in studies made in this group and is discussed in a review by Hardacre[44]

Nuclear magnetic resonance (NMR) and mass spectrometry were used by Lecocq *et al.*[45] to analyse the eutectics formed between zinc chloride and 1-butyl-2,3-dimethylimidazolium chloride [BMMIM][Cl] with the content of $ZnCl_2$ ranging between 0 and 0.75 mol. They showed that analogous to the aluminium systems, $Cl^-$ and $[ZnCl_3]^-$ are present in Lewis basic liquids, and $[ZnCl_3]^-$ and $[Zn_2Cl_5]^-$ are observed in Lewis acidic liquids. Pyridine was used as

a probe with infra red spectroscopy to quantify the Lewis acidity. High temperature (110 $^\circ$C) NMR experiments showed that the Cl$^-$ ligand switched between being associated with the imidazolium cation and the metal halide.

Ferric chloride is different from $SnCl_2$ and $ZnCl_2$ in that it forms two eutectic points at 33 and 67 mol % $FeCl_3$ which is analogous to the $AlCl_3$:EMIMCl system. These systems have been studied by a number of authors.[46,47,48] Speciation studies of $FeCl_2$ and $FeCl_3$ were carried out by Sitze *et al.* who found that [BMIM] Cl formed liquids with $FeCl_2$ in the molar ratio 0.3 $FeCl_2$: 1 [BMIM] Cl whereas the $FeCl_3$ formed in the molar ratio 0.53 to 1.7. Raman scattering was used to calculate the anion in the iron system and it was shown that ferrous ($FeCl_4^{2-}$) and ferric chloride ($FeCl_4^-$ and $Fe_2Cl_7^-$) were both present. It was also seen that Zn and Al systems were similar to Fe systems, as the relative concentrations were found to be dependent upon the Lewis acidity. The [BMIM]$FeCl_4$ liquid was also shown to be ferromagnetic.

As defined above, systems with low melting point halides should produce DESs. It is therefore not surprising that eutectic mixtures of imidazolium chloride with $GaCl_3$ and $InCl_3$ have also been reported.[49, 50] These have been used for the electrodeposition of semiconductors.[51, 52] Other metal halides that have been studied[53, 54] include $AuCl_3$, $NiCl_2$ and $CoCl_2$ but their applications have been limited to synthesis. Some more exotic metals have also been formulated into ionic liquids which include [EMIM]$_2$[UCl$_6$] [55] and niobium and tantalum in the form of [EMIM]TaF$_6$ and [EMIM]NbF$_6$.[17] As can be seen from the systems listed above most studies have concentrated upon halides but Noguera *et al.*[56] demonstrated that metal oxides in the form of $CrO_3$ and $Na_2MoO_4$ could also be used to prepare ionic liquids.

In general, imidazolium-based liquids have lower viscosities and higher conductivities than the corresponding pyridinium or quaternary ammonium eutectics formed under the same conditions. This is because the imidazolium cation has very low symmetry and ethyl methyl-imidazolium chloride is one of the lowest melting point chlorides.


## 1.4.2 Type II eutectic

Type II eutectics were developed in an attempt to include other metals into the DES formulations. It was found that metal hydrates have a lower melting point than the corresponding anhydrous salt. Clearly the water of hydration decreases the melting point of metal salts because it decreases the lattice energy. As **Figure 1.2** shows a lower melting point

of the pure metal salt, $T_f^*$, will produce a smaller depression of freezing point $\Delta T_f$. This correlation can be seen in **Figure 1.2** for the data presented in ref.[14] and arises because salts with a lower lattice energy will tend to have smaller interactions with the chloride anion.
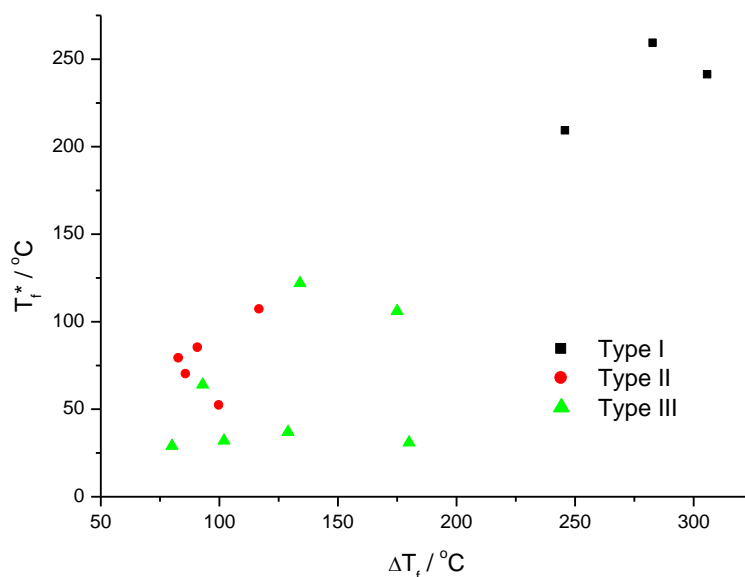


**Figure 1.2:** *Correlation between the freezing temperature ($T_f^*$) and the depression of freezing ($\Delta T_f$) point for metal salts and amides when mixed with choline chloride in 2:1 ratio.(compiled from data in ref .* [14]

Very few studies have been carried out on Type II eutectics and the role of the water molecules is still largely unknown. The authors claim that the water does not act in the same way as bulk water *i.e.* hydrogen evolution is a lot less common when chromium is electrodeposited. Chromium was reduced with high current efficiency and this is unaffected by the addition of up to 10 wt% water, suggesting that the water is strongly associated with the chloride anions or the metal centre.[26] It is only the chromium system which has been published to date. [33] in the area also shows that metals such as Co, Cu, Ni, Al, Ca and Fe also form liquids from the metal halides particularly with the hexahydrates. The deposition of metals such as Al and Ca is, however, not possible due to the limited potential window of these liquids.

### 1.4.3 Type III eutectic

Type III eutectics use a simple hydrogen bond donor such as amides, carboxylic acids and alcohols to form a complex with a quaternary ammonium halide. As can be seen from **Figure**

**1.2** these compounds tend to have lower freezing points than the metal halides and the depression of freezing point is accordingly lower. These liquids will be the subject of this thesis. Type III fluids have interesting solvent properties and a wide variety of solutes exhibit high solubilities.[34, 35] These eutectic systems have a large depression of freezing point. For example, the oxalic acid–choline chloride system show a depression of freezing point of 212 $^\circ$C and in the the choline chloride–urea system it is 178 $^\circ$C [35]. The freezing point depressions are not as large as the choline chloride–zinc chloride system[30] (272 $^\circ$C) due to the covalent bonds formed in the metal chloride case. The type III eutectic mixtures are easy to prepare and are relatively inexpensive meaning that they can be used for large scale applications such as metal finishing which is the subject of this thesis.

Type III eutectics rely on the formation of hydrogen bonds between the polar organic and the chloride anion. The existence of hydrogen bonding was shown using Heteronuclear overhauser effect spectroscopy (HOESY) for the choline fluoride / urea system.[34] The presence of a complex between Cl$^-$ and two urea molecules was observed using FAB-MS (M$^-$ = 155) a signal was also identified for one Cl$^-$ with one urea (M$^-$ = 95) was also observed.

The freezing point of the HBD- salt mixtures will be dependent upon the lattice energies as aresult from the interaction between the molecules of the salt and HBD and how these are counteracted by the anion-HBD interaction and the entropy changes arising from forming a liquid. For

The complexation reaction of chloride ions with urea is actually driven by hydrogen bonding between them assisted by high temperature conditions; therefore the reduction in freezing point is a measure of the entropy change. [35] These liquids have been used in numerous studies for the electrodeposition of a variety of metals and alloys. This has been reviewed recently in a variety of articles.[57-61]

## 1.5 Parameters of deposition characteristics

Ionic liquids are clearly different from aqueous solutions for metal electrodeposition. This is due primarily to the differences in the way that the solvent acts as a ligand for the metal cation and the ionic structure of the liquid as opposed to a molecular one. A more in depth analysis of the parameters that affect metal deposition is given in a review by McKenzie *et al* [62]. The information below is a summary of that review which has been updated where applicable.

## 1.5.1 Temperature

The liquid temperature range of ionic liquids varies from -50 to 250 $^{\circ}$C, which potentially leads to greater control of thermodynamics than in aqueous solutions. This has not really been used to any great extent with ionic liquids and most studies have been limited to below 100 $^{\circ}$C. Prolonged thermal stability of ionic liquids has not yet been demonstrated. For most applications of ionic liquids to metal deposition it is likely that one would want to operate around ambient temperature for ease of use and energy considerations.

## 1.5.2 Brighteners

Brighteners are added to most electroplating systems and work by either complexing the metal ions, thereby decreasing the reduction potential to make it more difficult to nucleate metal clusters or, by adsorption of an organic species on the electrode surface blocking nucleation and modifying growth.

In aqueous solutions, brighteners function by making large flat crystals. The brighteners therefore control the rate at which the metal phase forms on the electrode surface. In ionic liquids, however, most studies have shown that the metal particles grow as nanocrystalline deposits and bright layers result from a more even particle distribution. It is therefore likely that brighteners used in aqueous solutions will not function in the same way in ionic liquids because of the difference in double layer structure and mass transport.

Brighteners that involve a complexation with a solution based species will depend upon the comparative strength of the ionic liquid–metal interactions. Some work has been carried out on strong complexants for nickel [60] and reagents such as ethylene diamine and EDTA have been shown to function as effective brighteners. All systems that have been studied until now that produce bright metallic finishes produce a nanocrystalline structure and tend to results in a progressive nucleation mechanism. The chloride anions act as a Lewis bases (electron donor) in eutectic based ionic liquids due to a decreased interaction between the metal salt and the brightener. The effect of the ligand on the redox potential is only just being studied and work by Abbott *et al* is just starting to investigate speciation in DESs and the effect that this has upon redox potentials. The first reported electrochemical series has recently been published from this research.[63]

Caporali [64] studied aluminium deposition and found that using 5 g l$^{-1}$ phenanthroline produced a semi-bright finish in a [BMIM]Cl/ AlCl$_3$ ionic liquid. There was no insight into the mechanism, however, and the results were only presented in conference proceedings.

Abbott also showed the use of brighteners in choline-based ionic liquids.[65] Abbott shows the effect on the deposit morphology of adding acetonitrile as brighteners to a ChCl: urea eutectic containing Cu(II).[26] Recent works by the same group studied a variety of brighteners used for zinc deposition. It studied $NH_3$, ethylenediamine and acetonitrile as additives and showed that all had an effect on the morphology of zinc deposition. The best brightening effect was shown by the strongest hydrogen bond donors in the ChCl: ethylene glycol based eutectics. This was thought to occur due to strong interaction between the hydrogen bond donors and $Cl^-$ ions preventing their specific adsorption at the electrode surface. [66]

### 1.5.3 Diluents

The addition of small molecules of organic compounds and aqueous solvents will have two effects: they decrease the surface tension of the liquid and increase the molar free volume (easier ion movement) and the diluent molecules make it easier for ions to move. Aromatic solvents such as toluene and benzene have been added to imidazolium based liquids for aluminium deposition.[67, 68] Abbott *et al* recently studied the role of toluene for the deposition of aluminium from an $EMIMCl/AlCl_3$ eutectic and found that the brightening effect was actually caused by the diluents improving the anodic dissolution rate.[69]

For electrodeposition, which is usually carried out in ambient conditions, a practical solution is often important and in some cases water may also be suitable for use as a diluent if less than 10 % is added.[29] The amount of water which can be added will depend upon the Lewis basicity of the anion since it will coordinate with water molecules. In addition the presence of chloride contamination, for example, increases the viscosity of the ionic liquids, whereas the presence of water, or other co-solvents, reduces the viscosity. The addition of a co-solvent is usually carried out to reduce the viscosity and so increase the conductivity.

Lane *et al* studied the electrochemistry of lithium in several ionic liquid-organic diluent mixtures and found that ethylene carbonate and vinylene carbonate improved the cyclability of the electrode but toluene and tetrahydrofuran did not improve performance and this was related to passivation of the electrode.[70] The conductivity of these systems was also reported by the same group.[71] Propylene carbonate was also used as a diluent by Sun *et al*.[31] who studied the electrodeposition of zinc on glassy carbon and nickel substrates from $ZnCl_2$-EMIC eutectics. It was found that the deposits produced from coating baths with higher propylene carbonate concentrations or at higher temperatures exhibited larger grain size with a less uniform distribution. It is expected that the addition of propylene carbonate decreases

the solution viscosity, which in turn increases the mass transfer rate of the $Zn^{2+}$ species toward the electrode, as well as the growth rate of the electrodeposits.[31]

## 1.5.4 Metal salts

In aqueous plating solutions the type and concentration of the metal salt is critical in controlling the morphology and coating rate of the metal film. The coordination chemistry and concentration of the metal complex is the key for the design of ionic deposition systems. **Table 1.2** lists some of the metal salts that are used in the most commonly used aqueous electroplating solutions.

| Metal | Bath | Electrolyte | Concentration of Metal salts/ g dm$^{-3}$ |
|---------|----------------|-------------------------------------|--------------|
| Chromium | Hard Chromium | $CrO_3$, $H_2SO_4$ | 250 - 450 |
| Copper | Acid Copper | $CuSO_4$, Potash alum,$H_2SO_4$ | 60 - 200 |
| Nickel | Watts Nickel | $NiSO_4$. $NiCl_2$, Boric acid | 200 - 350 |
| Silver | Zonax Silver | Ag salts (various) | 80 - 200 |

*Table 1.2 Typical concentration of metal salts used in commercial aqueous solution*

For many of the ionic liquid systems discussed above metal deposition has been performed using chlorides and the metal complexes formed are dependent upon the Lewis acidity of the metal and Lewis basicity of the ionic liquid. Type I eutectic based ionic liquids necessarily have a high metal concentration and will have a tendency to promote small metal nuclei on the electrode surface.

The addition of strong complexing agents to hinder metal nucleation may not be trivial as it will also affect the charge on the metal complex and affect the interaction between the metal centre and the chloride anion due to the properties of the ionic liquids being altered by changing the speciation. In addition, some metal oxides have been dissolved in high concentrations in Type III eutectics.[39] Abbott [65, 26] showed the first example of the anion effects on the reduction potential for the $Cu^{2+}$ /$Cu^+$ and $Cu^+$ /$Cu$ couples for various copper salts in a variety of ionic liquids.

Another issue is that in all ionic liquids, the metal complex will tend to dissolve to form anionic species and these will have a significant effect on viscosity and mass transport and hence the effect of the concentration of the metal ions on the reduction current will not be linear. This effect on viscosity leads to an extremely complicated effect of the metal salt on

the deposition characteristics. This has recently been demonstrated by Abbott *et al*. who showed that there was almost no effect when the HBD was exchanged for ethylene glycol.[66]

### 1.5.5 Electrolyte

Ionic liquids have conductivities which are lower than aqueous solutions but higher than non-aqueous solvents. One way to increase the conductivity of ionic liquids could be to add a small inorganic salt such as LiCl that could have an increased mobility compared to the large organic cations. The addition of chloride to the electrolytes has already been shown to have an effect on the structure of the double layer and change the nucleation mechanism. Surprisingly few studies have been carried out into the double layer structure of ionic liquids.[72] Initial studies into the double layer structure in imidazolium with salts such as triflate, $(F_3CSO_2)_2N^-$ and $BF_4^-$ suggested that a layered model of alternating anion and cation layers was appropriate to describe the structure.[73, 74] The double layer structure is influenced by cation/ anion interaction (Helmholtz layer) and is very important to the mechanism of nucleation and growth in ionic liquids. In ionic liquids with discrete anions the presence of Group 1 metal ions can be detrimental to the deposition of reactive metals such as Al and Ta where they have been shown to be co-deposited, although their presence is in trace concentrations.[14]

### 1.5.6 Anode material

Generally, the two types of anode, soluble and insoluble are used for electroplating in aqueous solutions. Insoluble anodes tend to produce oxygen bubbles which are disrupting to the flow of ions and electric current to the growing surface. The use of insoluble anodes tends to lead to the breakdown of the ionic liquid which is clearly undesirable. For this reason, soluble anodes are generally used in ionic liquids. One disadvantage of the soluble anode is that it can release particles into the plating solution if the dissolving electrode fragments. Another disadvantage of using soluble anodes is passivation which can occur depending on a variety of factors including the process conditions and anode material. Surprisingly, almost no work has been carried out into the anodic dissolution of metals in ionic liquids. New strategies will therefore have to be developed to use soluble anodes, where possible, or add a sacrificial species that is oxidized to give a benign gaseous product. Abbott *et al*. showed that the anodic reaction can affect the morphology of the deposit at the cathode. The dissolution

of aluminium was shown to be rate determining due to the lack of suitable ligand in ethyl-imidazolioum chloroaluminate in the range of potentials at which the solvent is stable. [69]

## 1.6 Potential window

The potential window depends on the oxidative and reductive stabilities of the selected solvent. In the case of ILs, the electrochemical potential window is mainly dependent on the resistance of the cation to reduction and the resistance of the anion to oxidation. The potential window of ILs is generally more than 2.0 V. However the side reaction between ILs and impurities will limit the electrochemical potential window. For example water can decrease both the anodic and the cathodic potential limits. The electrochemical potential window of [BMIM][BF$_4$] was found to be reduced from 4.10 V to 1.95 V after addition of 3% water by weight, as shown in **Figure 1.3**. In addition, water can react with ILs to create electroactive species.[75, 76]

For electrochemical application, the potential window of the electrolyte solution is one of the most important properties. The potential window is governed not only by the chemical structure of the materials used but also by the electrode materials, sweep rate of the potential, temperature, atmosphere, solvent, impurities and so on. The use of a different reference electrode to determine cathodic and anodic limits of an ionic liquid solution makes the situation even more complicated.

The potential window is determined by cyclic voltammetry or linear sweep voltammetry. In the cyclic voltammetry method, it must be noted that the electrochemically oxidized or reduced products of the first sweep can affect the voltammograms of the reverse sweeps. In both cases, the anodic and cathodic limits are defined as the voltage where the current density reaches 1.0 mA cm$^{-2}$ with a sweep rate of 50 mV s$^{-1}$. [15]
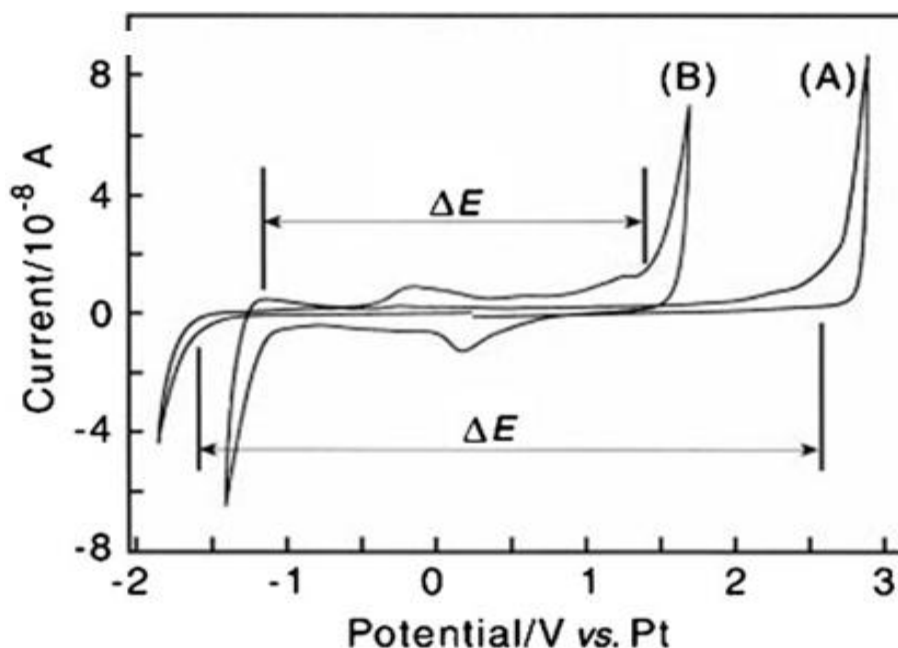
***Figure 1.3*** *Cyclic voltammograms recorded in BMIM BF$_4$ at a 50 μm Pt disc electrode: (A) without water pure IL and (B) with a water content 3% in the IL (scan rate 100 mV s$^{-1}$) where ΔE is the potential windows .Image taken from ref.* [76]

The potential widows of imidazolium salts are typically about 4 V and this is generally limited by the relatively acidic proton on the carbon between the two nitrogen atoms on the aromatic ring. When the imidazolium has the proton in the 2-position substituted by an alkyl chain, the potential window increases to more than 4 V.[77] Some ionic liquids have excellent electrochemical stability and are good for application as electrolyte materials.

The potential window of the choline chloride with urea eutectic mixture is relatively small on a platinum electrode (- 1.2 to + 1.25 V *vs* Ag). However, metals can be deposited with high current efficiencies because the reduction kinetics of the eutectic are quite slow.[39] Also the potential windows of 1:2 choline chloride/MX$n$ (MX$n$ = ZnCl$_2$, SnCl$_2$, FeCl$_3$) have been investigated by Abbott *et al.*[21, 36] The zinc chloride melt has the largest potential window of around 2 V, whereas the tin and iron analogues have potential windows around 1.5 and 0.5 V, respectively.

## 1.7 Charge and mass transfer

The biggest difference between ionic liquids and molecular solvents is the viscosity and the resultant change in mass transport. The conductivity and viscosity of an ionic liquid is

strongly dependent upon temperature. It has been shown that the conductivity, σ changes in an Arrhenius manner with temperature:

$$Ln\sigma = Ln\sigma_{\circ} - \frac{E_A}{RT}$$
(1.6)

where $E_A$ is the activation energy for conduction and $\sigma_0$ is a constant R is rate constant, T temperature in K. An analogous relationship has been found for the change in viscosity with temperature. Many authors have noted the close correlation between conductivity and viscosity and have invoked the Walden rule

$$\Lambda_o\, \eta_o = \text{constant}$$
(1.7)

where $\Lambda_o$ is the molar conductivity at infinite dilution and $\eta_o$ is the viscosity at infinite dilution.

The Walden rule was first based on observations of the properties of a given salt in dilute organic solutions, but has recently been applied to ionic liquids. Researchers have described a qualitative approach to this question based on **equation 1.7**.[78-80] This rule is only valid for ions at infinite dilution and ignores ion-ion interactions and so it should not be valid in ionic liquids.

The Walden rule is a totally empirical relationship which is observed for a group of electrolytes that have similar ion sizes and it should therefore be questioned why this works if the ions are not at infinite dilution. Schreiner *et al.* recently published a critique of the use of the Walden rule with ionic liquids.[81] They suggested that use of the empirical approach from Stokes (**equation 1.8**) explains the deviations from the so-called ideal Walden plot since each salt will have a different value of $C$ and α.

$$\log \Lambda_m{}^0 = \log C + \alpha \log \eta^{-1}$$
(1.8)

where $\Lambda_m{}^0$ is the limiting molar conductivity, $\eta$ is the pure solvent's viscosity, C is constant for infinitely diluted electrolyte solutions, α is a constant between zero and unity.

One approach to explain this observation has been to invoke a model of charge mobility occurring via hole transfer which was developed by Fürth [82] and applied to molten salts by Bockris.[65] The model did not fit experimental data for high temperature systems due to the large number of suitably sized holes at high temperatures which were able to take the small charge carriers. Ionic association decreased the number of charge carriers and hence the

model broke down. The same basic model was applied to ionic liquids and found to fit extremely accurately.[83, 84]

It was proposed that the reason that ionic liquids fit this model so accurately is due to the small number of suitably sized holes available at ambient temperatures that are able to accommodate the exceptionally large ions. Under these conditions the holes are effectively at infinite dilution and migration and can be described by a combination of the Stokes–Einstein and Nernst–Einstein equations. (**Equation 1.9**)

$$\lambda_+ \ = \ \frac{Z^2 Fe}{6\pi\eta R_+} \tag{1.9}$$

where $z$ is the charge on the ion, $F$ is the Faraday constant and $e$ is the electronic charge, $\lambda_+$ is the limiting molar conductivities of the cation, $R_+$ is the radii of the cation. This shows the validity of the Walden rule for studies of conductivity in ionic fluids since rearranging **equation 1.9** yields the observation that for a given electrolyte $\Lambda \eta$ = constant.

Abbott showed that the viscosity of an ionic liquid could be accurately modelled using a gas-like model where mobility was hindered by the probability of finding a hole large enough for an ion to move into.[83, 84] The liquids which do not fit hole theory tend to be those whose ions are less spherical. Modifications to this theory have been made by Zhao *et al.* who took into account the asymmetric nature of the cation and this significantly improved the prediction of the conductivity of long chain salts.[85]

An alternative approach has been to explain deviations from the Walden plot as arising from ion pairing or systems that are not true ionic liquids.[86-88] This work, along with all other diffusion studies in ionic liquids depends on the validity of the Stokes-Einstein equation and this has recently been shown to be invalid in ionic liquids.[80, 89] The breakdown of the Stokes-Einstein equation results from the fact that an ionic liquid cannot be viewed as a structureless continuum. Instead it is shown that species diffuse by jumping between suitable holes which are similar in size to those determined from the surface tension.

## 1.8 Electrodeposition of metals

Because ionic liquids have a much larger potential window than organic solvents, certain metals can be electrochemically deposited that are otherwise inaccessible to organic solvents.[90, 91] The wider potential window reduces the possibility of any side reactions occurring that can affect the deposition of the metal onto the substrate, such as hydrogen

evolution. As a result it has been possible to use a variety of chloroaluminate ionic liquids to deposit aluminium onto various substrates by various electrochemical methods.[92-94] The aluminium deposits on the substrate are affected by the current density, with higher current densities forming smaller crystals.[95] The deposition of aluminium from ionic liquids can be a complex issue, due to the air and moisture sensitivity of the chloroaluminate liquid. However, many other elements can be deposited easily, such as silver, copper and palladium. Furthermore, technically important alloys such as Al/ Mg, Al/ Cr and others can be made by electrochemical means. Addition of organic solvents such as benzene [68] or toluene [96] has shown that bright finishes can be obtained after deposition. The miscibility of the chloroaluminate based ionic liquids with organic solvents such as toluene and benzene. means that the ionic liquid can be cleaned away from the sample after deposition has taken place. The scope for electrochemicaly depositing metals successfully is large with the use of ionic liquids. Metals such as $Ag^{97}$, $Cu^{98}$, $Pd^{99}$, $In^{100}$, $Sb^{101}$, $Te^{102}$, $Cd^{103}$ and others have been deposited. Today about 300 different ionic liquids with different qualities are commercially available from a wide range of companies.[11]

## 1.9 Deposition of metals from non-chloroaluminate eutectic mixtures

Electrodeposition has been demonstrated for the majority of metals from ambient-temperature ionic liquids. However, this does not necessarily mean that the liquid with the widest potential window will negate the use of all other ionic liquids. These use organic cations based principally around ammonium, sulphonium and phosphonium moieties to produce ILs. Ionic liquids formed with inorganic cations have a higher charge density and do not tend to form room temperature electrolytes. Gambino *et al.*[104, 105] has developed mixtures of alkali metal halides with urea which form eutectics with melting points around 140 $^o$C. According to Abbott, this idea has been built upon and some transition metal salts were studied, such as those already used in type I eutectics to create ambient-temperature ionic liquids. The formation of room temperature eutectics with urea, acetamide, ethylene glycol and 1,6-hexanediol has been studied.[106]  In this case, choline chloride has been devolved as precursor for the preparation of eutectic ionic liquids which as the liquids are easy to prepare, as shown in **Reaction 1.2**, and relatively inexpensive.[34]

$$Z = H_2NCONH_2, HOOCCOOH, HOHC(CH_2OH)_2, ZnCl_2, SnCl_2, FeCl_3$$
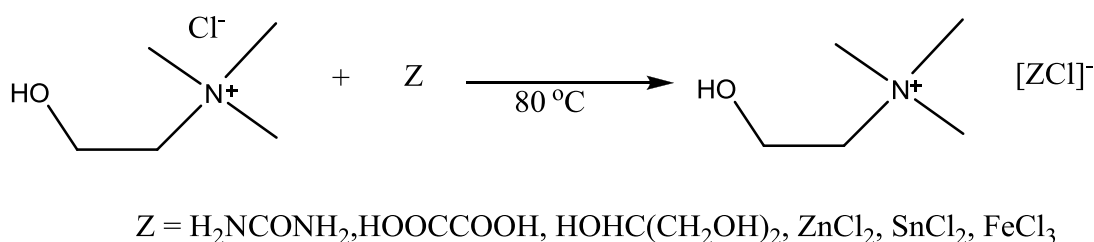
**Reaction 1.2** *Choline chloride reaction with complexing agents to produce eutectic ILs* [107]

Type I eutectics will probably be the most suitable for Ga, Al and Ge deposition. Type II eutectics are most suitable for Cr deposition and Type III are most suited to the deposition of Cu, Ag, Zn and associated alloys. In addition, Type III eutectics are widely used in many applications, such as metal winning, oxide recycling and electropolishing.[26]

The successful electrodeposition of zinc, tin, copper and zinc–tin alloys from these eutectic solvents depends on the choice of the hydrogen bond and the components in solution which affect the metal alloy deposition.[57-59] To date the most practically important metals have been electrodeposited from ionic liquids and a comprehensive review is given in articles by Abbott [26] and Endres.[90, 11, 108] The deposition methods of metals from eutectic based ionic liquids which are not predominantly AlCl$_3$ have been developed since the end of the 1990s. **Figure 1.4** shows just some of the metals that have been deposited from type (I), (II), and (III) of eutectics.[14]
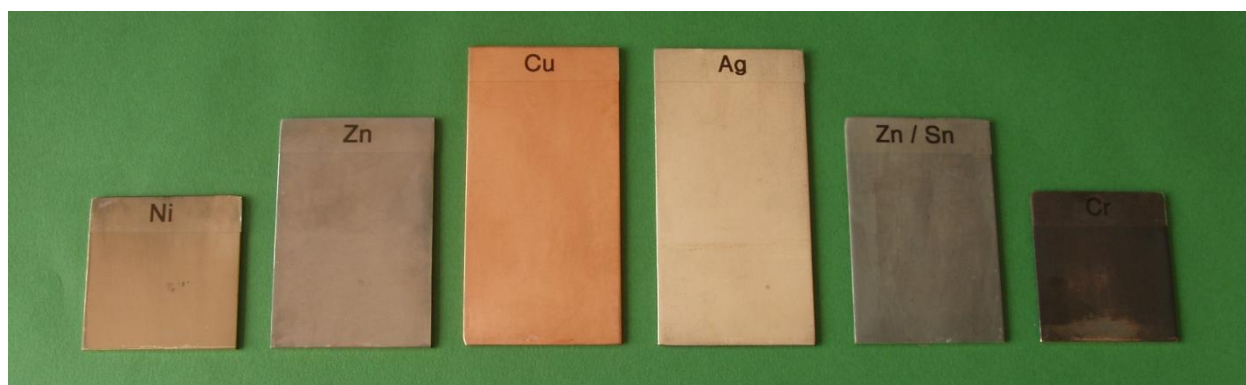


**Figure 1.4** *A range of metal and metal alloy coatings deposited electrolytically from type II (Cr far right) and type III (Ni, Cu, Zn, Sn and Ag) choline chloride-based ionic liquids.*

For example, Lewis acid chlorozincate ionic liquids can be obtained by mixing ZnCl$_2$ with various organic chloride salts (RCl), such as choline chloride and EMIC, to produce various

species such as $ZnCl_3^-$, $Zn_2Cl_5^-$, and $Zn_3Cl_7^-$, as shown in **Reaction 1.2**. Sun *et al.*[109] studied the electrochemical deposition of Ni–Zn alloy filament arrays from a zinc chloride based ionic liquid. Dale and co-workers have demonstrated gallium and copper–gallium alloy electrodeposition from Reline (a choline chloride/ urea based ionic liquid) for the fabrication of wide gap $CuGaSe_2$ solar cells. It was shown that deposits with a large Ga composition can be obtained from Reline with high current efficiency. The successful electrodeposition of Cu–Ga alloy films in one step was also shown from Reline.[110] The SEM images of electrodeposited thin film Cu-Ga alloys on Mo from Reline mixed with 25: 50 m mol $dm^{-3}$ $CuCl_2$: $GaCl_3$ at various potentials a) -0.7, b) -0.9 and c) -1.1 V for 30 minutes at 60 $^o$C are shown in **Figure 1.5**.
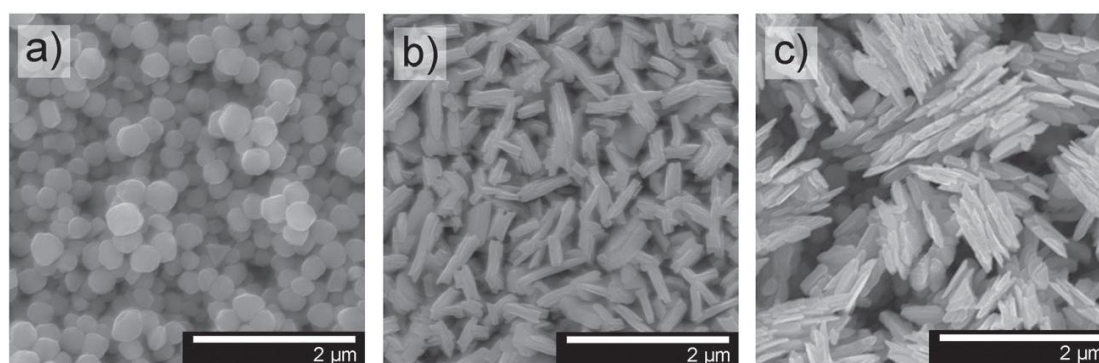


***Figure 1.5*** *SEM images of Cu-Ga alloys deposited on Mo from Reline $CuCl_2$: $GaCl_3$ 25: 50 mmol $dm^{-3}$ at different potentials; (a) -0.7 V, (b) -0.9 V and (c) -1.1 V for 30 minutes at 60 $^o$C. Figure from Ref [110]*

The different morphologies may be related to the percentage of Ga in the alloy composition film. EDX analysis shows that the gallium content increases in the alloy with an increase in the potential; at -0.7 V Cu is almost 100% but at approximatly -1.1 V the percentage decreased to 40.1%.

## 1.10 Summary of alloy deposition using ionic liquids (mostly Al & Zn)

### 1.10.1 Chloroaluminate

Generally, the most widely used system is the aluminium chloride-1-ethyl-3-methylimidazolium chloride ionic liquid, which is liquid at room temperature.[6] These

chloroaluminate systems have been used in the literature for applications such as batteries, chemical synthesis and electrodeposition.[111, 112]

Chloroaluminate liquids have been used for the electrodeposition of non-aluminium containing alloys such as Cu-Zn and Co-Zn however these are contaminated with Al. The electrodeposition of transition metal-aluminium alloys have been investigated from Lewis acid chloroaluminate ionic liquids at room temperature. Binary aluminium alloy films have been successfully deposited from aluminium chloride-1-methyl-3-ethylimidazolium chloride ionic liquids including species such as Al-V,[113] Al-Ti,[114] Al-Mo,[115] Al-Zr,[116] Al-Mg,[117] Co-Al[118] and Ni-Al.[119] It was also possible to deposit ternary alloys such as Al-In-Sb,[120] Al-Mo-Ti,[121] and Al-Mo-Mn.[122] The Al–Ce alloys were deposited from $AlCl_3$/ BMIM-Cl (1-butyl-3-methylimidazolium chloride) ionic liquid with cerium chloride. The main factor in this alloy deposition is the concentration of aluminium chloride in the solution, which influences the composition of the deposited alloy and the properties of the film.[123]

Electrodeposition of Al–Zn alloy onto a magnesium alloy substrate from a Lewis acidic aluminium chloride-1-ethyl-3-methylimidazolium chloride ($AlCl_3$-EMIC) ionic liquid containing various concentrations of $ZnCl_2$ has been successfully investigated.[124, 125] It is clearly shown that the amount of Zn in the deposit increases with increasing concentration of $ZnCl_2$ in the mixed bath but decreases with increasing magnitude of cathodic potential. In addition, increasing the surface roughness also depends on the presence of Zn in the coating, when compared with pure Al deposition. In addition, Co-Al and Ag-Al alloys have been deposited from $AlCl_3$-EMIC room temperature ionic liquids which were investigated by Carlin *et al.*[126] and Zhu[127], respectively. According to Ali [128], the electrodeposition of Al-Cr alloys could be achieved from a 2: 1 $AlCl_3$-N-(n-butyl) pyridinium chloride room temperature molten salt with varying concentrations of chromium from 0 – 94%. The electrodeposition of a layer of Al-Cr alloy onto Pt and mild steel substrates has been carried out by controlling the deposition parameters, such as $Cr^{3+}$ concentration in the bath, applied potential and current density. The large electrochemical potential window of the $AlCl_3$-$[C_4mim]^+Cl^-$ (1:1) melt containing $SbCl_3$ has been used to study the nanoscale electrocrystallization of pure Sb and the compound semiconductor AlSb on Au(111). [129] A more comprehensive review of aluminium and aluminium alloy deposition is given in a recent review.[69]

**1.10.2 Chlorozincate**

The $ZnCl_2$–1-ethyl-3-methylimidazolium chloride (EMIC) ionic liquid is less sensitive to air and moisture in comparison to chloroaluminate ILs and this has been used for the deposition of Zn and its alloys. The electrodeposition of copper and copper-zinc alloys from a Lewis acidic zinc chloride-1-ethyl-3-methylimidazolium chloride molten salt containing copper(I) has been investigated under different conditions onto tungsten and nickel electrodes.[130] Evaluation of the chronoamperometric transient behaviour during electrodeposition suggests that pure copper electrodeposition proceeds via 3-D instantaneous nucleation with diffusion-controlled growth. The surface morphologies and the compositions of the electrodeposited Cu-Zn alloys were examined with scanning electron microscopy (SEM) and X-ray diffraction.

According to the literature review[131] the anomalous co-deposition of Zn-Co alloys from aqueous plating baths shows a strange type of co-deposition alloy, in fact that cobalt content in this alloy was very low, because the Co has a greater nobility than Zn. On the other hand, the Zn-Co alloys can be deposited from two systems of ionic liquids, Lewis acid zinc chloride-1-ethyl-3-methylimidazolium chloride molten salt and $CoCl_2$-$ZnCl_2$-l-butylpyridinium chloride with varied Co content from Co-rich to Zn-rich.[132, 133]

Huang and Sun have reported the electrodeposition of zinc alloys from Lewis acidic zinc chloride-1-ethyl-3-methylimidazolium chloride ionic liquid such as Zn–Pt,[134, 135] Zn–Fe,[136] Zn–Sn,[137] Zn–Ni,[138] Cd-Zn [139] and Zn-Pd.[140] Electrochemical alloying and dealloying of a Au-Zn alloy in a $ZnCl_2$–EMIC ionic liquid to fabricate functional nanoporous gold has also been investigated.[141] However, the phase composition and the mechanism of the Zn–Au alloys bulk deposition have been reported several years later. In 2010 Borissov[142] studied the phase composition and the mechanism of alloy formation of the Zn–Au alloy by electrochemical deposition of zinc on gold from an ionic liquid comprising of 60.0–40.0 mol% $ZnCl_2$ and 1-butyl-3-methylimidazolium chloride (BMIC) at 50 $^{\circ}$C. It has been confirmed that zinc electrodeposition results in the formation of two phase cubic Au–Zn intermetallics, which at 75% zinc produce $AuZn_3$ and at 50% zinc produces AuZn. At higher than 75% zinc concentrations, the Au–Zn alloys exhibit a transformation to hexagonal $Au_{1.2}Zn_{8.8}$ phase. Zn-Mg alloys were also deposited from two different ionic liquids; firstly, from Lewis basic 1-ethyl-3-methylimidazorium bromide(EMIB)-$ZnBr_2$-$MgBr_2$-ethylene glycol molten salts [143] and secondly from a bath of trimethyl propylammonium bis((trifluoromethyl)sulfonyl)imide (TMPATFSI) at the same temperature of 120 $^{\circ}$C.[144]

## 1.11 Copper deposition using ionic liquids

The electrodeposition of copper in RTILs has been widely investigated. In almost all systems two steps were found for the reduction of $Cu^{2+}$ to the metallic state.[98, 145, 146] The electrodeposition of Cu from trimethyl-n-hexylammonium bis (trifluoromethylsulfonyl) amide (TMHA-Tf$_2$N) IL has been investigated by Murase [147] and co-workers and they have stated that the Cu deposition and dissolution involved a monovalent redox reaction of $Cu^+$. Endres *et al.*[148] also obtained nanocrystalline Cu by electrodeposition from the same IL.[75]

The new IL system, air and water stable ionic liquid at room temperature 1-ethyl-3-methylimidazolium dicyanamide (EMI-DCA) was employed for the electrodeposition of copper, as CuCl and CuCl$_2$ are very soluble in EMI-DCA. The results of $Cu^+$ in EMI–DCA were compared by cyclic voltammetry with the corresponding tetrafluoroborate bis(trifluoromethane-sulfonyl)imide. The basicity of the two ionic liquids EMI-DCA and EMI-BF$_4$ are shown by the redox potentials of both the $Cu^{2+}/Cu^+$ and $Cu^+/Cu$ occurring at potentials less positive than those that were observed in the EMI-TFSI ionic liquid.[149] It is also shown that the EMI-DCA ionic liquid has less peak potential separation between the cathodic and the anodic peak for the $Cu^{2+}/Cu^+$, whereas the peak currents are higher due to increased mass transport. In fact these results show that the type of the anions in the ILs can play significant roles in the chemical behaviour of the metal species.

The electrodeposition of different copper components such as CuCl$_2$,[59, 150] Cu$_2$O[151, 152] and CuCl$_2$ (anhydrous) [145] salt, in deep eutectic solvents have also been investigated. The three different types of deep eutectic solvents used for studying the electrodeposition of Cu were 1:2 choline chloride: glycerol (Glyceline), 1: 2 choline chloride: ethylene glycol (Ethaline) and 1: 2 choline chloride: urea (Reline).

## 1.12 Project aims

Electroplating of mixed-metal species from a solution containing different metal salts is relatively straight forward. In principle solid-solution phases (alloys) can be obtained by co-deposition where the composition of the alloy is determined by the ratio of metal ions in solution. In practice these coatings are usually applied by controlling the cathode potential at a value that is substantially negative of the metal ion with the most cathodic reduction potential. This is intended to ensure that mass-transport is rate limiting for both metal ions.

Alternatively it is possible to control the composition of the deposit by careful positioning of the applied potential but this method of kinetic control is notoriously unreliable. Despite the seductive simplicity of this approach the compositions of alloys and mixed phase deposits often bear no resemblance to the composition of the electrolyte from which they were deposited. This is often because of large differences in the redox potentials of the two metal ions, disparate electrode kinetics (slow ligand exchange or electron-transfer) or side reactions from the solvent or electrolyte. It has been previously shown that the range of metal ion redox potentials is compressed in ionic liquids compared to the equivalent species in aqueous solution and also that the potential window within ionic liquids is often much larger that aqueous electrolytes. These combined observations have led to the expectation that ionic liquids can be used effectively for electrolytic deposition of alloys from binary metal ion mixtures that would not be possible in conventional aqueous electrolytes. This has already been demonstrated for the Zn and Sn[58] alloy deposit.

The aims of this project are to study the deposition of strategic alloys from type III ionic liquids containing binary mixtures of metal ions under potential (mass transport) control. In addition, it is also the intention to develop a general system of gravimetric analysis that can probe the composition (mass and charge) of an electrolytic deposit during the experiment in real time. The results of this project on Cu alloy mixtures (Cu-Ag, Cu-Sn and Cu-P) have all been described from the perspective of the technique development, including benefits and limitations but also in terms of the intrinsic properties of the Cu alloys' deposits.

**1.13 References**

1.  C. Chiappe and D. Pieraccini, *Journal of Physical Organic Chemistry*, 2005, **18**, 275-297.

2.  P. Walden, *Bull. Acad. Imper. Sci*, 1914, 1800.

3.  Hurley, *J. Electrochem. Soc.*, 1951, **98**, 207.

4.  H. L. Chum, V. R. Koch, L. L. Miller and R. A. Osteryoung, *Journal of the American Chemical Society*, 1975, **97**, 3264-3265.

5.  J. Robinson and R. A. Osteryoung, *Journal of the American Chemical Society*, 1979, **101**, 323-327.

6.  J. S. Wilkes, J. A. Levisky, R. A. Wilson and C. L. Hussey, *Inorganic Chemistry*, 1982, **21**, 1263-1264.

7.  T. B. Scheffler, C. L. Hussey, K. R. Seddon, C. M. Kear and P. D. Armitage, *Inorganic Chemistry*, 1983, **22**, 2099-2100.

8.  D. Appleby, C. L. Hussey, K. R. Seddon and J. E. Turp, *Nature*, 1986, **323**, 614-616.

9.  C. L. Hussey, *Adv. Molten Salt Chem*, 1983, **5**, 185.

10. J. S. Wilkes and M. J. Zaworotko, *Journal of the Chemical Society-Chemical Communications*, 1992, 965-967.

11. F. Endres and S. Z. El Abedin, *Physical Chemistry Chemical Physics*, 2006, **8**, 2101-2116.

12. P. Wasserscheid, T. Welton (Eds.) *Ionic liquids in synthesis*, Wiley-VCH, Weinheim 2003.

13. P. Wasserscheid, T. Welton , *Ionic liquids in synthesis*, John Wiley -VCH, 2nd edn., 2007, p. 776.

14. F. Endres, P. Abbott Andrew and D. R. MackFarlane, in *Electrodeposition from Ionic Liquids*, John wiley, 2008, p. 410.

15. H. Ohno, *Electrochemical Aspects of Ionic Liquids*, John Wiley, 2005.

16. K. R. Seddon, A. Stark and M. J. Torres, *Pure and Applied Chemistry*, 2000, **72**, 2275-2287.

17. K. Matsumoto, R. Hagiwara and Y. Ito, *Journal of Fluorine Chemistry*, 2002, **115**, 133-135.

18. M. L. Patil, C. V. L. Rao, K. Yonezawa, S. Takizawa, K. Onitsuka and H. Sasai, *Organic Letters*, 2006, **8**, 227-230.

19.     I. Newington, J. M. Perez-Arlandis and T. Welton, *Organic Letters*, 2007, **9**, 5247-5250.

20.     R. A. Osteryoung, R. J. Gale, J. Robinson, H. Linga and G. Cheek, *Journal of the Electrochemical Society*, 1981, **128**, C79-C79.

21.     A. P. Abbott, G. Capper, D. L. Davies, H. L. Munro, R. K. Rasheed and V. Tambyrajah, *Chemical Communications*, 2001, 2010-2011.

22.     C. J. Bradaric, A. Downard, C. Kennedy, A. J. Robertson and Y. H. Zhou, in *Ionic Liquids as Green Solvents: Progress and Prospects*, eds. R. D. Rodgers and K. R. Seddon, 2003, vol. 856, pp. 41-56.

23.     C. J. Bradaric, A. Downard, C. Kennedy, A. J. Robertson and Y. H. Zhou, *Green Chemistry*, 2003, **5**, 143-152.

24.     L. Xiao and K. E. Johnson, *Canadian Journal of Chemistry-Revue Canadienne De Chimie*, 2004, **82**, 491-498.

25.     S. Zein El Abedin, E. M. Moustafa, R. Hempelmann, H. Natter and F. Endres, *Chemphyschem*, 2006, **7**, 1535-1543.

26.     A. P. Abbott and K. J. McKenzie, *Physical Chemistry Chemical Physics*, 2006, **8**, 4265-4279.

27.     T. Welton, *Chemical Reviews*, 1999, **99**, 2071-2083.

28.     P. Wasserscheid and W. Keim, *Angewandte Chemie-International Edition*, 2000, **39**, 3772-3789.

29.     A. P. Abbott, G. Capper, D. L. Davies, R. K. Rasheed, J. Archer and C. John, *Transactions of the Institute of Metal Finishing*, 2004, **82**, 14-17.

30.     S. I. Hsiu, J. F. Huang, I. W. Sun, C. H. Yuan and J. Shiea, *Electrochimica Acta*, 2002, **47**, 4367-4372.

31.     Y. F. Lin and I. W. Sun, *Electrochimica Acta*, 1999, **44**, 2771-2777.

32.     L. Heerman and W. D'Olieslager, *Inorganic Chemistry*, 1985, **24**, 4704-4707.

33.     A. P. Abbott, G. Capper, D. L. Davies and R. K. Rasheed, *Chemistry – A European Journal*, 2004, **10**, 3769-3774.

34.     A. P. Abbott, G. Capper, D. L. Davies, R. K. Rasheed and V. Tambyrajah, *Chemical Communications*, 2003, 70-71.

35.     A. P. Abbott, D. Boothby, G. Capper, D. L. Davies and R. K. Rasheed, *Journal of the American Chemical Society*, 2004, **126**, 9142-9147.

36.     A. P. Abbott, G. Capper, D. L. Davies and R. Rasheed, *Inorganic Chemistry*, 2004, **43**, 3447-3452.

37.    A. P. Abbott, G. Capper, D. L. Davies, H. Munro, R. K. Rasheed and V. Tambyrajah, *Ionic Liquids as Green Solvents: Progress and Prospects*, 2003, **856**, 439-452.

38.    A. P. Abbott, C. A. Eardley, N. R. S. Farley, G. A. Griffith and A. Pratt, *Journal of Applied Electrochemistry*, 2001, **31**, 1345-1350.

39.    A. P. Abbott, G. Capper, D. L. Davies, R. K. Rasheed and P. Shikotra, *Inorganic Chemistry*, 2005, **44**, 6497-6499.

40.    A. P. Abbott, G. Capper, B. G. Swain and D. A. Wheeler, *Transactions of the Institute of Metal Finishing*, 2005, **83**, 51-53.

41.    A. P. Abbott, G. Capper, D. L. Davies, K. J. McKenzie and S. U. Obi, *Journal of Chemical and Engineering Data*, 2006, **51**, 1280-1282.

42.    E. N. Golubeva, A. I. Kokorin, D. I. Kochubei, V. I. Pergushov and V. V. Kriventsov, *Kinetics and Catalysis*, 2002, **43**, 408-411.

43.    A. P. Abbott, J. C. Barron, G. Frisch, S. Gurman, K. S. Ryder and A. F. Silva, *Physical Chemistry Chemical Physics*, 2011, **13**, 10224-10231.

44.    V. I. Parvulescu and C. Hardacre, *Chemical Reviews*, 2007, **107**, 2615-2665.

45.    V. Lecocq, A. Graille, C. C. Santini, A. Baudouin, Y. Chauvin, J. M. Basset, L. Arzel, D. Bouchu and B. Fenet, *New Journal of Chemistry*, 2005, **29**, 700-706.

46.    M. S. Sitze, E. R. Schreiter, E. V. Patterson and R. G. Freeman, *Inorganic Chemistry*, 2001, **40**, 2298-2304.

47.    Q. G. Zhang, J. Z. Yang, X. M. Lu, J. S. Gui and Z. Huang, *Fluid Phase Equilibria*, 2004, **226**, 207-211.

48.    S. Hayashi and H. O. Hamaguchi, *Chemistry Letters*, 2004, **33**, 1590-1591.

49.    W. G. Xu, X. M. Lu, Q. G. Zhang, J. S. Gui and J. Z. Yang, *Chinese Journal of Chemistry*, 2006, **24**, 331-335.

50.    J. Z. Yang, P. Tian, L. L. He and W. G. Xu, *Fluid Phase Equilibria*, 2003, **204**, 295-302.

51.    M. W. Verbrugge and M. K. Carpenter, *Aiche Journal*, 1990, **36**, 1097-1106.

52.    M. K. Carpenter, *J. Electrochem. Soc.*, 1987, **87-7**, 591.

53.    E. R. Schreiter, J. E. Stevens, M. F. Ortwerth and R. G. Freeman, *Inorganic Chemistry*, 1999, **38**, 3935.

54.    M. Hasan, I. V. Kozhevnikov, M. R. H. Siddiqui, A. Steiner and N. Winterton, *Inorganic Chemistry*, 1999, **38**, 5637-5641.

55.    P. B. Hitchcock, T. J. Mohammed, K. R. Seddon, J. A. Zora, C. L. Hussey and E. H. Ward, *Inorganica Chimica Acta*, 1986, **113**, L25-L26.

56. G. Noguera, J. Mostany, G. Agrifoglio and R. Dorta, *Advanced Synthesis & Catalysis*, 2005, **347**, 231-234.

57. A. P. Abbott, J. C. Barron and K. S. Ryder, *Transactions of the Institute of Metal Finishing*, 2009, **87**, 201-207.

58. A. P. Abbott, G. Capper, K. J. McKenzie and K. S. Ryder, *Journal of Electroanalytical Chemistry*, 2007, **599**, 288-294.

59. A. P. Abbott, K. El Ttaib, G. Frisch, K. J. McKenzie and K. S. Ryder, *Physical Chemistry Chemical Physics*, 2009, **11**, 4269-4277.

60. A. P. Abbott, K. El Ttaib, K. S. Ryder and E. L. Smith, *Transactions of the Institute of Metal Finishing*, 2008, **86**, 234-240.

61. A.-M. Popescu, V. Constantin, A. Cojocaru and M. Olteanu, *Revista De Chimie*, 2011, **62**, 206-211.

62. K. J. McKenzie, *Physical chemistry chemical physics : PCCP*, 2006, **8**, 4265-4279.

63. A. P. Abbott, G. Frisch, H. Garrett and J. Hartley, *Chemical Communications*, 2011, **47**, 11876-11878.

64. Caporali, *Private communication by Prof. Andrew Abbott*

65. J. O'M. Bockris and A. K. N. Reddy, *Modern Electrochemistry, Vol.1*, Plenum Press, New York, 1970, Chapter 6.

66. A. P. Abbott, J. C. Barron, G. Frisch, K. S. Ryder and A. F. Silva, *Electrochimica Acta*, 2011, **56**, 5272-5279.

67. Q. Zhu, C. L. Hussey and G. R. Stafford, *Journal of the Electrochemical Society*, 2001, **148**, C88-C94.

68. Q. Liao, W. R. Pitner, G. Stewart, C. L. Hussey and G. R. Stafford, *Journal of the Electrochemical Society*, 1997, **144**, 936-943.

69. A. P. Abbott, F. Qiu, H. M. A. Abood, M. R. Ali and K. S. Ryder, *Physical Chemistry Chemical Physics*, 2010, **12**, 1862-1872.

70. G. H. Lane, A. S. Best, D. R. MacFarlane, M. Forsyth, P. M. Bayley and A. F. Hollenkamp, *Electrochimica Acta*, 2010, **55**, 8947-8952.

71. P. M. Bayley, G. H. Lane, N. M. Rocher, B. R. Clare, A. S. Best, D. R. MacFarlane and M. Forsyth, *Physical Chemistry Chemical Physics*, 2009, **11**, 7202-7208.

72. Y.-Z. Su, Y.-C. Fu, Y.-M. Wei, J.-W. Yan and B.-W. Mao, *Chemphyschem*, 2010, **11**, 2764-2778.

73. C. Nanjundiah, S. F. McDevitt and V. R. Koch, *Journal of the Electrochemical Society*, 1997, **144**, 3392-3397.

74. C. Nanjundiah, J. L. Goldman, S. F. McDevitt and V. R. Koch, *Proceedings of the Symposium on Electrochemical Capacitors Ii*, 1997, **96**, 301-312.

75. H. Liu, Y. Liu and J. Li, *Physical Chemistry Chemical Physics*, 2010, **12**, 1685-1697.

76. U. Schroder, J. D. Wadhawan, R. G. Compton, F. Marken, P. A. Z. Suarez, C. S. Consorti, R. F. de Souza and J. Dupont, *New Journal of Chemistry*, 2000, **24**, 1009-1015.

77. N. V. Ignat'ev, U. Welz-Biermann, A. Kucheryna, G. Bissky and H. Willner, *Journal of Fluorine Chemistry*, 2005, **126**, 1150-1159.

78. W. Xu, E. I. Cooper and C. A. Angell, *Journal of Physical Chemistry B*, 2003, **107**, 6170-6178.

79. E. I. Cooper and C. A. Angell, *Solid State Ionics*, 1983, **9-10**, 617-622.

80. D. R. MacFarlane, M. Forsyth, E. I. Izgorodina, A. P. Abbott, G. Annat and K. Fraser, *Physical Chemistry Chemical Physics*, 2009, **11**, 4962-4967.

81. C. Schreiner, S. Zugmann, R. Hartl and H. J. Gores, *Journal of Chemical and Engineering Data*, 2010, **55**, 4372-4377.

82. R. Fürth, *Mathematical Proceedings of the Cambridge Philosophical Society*, 1941, **37**, 281-290.

83. A. P. Abbott, *Chemphyschem*, 2004, **5**, 1242-1246.

84. A. P. Abbott, *Chemphyschem*, 2005, **6**, 2502-2505.

85. H. Zhao, Z. C. Liang and F. Li, *Journal of Molecular Liquids*, 2009, **149**, 55-59.

86. H. Tokuda, K. Hayamizu, K. Ishii, M. Abu Bin Hasan Susan and M. Watanabe, *Journal of Physical Chemistry B*, 2004, **108**, 16593-16600.

87. H. Tokuda, K. Hayamizu, K. Ishii, M. Susan and M. Watanabe, *Journal of Physical Chemistry B*, 2005, **109**, 6103-6110.

88. H. Tokuda, K. Ishii, M. Susan, S. Tsuzuki, K. Hayamizu and M. Watanabe, *Journal of Physical Chemistry B*, 2006, **110**, 2833-2839.

89. C. D'Agostino, R. C. Harris, A. P. Abbott, L. F. Gladden and M. D. Mantle, *Physical Chemistry Chemical Physics*, 2011, **13**, 21383-21391.

90. F. Endres, *Chemphyschem*, 2002, **3**, 144.

91. M. C. Buzzeo, R. G. Evans and R. G. Compton, *Chemphyschem*, 2004, **5**, 1106-1120.

92. P. K. Lai and M. Skyllaskazacos, *Journal of Electroanalytical Chemistry*, 1988, **248**, 431-440.

93. Y. Zhao and T. J. VanderNoot, *Electrochimica Acta*, 1997, **42**, 3-13.

94. M. R. Ali, A. Nishikata and T. Tsuru, *Indian Journal of Chemical Technology*, 1999, **6**, 317-324.

95. K. R. Seddon, A. Stark and M. J. Torres, in *Clean Solvents - Alternative Media for Chemical Reactions and Processing*, eds. M. A. Abraham and L. Moens, 2002, **vol. 819**, pp. 34-49.

96. S. Takahashi, *Hyomen Gijutsu* 1989, **40**, 134.

97. X. H. Xu and C. L. Hussey, *Journal of the Electrochemical Society*, 1992, **139**, 1295-1300.

98. C. L. Hussey, L. A. King and R. A. Carpio, *Journal of the Electrochemical Society*, 1979, **126**, 1029-1034.

99. H. C. Delong, J. S. Wilkes and R. T. Carlin, *Journal of the Electrochemical Society*, 1994, **141**, 1000-1005.

100. J. S.-Y. Liu and I. W. Sun, *Journal of the Electrochemical Society*, 1997, **144**, 140-145.

101. M. Lipsztajn and R. A. Osteryoung, *Inorganic Chemistry*, 1985, **24**, 3492-3494.

102. E. G. S. Jeng and I. W. Sun, *Journal of the Electrochemical Society*, 1997, **144**, 2369-2374.

103. M. A. M. Noel and R. A. Osteryoung, *Journal of Electroanalytical Chemistry*, 1990, **293**, 139-150.

104. M. Gambino and J. P. Bros, *Thermochimica Acta*, 1988, **127**, 223-236.

105. M. Gambino, P. Gaune, M. Nabavian, M. Gaune-Escard and J. P. Bros, *Thermochimica Acta*, 1987, **111**, 37-47.

106. A. P. Abbott, J. C. Barron, K. S. Ryder and D. Wilson, *Chemistry-a European Journal*, 2007, **13**, 6495-6501.

107. Shamsuri, *Singapore Journal of Scientific Research* 2011, 1-7.

108. F. Endres, *Zeitschrift Fur Physikalische Chemie-International Journal of Research in Physical Chemistry & Chemical Physics*, 2004, **218**, 255-283.

109. J. M. Yang, S. P. Gou and I. W. Sun, *Chemical Communications*, 2011, **46**, 2686-2688.

110. M. Steichen, M. Thomassey, S. Siebentritt and P. J. Dale, *Physical Chemistry Chemical Physics*, 2011, **13**, 4292-4302.

111. J. S. Wilkes, J. A. Levisky, R. A. Wilson and C. L. Hussey, *Inorganic Chemistry*, 1982, **21**, 1263-1264.

112. C. L. Hussey, *in Chemistry of Nonaqueous Solvents: Current Progress,* G. Mamantov and A. I. Popov, Editors, p. 227, VCH, New York (1994).

113. T. Tsuda and C. L. Hussey, *Magnetic Materials, Processes, and Devices Vii and Electrodeposition of Alloys, Proceedings*, 2003, **2002**, 637-648.

114. T. Tsuda, C. L. Hussey, G. R. Stafford and J. E. Bonevich, *Journal of the Electrochemical Society*, 2003, **150**, C234-C243.

115. T. Tsuda, C. L. Hussey and G. R. Stafford, *Journal of the Electrochemical Society*, 2004, **151**, C379-C384.

116. T. Tsuda, C. L. Hussey, G. R. Stafford and O. Kongstein, *Journal of the Electrochemical Society*, 2004, **151**, C447-C454.

117. M. Morimitsu, N. Tanaka and M. Matsunaga, *Chemistry Letters*, 2000, **9**,1028-1029.

118. J. A. Mitchell, W. R. Pitner, C. L. Hussey and G. R. Stafford, *Journal of the Electrochemical Society*, 1996, **143**, 3448-3455.

119. W. R. Pitner, C. L. Hussey and G. R. Stafford, *Journal of the Electrochemical Society*, 1996, **143**, 130-138.

120. T. Tsuda and C. L. Hussey, *Thin Solid Films*, 2008, **516**, 6220-6225.

121. T. Tsuda, S. Arimoto, S. Kuwabata and C. L. Hussey, *Journal of the Electrochemical Society*, 2008, **155**, D256-D262.

122. T. Tsuda, C. L. Hussey and G. R. Stafford, *Journal of the Electrochemical Society*, 2005, **152**, C620-C625.

123. A. Lisenkov, M. L. Zheludkevich and M. G. S. Ferreira, *Electrochemistry Communications*, 2010, **12**, 729-732.

124. S.-J. Pan, W.-T. Tsai and I. W. Sun, *Electrochemical and Solid-State Letters*, 2010, **13**, D69-D71.

125. S.-J. Pan, W.-T. Tsai, J.-K. Chang and I. W. Sun, *Electrochimica Acta*, 2010, **55**, 2158-2162.

126. R. T. Carlin, P. C. Trulove and H. C. De Long, *Journal of the Electrochemical Society*, 1996, **143**, 2747-2758.

127. Q. Zhu, C. L. Hussey and G. R. Stafford, *Journal of the Electrochemical Society*, 2001, **148**, C88-C94.

128. M. R. Ali, A. Nishikata and T. Tsuru, *Electrochimica Acta*, 1997, **42**, 2347-2354.

129. O. Mann, C. L. Aravinda and W. Freyland, *The Journal of Physical Chemistry B*, 2006, **110**, 21521-21527.

130. P. Y. Chen, M. C. Lin and I. W. Sun, *Journal of the Electrochemical Society*, 2000, **147**, 3350-3355.

131. A. Brenner, *electrodeposition of alloys*, Acadimic Press edn., New York, 1963.

132. P. Y. Chen and I. W. Sun, *Electrochimica Acta*, 2001, **46**, 1169-1177.

133. N. Koura, T. Endo and Y. Idemoto, *Journal of Non-Crystalline Solids*, 1996, **205-207**, 650-655.

134. J. F. Huang and I. W. Sun, *Electrochimica Acta*, 2004, **49**, 3251-3258.

135. J. F. Huang and I. W. Sun, *Chemistry of Materials*, 2004, **16**, 1829-1831.

136. J. F. Huang and I. W. Sun, *Journal of the Electrochemical Society*, 2004, **151**, C8-C14.

137. J. F. Huang and I. W. Sun, *Journal of the Electrochemical Society*, 2003, **150**, E299-E306.

138. S. P. Gou and I. W. Sun, *Electrochimica Acta*, 2008, **53**, 2538-2544.

139. J. F. Huang and I. W. Sun, *Journal of the Electrochemical Society*, 2002, **149**, E348-E355.

140. H. Y. Hsu and C. C. Yang, *Zeitschrift Fur Naturforschung Section B-a Journal of Chemical Sciences*, 2003, **58**, 1055-1062.

141. J. F. Huang and I. W. Sun, *Advanced Functional Materials*, 2005, **15**, 989-994.

142. D. Borissov, A. Pareek, F. U. Renner and M. Rohwerder, *Physical Chemistry Chemical Physics*, 2010, **12**, 2059-2062.

143. T. Iwagishi, K. Sawada, H. Yamamoto, K. Koyama and H. Shirai, *Electrochemistry*, 2003, **71**, 318-321.

144. H. Yamamoto, H. Kinoshita, H. Shirai, M. Morishita and K. Koyama, *Journal of The Surface Finishing Society of Japan*, 2006, **57**, 540.

145. A. M. Popescu, V. Constantin, A. Cojocaru and M. Olteanu, *Revista De Chimie*, 2011, **62**, 206-211.

146. C. Nanjundiah and R. A. Osteryoung, *Journal of the Electrochemical Society*, 1983, **130**, 1312-1318.

147. K. Murase, K. Nitta, T. Hirato and Y. Awakura, *Journal of Applied Electrochemistry*, 2001, **31**, 1089-1094.

148. S. Z. El Abedin, A. Y. Saad, H. K. Farag, N. Borisenko, Q. X. Liu and F. Endres, *Electrochimica Acta*, 2007, **52**, 2746-2754.

149. T.-I. Leong, I. W. Sun, M. J. Deng, C.-M. Wu and P.-Y. Chen, *Journal of the Electrochemical Society*, 2008, **155**, F55-F60.

150. B. G. Pollet, J. Y. Hihn and T. J. Mason, *Electrochimica Acta*, 2008, **53**, 4248-4256.

151. T. Tsuda, L. Boyd, S. Kuwabata and C. L. Hussey, *ECS Transactions*, 2009, **16**, 529-540.

152. T. Tsuda, L. E. Boyd, S. Kuwabata and C. L. Hussey, *Journal of the Electrochemical Society*, 2010, **157**, F96-F103.

**Chapter 2: Experimental**

**2.1 Preparation of deep eutectic solvent and electrochemical deposition.**

**2.2 Electrochemical methods**

2.2.1. Cell design

2.2.2. Cyclic voltammetry and chronoamperometry

2.2.3. Qurtz crystal microbalance

**2.3. Microchemical and microstructural analyses**

2.3.1. Atomic force microscope.

2.3.2. Scanning electron microscope

2.3.3. X-ray diffraction

2.3.4. Tensile test

**2.4. Viscosity**

**2.5. References**

## 2.1 Preparation of deep eutectic solvent and electrochemical deposition

Choline chloride ($HOC_2H_4N^+(CH_3)_3$ $Cl^-$) ChCl 99% and ethylene glycol (EG) > 99% and urea > 98% were sourced from Aldrich and used as obtained. The eutectic mixture was formed by mixing the 1:2 molar ratios of two components ChCl: hydrogen bond donor with heating and stirring at 80 $^oC$ until a homogeneous colourless liquid was formed. The metal halide salts $CuCl_2.2H_2O$ (Aldrich $\geq$ 99%), $SnCl_2.2H_2O$ (Aldrich $\geq$ 98%), $NiCl_2.6H_2O$ (Aldrich $\geq$ 98%) were used as received. The $AgNO_3$ (Aldrich $\geq$ 99%) and sodium hypophosphite ($NaH_2PO_2$) (Aldrich $\geq$ 98%) were used as obtained. The organic additives a) boron trimethyl amine complex, b) sodium 2-ethylhexyl sulfate and c) *1,10-phenanthroline 99%* were all from Aldrich and used as received. Generally, the organic additives were added to the Cu-Sn alloy electroplating bath to a concentration of 1 wt%.

## 2.2 Electrochemical methods

### 2.2.1 Cell design

All the electrochemical experiments were made using a conventional three-electrode cell, connected to an Ecochemiem Autolab type III potentiostat. The counter electrode was 0.5 mm diameter platinum disc, the reference electrode was a silver wire. The working electrode consisted of a Pt flag.

### 2.2.2 Cyclic voltammetry and chronoamperometry

All voltammetry and chronoamperometry investigations were carried out using an Autolab PGSTAT 20 potentiostat (Ecochemie, Holland) controlled with GPES software. Experiments were carried out in the ionic liquid as seen in **Figure 2.1**. The two systems each consisted of three electrodes: platinum microelectrode (0.19625 $mm^2$ area) (made in-house), a platinum flag counter electrode and a silver wire reference electrode. The working electrodes were polished with 0.3μm alumina paste, rinsed with water and dried prior to all measurements. All cyclic voltammograms were performed at room temperature.
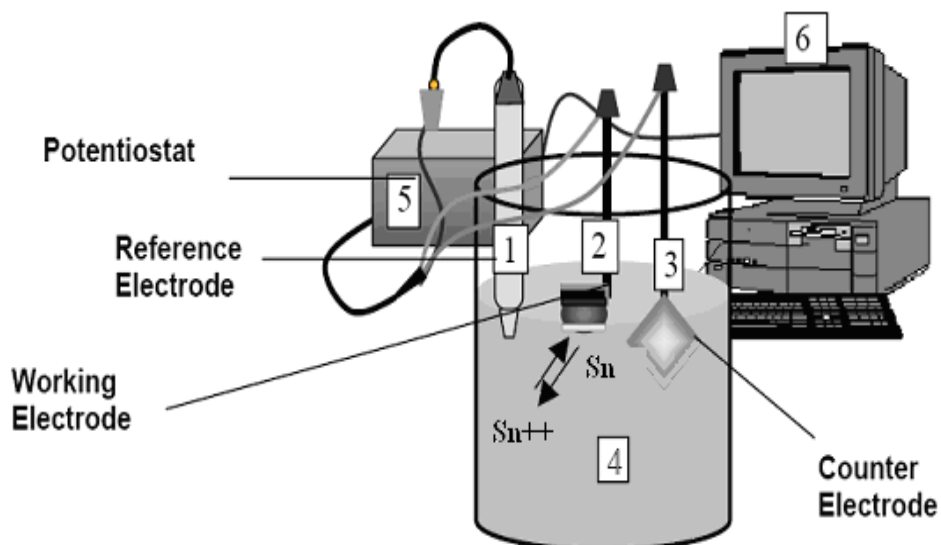
**Figure 2.1** *Electrochemistry Setup. The electrochemical cell contained the following: 1) a silver wire as a reference electrode; 2) a working electrode; 3) a platinum counter disc electrode; 4) an electrolyte based in ionic liquid 5) an Autolab PGSTAT 20 Potentiostat and 6) a computer to record the data.*

### 2.2.3 Quartz crystal microbalance

A quartz crystal microbalance (QCM) has been used to measure the deposition and dissolution of of metals and alloys in the electrolyte solution, mass growth and viscosity of liquids. In addition, the sensitivity of the QCM to all these variables, while the resonant oscillation frequency in a solution depends on the properties of three main factors: thickness and type of quartz, rigidly attached film and the viscosity of the liquid itself.

An electrochemical quartz crystal microbalance model (Agilent/ HP E5061A) network analyser with a 10 MHz AT-cut gold quartz crystal (International Crystal Manufacturing Co., Oklahoma City, USA) was used.

A three-electrode compartment cell (Teflon cell) with an unpolished gold coated crystal as a working electrode, silver wire as a reference electrode and Pt sheet as a counter electrode were used. QCM was connected with Autolab potentiostat (Potentiostat/ gelvanostat – Model 263A) used for I/ E data recording. The quartz crystal has 0.23 cm$^{-2}$ piezoelectric active areas. From the experiment, the additional thickness of plated metal on the quartz crystal over time

causes an increase of wavelengths which reduces the standing wave frequency. When the crystal is immersed in the solution, the frequency shifted to lower value as observed **Equation 2.1.**

$$\Delta f = \Delta f_m + \Delta f_P + \Delta f_\eta + \Delta f_r \qquad (2.1)$$

Where $\Delta f_m$ is the effect of additional mass or film formation, $\Delta f_P$ is the pressure of the fluid, $\Delta f_\eta$ is the viscous effect and $\Delta f_r$ is the roughness of the surface of the crystal. Sauerbrey[1] expressed the mass effect by **Equation 2.2**

$$\Delta f = - \left( 2f_o^2 / \rho \upsilon \right) \frac{\Delta m}{A} \qquad (2.2)$$

Where $\rho$ is the density of quartz and $\upsilon$ the wave velocity, $f_o$ is the resonance frequency prior to the mass change and $\Delta m$ is the mass change and A is the surface area of the resonator. If the deposition mass is non–rigid then the Sauerbrey equation cannot be used to get an accurately calculated mass change.

Data acquisition and review software were used throughout. Analysis, modeling and fitting of a large array of data sets was performed using Visual Basic for Applications (VBA) inside Microsoft Excel. Also the literature has deeply described the fitting admittance, which is caused by changes in the electrical measurements by a Lorentzian equivalent circuit model **Equation 2.3**.

$$U(f) = a + \left[ \frac{R}{R^2 + 16\pi^2 \, L^2 (f - f_o)} \right] \qquad (2.3)$$

Where $U(f)/\Omega^{-1}$ is the admittance measured peak as a function of applied frequency, $f$, is the real component of acoustic impedanc , $Z$, $L$ is the inductance, $f_o$ is the centre frequency and $a$ is the baseline offset. The latter was used during fitting to compensate for variations in the static calibration of the network analyser.[2] In addition, the running HP VEE program was recording the admittance spectra every 3-4 s. Only one side of the crystal was to be exposed to the solution and was fixed on the cell. All measurements were obtained at room temperature ($20 \pm 2$ °C).

## 2.3 Microchemical and microstructural analyses

### 2.3.1 Atomic force microscope

Atomic force microscope (AFM) images were acquired using a Digital Instruments (DI) Nanoscope IV, Dimension 3100 instrument with software version 6.12 in either resonant (tapping) or contact mode. AFM images are obtained by measurement of the force on a sharp tip (any substrate) formed by the proximity of the surface of the sample. In addition, the tip will follow the surface contours.

### 2.3.2 Scanning electron microscopy

The surfaces of alloys deposited were analyzed qualitatively for the presence of copper alloys using scanning electron microscopy/ energy dispersive spectroscopy or ESEM/ EDAX. ESEM and EDAX elemental analysis was carried out under vacuum using a Philips XL30 ESEM instrument with a voltage between $15 - 20$ KeV giving an average beam current of ca. 120 μA.

### 2.3.3 X-ray diffraction

X-ray diffraction patterns of alloy phases were measured using a Phillips model PW 1730 X-ray generator, with a PW 1716 diffractometer and PW 1050/25 detector. The copper tube used as the anode filtered Cu-K$_\alpha$ radiation at a wavelength is 0.1540 nm. The running conditions for the X-Ray tube were 40 kV and 40 mA, scanned between 20 and 85° (2θ) with

a step size of 0.02° (2θ). Angle calibration was carried out using a synthetic Si sintered standard.

## 2.4.4 Tensile testing of thin film of Cu and Cu-P alloy

The tensile testing of the dog-bone shaped Cu and Cu-P alloy sheet was carried out using an Instron 3343 tensile apparatus (Instron Ltd, Assembled, USA) with a load cell of 500N. The material strain and stress was controlled by Instron bluehill`2 software. A Ceast model 8047-020 cutter was used to cut the sheet of Cu and Cu-P alloy as a dog-bone.

## 2.4 Viscosity of three systems of Cu-Ag alloys

The viscosity of the ionic liquids was measured at 35 $^{o}$C. A Brookfield viscometer model LVDV-II+P (Brookfield Instruments, USA), with a small scale sample adapter with different spindle was used to measure the viscosity of these samples. A thermo-regulated bath type Refrigerated Bath RB-5 was fitted to maintain the temperature of the sample by a water jacket. It was maintained with an accuracy of temperature ±1 $^{o}$C. The average of three reading of viscosity was used for the analysis.

## 2.5 References

1.      G. Sauerbrey, *Z. Physik* 1959, **155**, 206.
2.      A. P. Abbott, S. Nandhra, S. Postlethwaite, E. L. Smith and K. S. Ryder, *Physical Chemistry Chemical Physics*, 2007, **9**, 3735-3743.

# Chapter 3: The Electrodeposition of Copper-Silver Alloys using Deep Eutectic Solvents

## 3.1 Introduction

The electrodeposition of copper is a strategically vital process and covers a range of applications from electronics, through coating process, to electroforming. The technology for electroplating is relatively mature but there is still a need to be able to develop new media for niche applications, such as water sensitive substrates and alloy deposition.

### 3.1.1 Electrodeposition of copper using aqueous solutions

The use of electrodeposited coatings has allowed new material properties to be developed that expand the physical properties beyond those of the substrate. Many electrochemical processes, such as the electrodeposition of copper in aqueous solvents are limited by reactions that limit the potential window, i.e. those involving the redox processes of the solvent.[1-4] Ionic liquids are considered suitable for electrodeposition as they exhibit potential windows up to 2.5 times wider than that of aqueous acid electrolytes.

Copper deposition has been carried out for decades from sulphate-sulphuric media for various applications.[5] Typical baths are prepared from sulphuric acid solutions and have a high copper ion content. Organic additives are commonly used to change the coating properties, such as surface active agents, brighteners, and levellers, which allow improvement of the electrical and mechanical properties of the metal deposited. The differences in the kinetics of the $Cu/Cu^+$ (fast) and $Cu^+/Cu^{2+}$ (slow) processes can control the overall deposition process.[5]

The co-deposition of Pd-Cu alloys of different composition was investigated using alkaline electrolytes. A rotating disk electrode was used to study the catalytic activity of these alloys and to also investigate the mechanism of the oxygen reduction reaction by a combination of electrochemical results and theoretical calculations.[6] The Pb-Cu alloys have been deposited onto steel sheet from baths containing mixtures of lead nitrate, copper nitrate and sodium gluconate.[7] Auger spectrum lines show a good agreement with the X-ray diffraction results for the structure composition of the Pb-Cu alloy deposition. The electrodeposition of brass (Cu-Zn alloys) onto steel substrates has been investigated from a variety of citrate-based Cu-Zn bath compositions. The fine-grained alloy deposition has been examined by scanning electron microscopy and X-ray diffraction.[8] The electrodeposition of Cu-Ni[9] and Cu-Co[10] alloys was carried out in aqueous solution, typically with citrate and boric acid as electrolytes in the solutions. The composition of these alloys deposited was studied, as influenced by bath composition, current density and temperature. It is clear that the compositions of these alloys

are dependent upon the applied current density. SEM and XRD have been used to follow the deposition of these alloys by examining the surface morphologies and structures. In addition, the acidic additive shows an effective increase of cobalt and nickel percentage in the deposited alloys. This process has been studied for Cu-Co by a number of authors and the processes were reviewed by Brenner [11] Fink and Hotton. [12] Electroplating Cu-Co alloys from ammonium sulphate containing a supporting electrolyte to improve the quality of deposition morphology has been investigated as a function of $Cu^{2+}$ and $Co^{2+}$ ions concentrations by Ignatova. [13]

### 3.1.2 Electrodeposition of copper using ionic liquids

Copper is easily deposited as an alloy with other metals, such as zinc. In the 1960s and 1970s copper deposition was studied in chloroaluminate ionic liquids.[14,15,16,17] In the 1990s copper was found to be easily deposited using ionic liquids containing anions such as $[BF_4]^-$, $[(F_3CSO_2)_2N]^-$ and $[Tf_2N]^-$. The air and moisture stability of these systems made them easier to apply.[18,19] Endres and co-workers studied copper deposition from (buthylmethyl pyrrolidinium) [BMP] $[Tf_2N]^-$ at different temperatures. However, this particular ionic liquid has limited solubility for copper compounds and copper cations had to be introduced into the liquid *via* anodic dissolution of a copper electrode.[20]

It has recently been shown that simple eutectic-based ionic liquids can be produced using the quaternary ammonium salts, $R_1R_2R_3R_4N^+X^-$, complexed with hydrogen bond donors, such as acids, amides and alcohols.[21, 22] These so called deep eutectic solvents (DES) have been used for electropolishing,[23,24,25] polymer synthesis,[26] organic synthesis and metal oxide processing.[27,28] The previous studies have concentrated on choline chloride as the quaternary ammonium salt, as it is environmentally friendly and is already used as a common constituent of various household and industrial products, such as detergents. The DESs formed with choline chloride and urea, or choline chloride and ethylene glycol, have successfully been employed for the electrodeposition of zinc, tin, and zinc–tin alloys.[29] This has also shown that the alloy is affected by the choice of hydrogen bond donor and that the electrochemistry of the components in solution, as well as the morphology of the coatings is also affected. A selection of reviews have discussed the detail of metal deposition by using ionic liquids.[30,20,31,32]

Pollet *et al* investigated the electrodeposition of copper from copper (II) chloride in aqueous potassium chloride and in mixtures of glycerol and choline chloride (2:1 ) (ionic liquid) (DES)

on Pt electrodes, in the potential range for copper deposition and dissolution. In addition, the current density was increased using ultrasound within the two different solvents, when compared with the silent solution. [33]

The electrolytic deposition of copper and copper composites from a solution of the metal chloride salt has been studied in choline chloride based deep eutectic solvents.[34] It was shown that the deposition kinetics and thermodynamics differ from the aqueous processes and that different complexes are formed. EXAFS (Extended X-ray Absorption Fine Structure) showed that the main species formed from the dissolution of $CuCl_2$ in Deep Eutectic Solvent is $[CuCl_4]^{2-}$. Bulk electrodeposition in DES results in different deposit morphologies to that encountered in aqueous solutions. The mechanism of copper nucleation was studied using chrono-amperometry and it was shown that progressive nucleation leads to a bright nano-structured deposit. The current efficiency of copper deposition in this system is near 100 %.

Abbott *et al.*[34] used a electrochemical quartz crystal microbalance, EQCM, to study the electrodeposition of copper composites. It was possible to calculate the amount of inert particulates (SiC, $Al_2O_3$ and PTFE) in the copper coatings and it has been shown that material was dragged onto the surface of the copper coating. The amount of micron-size particles of $Al_2O_3$ and SiC incorporated in the copper deposit is related to the amount of species in the solution. [35]

In this chapter the electrodeposition of copper alloys is demonstrated using copper-silver as a test system. Both metals have been studied individually in Deep Eutectic Solvents, but never together.


**3.2 The electrodeposition of Cu-Ag alloys**


Copper and its alloys are important metals for industrial applications because of their excellent conductivity, good solderability and high catalytic activities for various chemical reactions. The copper - silver system is a binary eutectic alloy. The simple phase diagram is shown in **Figure 3.1**. For two component systems, and three single-phase regions, $\alpha$, $\beta$ and liquid are often observed, $\alpha$ and $\beta$ are the two solid solutions phases rich in copper and silver, respectively. The solubility in each of these solid phases is limited at any temperature below *(BEG)* 779 $^oC$. The amount of Ag increases with temperature to a maximum of 8.0 Wt % Ag at 779 $^oC$ at point *B,* then decreases to zero at *A* (1085 $^oC$).[36, 37] The solvus line separates one solid solution from a mixture of solid solutions, as shown in **Figure 3.1**. At point *G,* 8.8 Wt

% Cu is the maximum solubility of copper in the $\beta$ phase. There are also three two- phase regions found for the Cu – Ag system: $\alpha + L, \beta + L$ and $\alpha + \beta$.

When silver is added to copper, the temperature at which the alloys become completely liquid decreases along the liquidus. It is the main theory behind the phase diagram, it shows the change of phase by decreasing the melting point of Cu when the added % of Ag is increased. This also holds true for the addition of Cu to Ag, where the temperature for complete melting, along the liquidus, is also reduced as the Cu% increases. Both liquidus lines meet at the eutectic point $E$, which is shown by Cu-Ag composition and temperature. [36, 37]
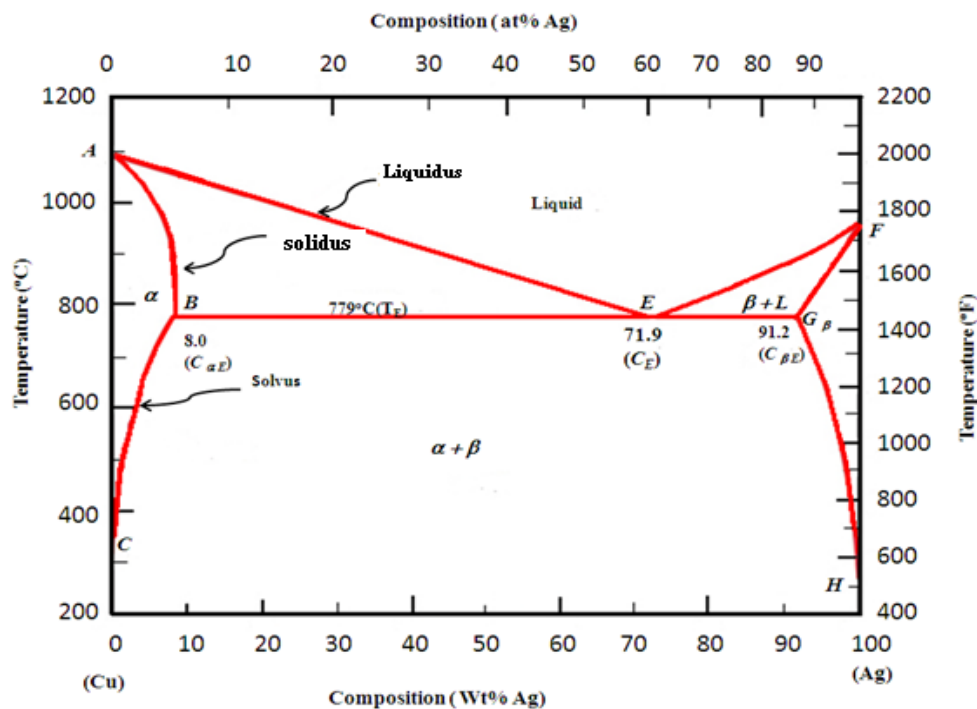


*Figure 3.1* *The binary Cu-Ag equilibrium alloy phase diagram. Image taken from ref* [37]

The Cu–Ag alloys are efficient conducting materials that have high strength and high conductivity and are easy to melt and cast. These materials have been shown to achieve strengths greater than 1000 MPa, combined with electrical conductivities greater than 75% ICSA (International Annealed Copper Standard). [38] Highly conductive materials with high strength are required for the development of high efficiency electrical conductors for future electrically-powered platforms. To achieve the desired Cu–Ag alloy material properties for a particular application, these alloys can be achieved by two different methods. Firstly, to reach these properties a thermomechanical treatment process can be used. Secondly, most of the more commonly used elements in copper alloys reduce conductivity; silver has little effect on

the overall conductivity. However, copper and silver are only slightly soluble in each other and do not form any intermediate phases. According to the phase diagram of the binary Cu-Ag system, the reciprocal solubility of copper and silver is a function of temperature, but remains quite small at ambient temperature.[39] As a result, all the alloys formed are two-phases, containing a mixture of solid solutions of copper in silver ($\alpha$-phase) and silver in copper ($\beta$-phase). Assaf *et al* [39] studied the electrochemical behaviour of the Cu-Ag alloys of different composition in NaOH solutions, under different experimental conditions, using cyclic voltammetry and XRD, and they found that the maximum currents for the anodic and cathodic peaks of the cyclic polarisation curves depend on the composition of the alloy.

The current study has been designed to investigate the influence of liquid formulation (*e.g.* ratio of metal ions in solution and type of hydrogen bond donor (HBD)) and to develop the techniques and methods to measure (as a function of time) the composition of the alloy formed. For these studies, the Cu-Ag alloy system has been chosen due to its simplicity and the large difference in mass and between the two metals makes it ideal for study using a EQCM. This simple system was selected for both tactical and strategic reasons; in the short term it provides a good mix of metal ion systems that are well behaved in type III, choline-based, ionic liquids. One of the key objectives here was to develop a technique for probing phase behaviour and, specifically, alloy composition *in situ* and in real time during electrolytic deposition in ionic liquids. The studies described here were carried out in Ethaline and Reline.


### 3.3 Cyclic voltammetry

Cyclic voltammetry (CV) was used to define the redox properties of the Cu-Ag alloy deposition processes. **Figure 3.2** shows the CV curves of the pure Cu and Ag deposition onto a Pt disc electrode from Ethaline and Reline. When the scan was performed from 1.0 V to -1.0 V, Cu deposition peaks were found at +0.5 V for $Cu^{2+}/Cu^{+}$ and -0.375 V for $Cu^{+}/Cu$ and an Ag reduction peak was found at - 0.1 V. When the potential was scanned in the reverse direction (from -1.0 V to a positive direction), Cu stripping peaks were observed at -0.3 V for $Cu/Cu^{+}$ and +0.4 V for $Cu^{+}/Cu^{2+}$, whereas the Ag oxidation peak appears at -0.1V in both ionic liquids, with little difference in the peaks position.
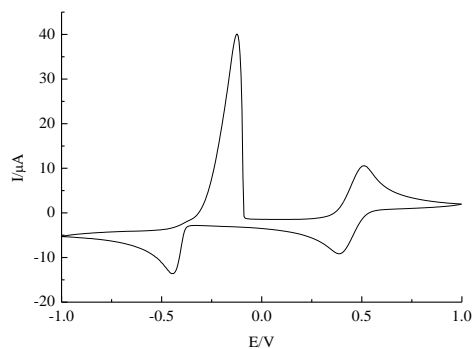
*a) 0.1 mol dm$^{-3}$ CuCl$_2$·2H$_2$O in Ethaline*
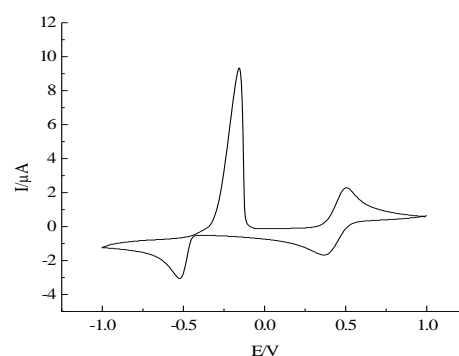


*b) 0.1 mol dm$^{-3}$ CuCl$_2$·2H$_2$O in Reline*
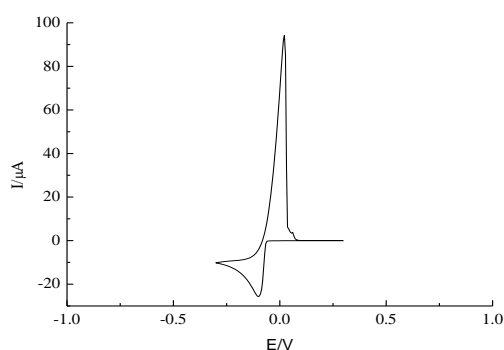


*c) 0.1 mol dm$^{-3}$ AgNO$_3$ in Ethaline*
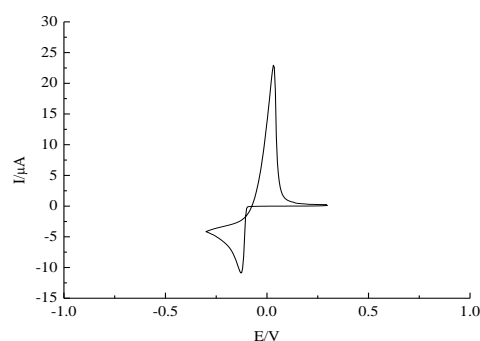


*d) 0.1 mol dm$^{-3}$ AgNO$_3$ in Reline*

**Figure 3.2** *CV for 0.1 mol dm$^{-3}$ CuCl$_2$·2H$_2$O 0.1 mol dm$^{-3}$ AgNO$_3$ in Ethaline and Reline at a Pt disk working electrode (dia. 0.5mm) vs. Ag. (5 mVs$^{-1}$scan rate)*

It can also be clearly seen that in Ethaline, the reduction charge for Ag$^+$, Cu$^+$ and Cu$^{2+}$ are different, despite being the same concentration, which means that Ag$^+$ reduction is kinetically faster than Cu$^+$. In Reline, the reduction potentials are similar to those in Ethaline.

The electrodeposition of copper–silver alloys was studied in the same two ionic liquids. The deposition was studied in three relative concentration regimes; equimolar Cu and Ag (0.10 mol dm$^{-3}$ of both CuCl$_2$·2H$_2$O and AgNO$_3$), 3: 1 Ag: Cu (0.15 mol dm$^{-3}$ of CuCl$_2$·2H$_2$O and 0.05 mol dm$^{-3}$ AgNO$_3$) and 1: 3 Ag: Cu (0.05 mol dm$^{-3}$ of CuCl$_2$·2H$_2$O and 0.15 mol dm$^{-3}$ AgNO$_3$). The CV of the system containing 0.10 mol dm$^{-3}$ CuCl$_2$·2H$_2$O: 0.10 mol dm$^{-3}$ AgNO$_3$ was recorded at a scan rate of 5 mV s$^{-1}$ and the results are shown in **Figure 3.3**. This approach was used to ensure that the metal concentration was constant through all experiments.

It has previously been shown that in some ionic liquids, the metal salt can significantly affect the viscosity of the fluid. **Table 3.1** shows the viscosity of Ethaline as a function of $CuCl_2 \cdot 2H_2O$: $AgNO_3$ ratio. Barron [40, 41] recently carried out similar experiments using $ZnCl_2$ as the metal salt. It was found that the metal salt had little effect upon the viscosity of the Ethaline solution, but had a more significant effect upon the viscosity of Reline. This was thought to occur because the metal salt broke up the hydrogen bond donor structure of the solution.

| | Viscosity /cP at 25 $^o$C | | | | |
|---|---|---|---|---|---|
| | No metal salt | 1:1 Cu: Ag | 3: 1 Cu: Ag | 1: 3 Cu: Ag | 0.05 mol dm$^{-3}$ $ZnCl_2$ (ref. [39]) |
| Ethaline | 23 | 11 | 14 | 22.7 | 22.5 |
| Reline | 800 | 520.3 | 464.3 | 504.8 | 500 |

*Table 3.1 The viscosity of Ethaline and Reline with various metal salts dissolved*

The data in **Table 3.1** show a similar trend for copper and silver as for zinc, although the copper salt appears to decrease the viscosity more than the silver salt. This is probably due to the waters of crystallisation being removed from the metal centre during solvation. Frisch[34] has recently shown using EXAFS spectroscopy that, irrespective of the salt being $CuCl_2$ or $CuCl_2.2H_2O$, the speciation around the Cu is the same i.e. the waters of crystallisation are removed.

**Figure 3.3a** shows the cyclic voltammetry of an equimolar mixture of $CuCl_2 \cdot 2H_2O$ and $AgNO_3$ in the EG-based liquid. Three distinct redox processes are clearly visible. The most cathodic of these at $-0.42$ V, shows the deposition and stripping response of a Cu rich phase. Similarly, the second process at $+0.05$ V, corresponds to the deposition and stripping response of an Ag rich phase. Finally at $+0.32$ V, a reversible 1 electron process corresponds to the reversible $Cu^{2+/+}$ couple.

Similar results are observed in the urea based liquid, although the silver and copper stripping peaks overlap to a larger extent. The redox potentials are largely similar to those of the individual metals in Ethaline and Reline.

The CV was obtained using a Pt disc electrode in the DES containing 3:1 $AgNO_3$: $CuCl_2 \cdot 2H_2O$ in Ethaline, which is shown in **Figure 3.3e** and, as expected, the current response for the silver rich phase increases with respect to that for copper. Abbott *et al.*[42]
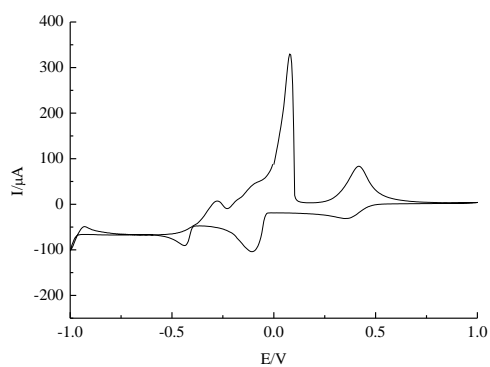
a) 1:1 Cu-Ag Ethaline
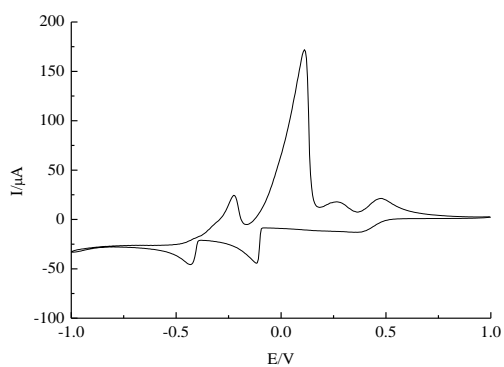
b) 1: 1 Cu: Ag Reline
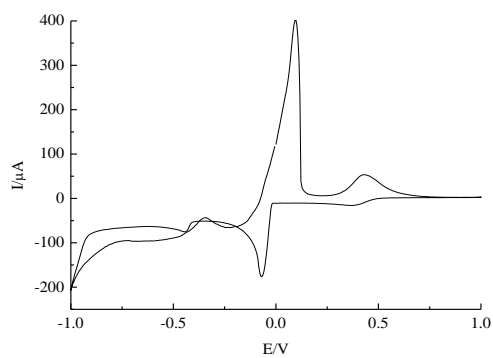
c) 1: 3 Cu: Ag Ethaline
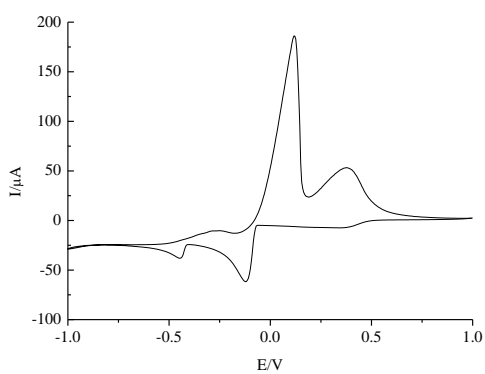
d) 1: 3 Cu: Ag Reline
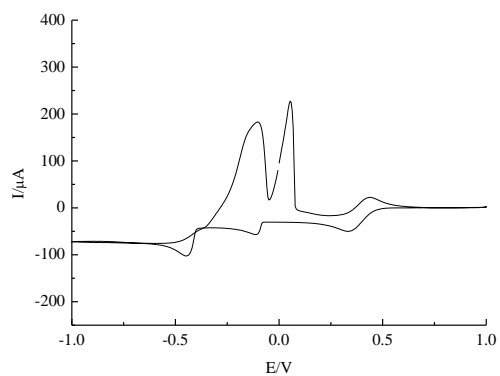
e) 3: 1 Cu: Ag Ethaline
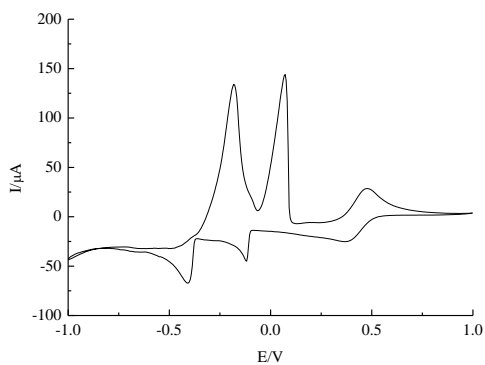
f) 3: 1 Cu: Ag Reline

**Figure 3.3** *Cyclic voltammograms of 1:1, 1:3 and 3:1 CuCl$_2$·2H$_2$O: AgNO$_3$ in both; Ethaline (a, c, and e) and Reline (b, d and f) at a Pt disk working electrode (dia. 0.5mm) using a silver wire pseudo reference electrode.*

have recently studied the effect of concentration upon the redox potential of the $Ag/Ag^+$ couple and the $Cu^{2+}/Cu^+$ couples. It was found that up to a concentration of 1 mol kg$^{-1}$, the redox potentials changed in a Nernstian manner i.e. they obeyed the Nernst equation;

$$E = E^0 + \frac{RT}{nF} \ln\left(\frac{a_{ox}}{a_{red}}\right) = E^0 + \frac{RT}{nF} \ln\left(\frac{m_{ox}}{m_{red}}\right) + \frac{RT}{nF} \ln\left(\frac{\gamma^2(ox)_\pm}{\gamma^2(red)_\pm}\right) \qquad (3.1)$$

where $E^0$ is the standard cell potential, $R$ is the gas constant, $T$ is absolute temperature, $F$ is the Faraday constant, $n$ is the number of electrons, $\gamma_\pm^2 = \gamma_+\gamma_-$ is the mean activity coefficient and $a$ and $m$ are the activity and molality of the solute, respectively. It was shown that the high ionic strength shielded the metal ions from each other and the third term in **Equation 3.1** could be ignored, as the activity coefficients of the reduced and oxidised species were both unity. It follows from this that the $Cu^{2+}/Cu^+$ and $Ag/Ag^+$ signals should overlap at high silver concentrations and the $Cu^+/Cu$ and $Ag/Ag^+$ signals should overlap at high copper concentrations, which is what is observed in **Figures 3.3c, d, e and f** for both systems.

From the CV scans of CuCl$_2$·2H$_2$O and AgNO$_3$, it has been found that copper and silver have reduction peaks at different positions, as mentioned above in **Figure 3.2a, b, c and d** for both ionic liquids. When both metals are together in the same solution, a broadening and negative shift of the peaks are observed. However, the charge for the copper rich phase increases with copper content in the alloy and the area under the current peak of silver species increases with increasing silver content. Changing the $Ag^+$ concentration from 0.05 to 0.15 mol dm$^{-3}$ will cause the potential to shift by only 28 mV. It is notable that the copper rich solution leads to two peaks. This could be due to the different phases, pure copper and a copper/ silver solid solution, or because the materials are deposited with different morphologies.

Abbott *et al* [40] showed that two stripping peaks are often obtained for the deposition of pure metals from eutectic based ionic liquids and these peaks were found to arise from different deposit morphologies. It was shown that for both Zn and Al, the less cathodic peaks results from nano crystalline material and the more cathodic peaks come from micro crystalline metal. The observation that **Figure 3.2** only has one peak suggests that it is due to two different compositions rather than two different morphologies.

The cyclic voltammograms recorded at the Pt electrode in Reline containing $Cu^{2+}$, $Ag^+$ with a concentration ratio of 1:1, 1: 3 and 3: 1 are shown in **Figures 3.3b, d and f**. By carefully examining these voltammograms, it can be found that the reduction peak of $Cu^+$ in the mixture is more positive than that observed in the solution containing $Cu^+$ alone, the same

response as seen in Ethaline. $Ag^+$ in the mixture was reduced to Ag at more positive potentials, as indicated by the positive shift in the reduction peak of $Ag^+$. This behaviour implies that $Cu^{2+}$ and $Ag^+$ may have specific interactions, forming some Cu and Ag containing compounds, resulting in a smaller separation of the reduction potentials. Chen *et al*. [43, 44] observed similar behaviour when mixed $Zn^{2+}/ Mn^{2+}$ and $Cu^{2+}/ Mn^{2+}$ systems were studied for alloy deposition. Clearly in both Ethaline and Reline, with two metals mixed the redox peaks move to more positive potentials compared to pure metal solutions. The Ag rich phase in Ethaline is moved more than in Reline, as shown in **Figure 3.3 c and d**.

## 3.4 Chronoamperometry

The nucleation and growth mechanism observed in the present study was investigated by chronoamperometric transients, recorded at a Pt electrode for varying copper–silver compositions. Initially, chronoamperometry was carried out for the nucleation and growth processes of the electrodeposition of pure systems (Cu and Ag) from Ethaline at the Pt electrode, by stepping the potential of the working electrode from a value where no reduction of $Cu^{2+}$ or $Ag^+$ would occur to potentials sufficiently negative to initiate a nucleation and growth mechanism. After a short induction time, $t_0$, the current increases due to the formation and growth of the nuclei and reaches a current maximum, $I_{Max}$, at time, $t_{Max}$, when the discrete diffusion zone of each of the growing crystallites begin to overlap. A collection of the current–time transients for the electrodeposition of pure Cu occurs at a Pt electrode between 320 and 330 mV *vs* Ag. These transients were normalized to $I/ I_{Max}$ and $t/ t_{Max}$ and then compared to the well known theoretical $[I/ I_{Max}]^2$ versus $t/ t_{Max}$ curves derived for instantaneous and progressive three-dimensional (3D) nucleation and growth models. The resulting plots shown in **Figure 3.4a** reveal that the electrodeposition of copper on the Pt electrode in Ethaline fits well to the model for 3D-instantaneous nucleation mechanism.[34] This is the same as found by Barin where an increase in the concentration of $Cu^{2+}$ in the solution causes the initial nucleation to change completely from progressive to instantaneous.[45]

The experimental current transients at different step potentials for the deposition process of silver onto a Pt electrode obtained in Ethaline solution are shown in **Figure 3.4** (with the raw data in the appendix **Figure 7.2).** As it can be seen, all current transients are of the same form with characteristic and well-defined current maxima. **Figure 3.4b** shows the representative

non-dimensional plots of silver deposition in Ethaline, along with the theoretical curves for the limiting cases of instantaneous and progressive 3D nucleation mechanism with diffusion controlled growth. The analysis of the experimental data under different over-potentials shows good agreement with the theoretical lines for instantaneous nucleation with diffusion controlled growth, up to $t_{Max}$. A mechanism of silver nucleation in the presence of 1-$n$-butyl-3-methylimidazolium hexafluorophosphate ([BMIM][PF$_6$]) and 1-$n$butyl-3-methylimidazolium tetrafluoroborate ([BMIM][BF$_4$]) RTILs and in KNO$_3$ aqueous solution was investigated at a glassy carbon electrode surface.[46] It has been found that silver nucleation closely follows a progressive nucleation in [BMIM][PF$_6$] and an instantaneous nucleation in KNO$_3$ aqueous solution. However, the deposition of silver in [BMIM][BF$_4$] deviated from both the instantaneous and progressive nucleation models. Azam [47] also shows instantaneous nucleation when depositing silver from Ethaline for a variety of silver salts and a variety of reaction conditions.

The nucleation mechanism of [CuCl$_2$·2H$_2$O] solutions in EG based ionic liquids was noted to be highly sensitive to experimental conditions, such as the concentration of reactant, applied potential, and temperature.[34] In this study, the chronoamperometric transients of copper–silver alloys were studied and these are shown in **Figures 3.4** (with raw data in the appendix **Figure 7.1**). Oliveira *et al*[48] studied the influence of EDTA (ethylenediaminetetraacetic acid, disodium salt) or HEDTA (*N*-(2-hydroxyethyl) ethylenediaminetriacetic acid, tri-sodium salt) on silver–copper electrodeposition from ammonium hydroxide solution and showed that at high current density in the Ag rich solution low values of $t_{Max}$ are observed and high silver compositions are obtained in the deposit. The transients are considered by an initial decrease of negative current due to charging of the double layer and the formation of the first nuclei on the Pt working electrode. This is followed by an increase in the negative current to a maximum value, $J_{Max}$, at a particular time, $t_{Max}$, which is attributed to the 3D growth of a metal over the nuclei, resulting in an increase of surface area.[49] The negative current decays when reaching the $t_{Max}$ and the position of $J_{Max}$ depends upon the magnitude of the applied potential. A lower value of $t_{Max}$ gives a higher negative potential. The model was taken to analyse the chronoamperometric data using dimensionless current and time plots for 3D instantaneous nucleation, **Equation (3.2)**, and progressive, **Equation (3.3)**, nucleation mechanisms where $J_{Max}$ and $t_{Max}$ represent the current per area and time coordinate values of the nucleation peak, respectively.[50]
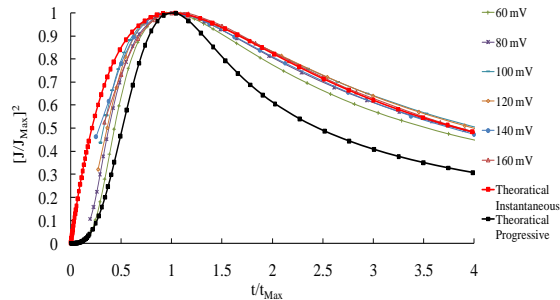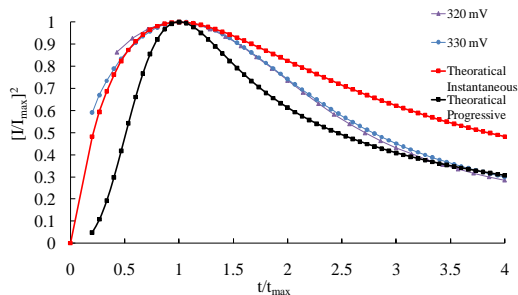
a) 0.1 mol dm$^{-3}$ CuCl$_2$·2H$_2$O in Ethaline

b) 0.1 mol dm$^{-3}$ AgNO$_3$ in Ethaline
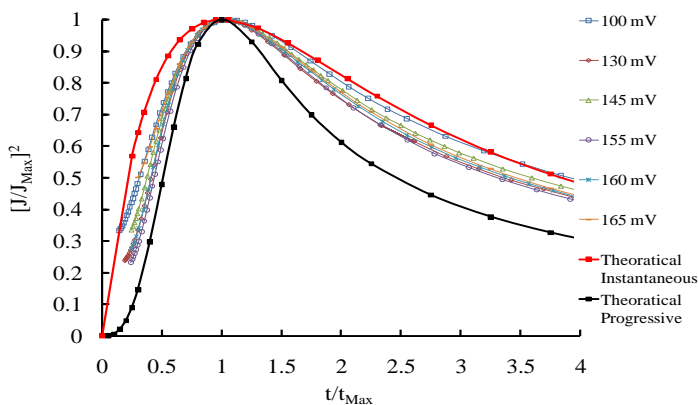
1: 1 Cu: Ag
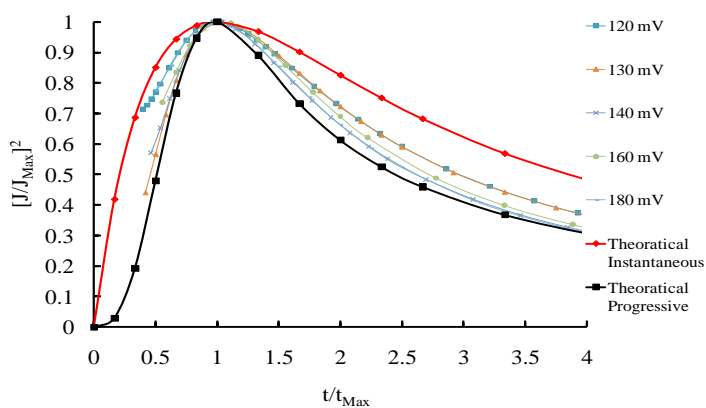
1: 3 Cu: Ag
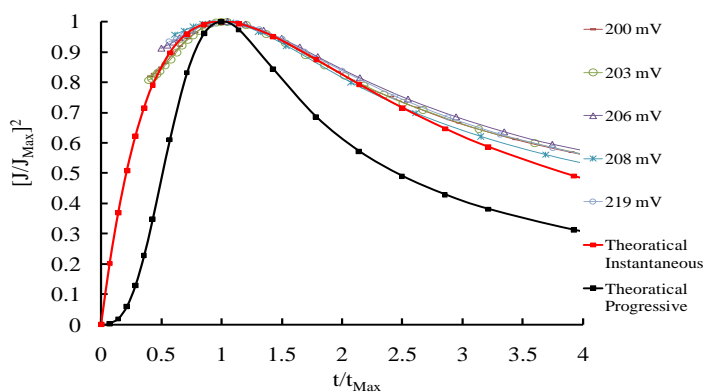
3: 1 Cu: Ag

***Figure 3.4*** *Comparison of the dimensionless and theoretical chronoamperometric curves of a) 0.1 mol dm$^{-3}$ CuCl$_2$·2H$_2$O, b) 0.1 mol dm$^{-3}$ AgNO$_3$, 1: 1 Cu: Ag, 1: 3 Cu: Ag and 3: 1 Cu: Ag from Ethaline. Applied potentials all in negative*

$$\left(\frac{J}{J_{Max}}\right)^2 = 1.9542\left(\frac{t_{Max}}{t}\right)[1 - e^{\left(-1.2564\left(\frac{t}{t_{Max}}\right)\right)}]^2 \qquad (3.2)$$

$$\left(\frac{J}{J_{Max}}\right)^2 = 1.2254\left(\frac{t_{Max}}{t}\right)[1 - e^{\left(-2.2367\left(\frac{t}{t_{Max}}\right)^2\right)}]^2 \qquad (3.3)$$

A comparison of these model curves with the experimental transients of the three different metal concentrations of Cu-Ag alloy deposition from Ethaline is presented in **Figures 3.4.** The equimolar Cu and Ag solution shows that the nucleation initially conforms to a 3D progressive mechanism, however, at longer time scales, the mechanism changes to an instantaneous growth mechanism.

It can be seen from the data presented in **Figure 3.4,** for the Ag rich solution shows a good fit to the 3D progressive, diffusion-controlled nucleation model proposed by Scharifker and Hills.[51] When increasing the concentration of Cu, such that it was the same as the silver concentration, the response in **Figure 3.4** corresponds to instantaneous nucleation. Finally, for the Cu rich solution, all time scale nucleation conforms to a 3D instantaneous mechanism, as shown in **Figure 3.4**. This transition indicates that the nucleation rate increases with an increase in the concentration of Cu in the alloys. The results of the present investigation have demonstrated that the mechanism of copper–silver alloy deposition on a platinum disc electrode is a function of the concentration of $Cu^{2+}$ ions in the ionic liquid. The initial nucleation changes completely from progressive at low Cu concentrations in IL to instantaneous when the copper concentration is increased. The results mentioned above are contrary to those expected from aqueous solutions, where the nucleation mechanisms are moved from progressive to instantaneous upon increasing concentration.[45, 52] To gain more information about the rate of metal growth chronocoulommetry was carried out the individual metal surfaces to see if the substrate affects the rate at which the two metals nucleate on each other.

The nucleation mechanism results from Cu-Ag alloy deposition are different from pure Cu, which is progressive and pure silver, which is instantaneous. A progressive nucleation can be observed in the rich silver phase. However, a high Cu with low Ag phase shows instantaneous nucleation mechanism. Clearly, an increase in the over potential allows deposition of the alloy in solution. The silver is laid down first, which is then followed by copper growth and this is probably very slow in comparison.

## 3.5 Chronocoulometry

Chronocoulometry (CC) is one of the classical electrochemical techniques commonly used in electroanalytical chemistry and measures charge as a function of time. The resulting plots can be understood by considering the concentration gradients in the solution adjacent to the electrode surface. Abbott *et al*[34] investigated chronocoulometry of Cu using a Pt disc electrode in 0.01 mol dm$^{-3}$ CuCl$_2$·2H$_2$O from Ethaline and found that metal growth was diffusion controlled.

In the current study, the same concentration (0.05 mol dm$^{-3}$ CuCl$_2$·2H$_2$O or 0.05 mol dm$^{-3}$ AgNO$_3$) was used and the chronocoulometric response of a Cu and Ag disc electrode was measured from Ethaline solutions. The charge measured (*Q*) was assumed to be directly proportional to the number of species deposited in moles (*N*) in accordance with Faraday's Law (*Q = nFN*) since both processes are approximately 100 % current efficient.

**Figure 3.5a** shows chronocoulometry plots that compare depositions on different substrates at an applied potential of -0.75 V for 1800 s. **Figure 3.5a** shows the silver growth is faster than copper due to a larger over-potential, this idea is the same as that found in cyclic voltammetry. The copper deposition kinetics on silver is slower than that on copper, which gives good agreement with the nucleation of the Cu rich phase having an instantaneous mechanism. The low deposition response at 0.05 mol dm$^{-3}$ Cu on a Cu disc is comparable with the 0.05 mol dm$^{-3}$ Ag deposit on a Cu disc electrode under the same conditions. However, the deposition from a 0.05 mol dm$^{-3}$ CuCl$_2$ solution on an Ag disc is lower than the deposition from 0.05 mol dm$^{-3}$ Ag NO$_3$ on an Ag disc electrode. In contrast, deposition from 0.05 mol dm$^{-3}$ AgNO$_3$ on Ag disc electrode under the same conditions yields a measured charge density of around 4.2 mC. The plots of charge versus t$^{1/2}$ are linear for Cu or Ag on Cu or Ag disc electrodes, suggesting that the processes are not purely diffusion controlled but become linear over longer times. Unlike the previous studies of Cu on Pt[34] the studies of Ag or Cu on a Cu disc electrode, shown in **Figure 3.5b,** show that neither process is diffusion controlled.

a)                                                                        b)
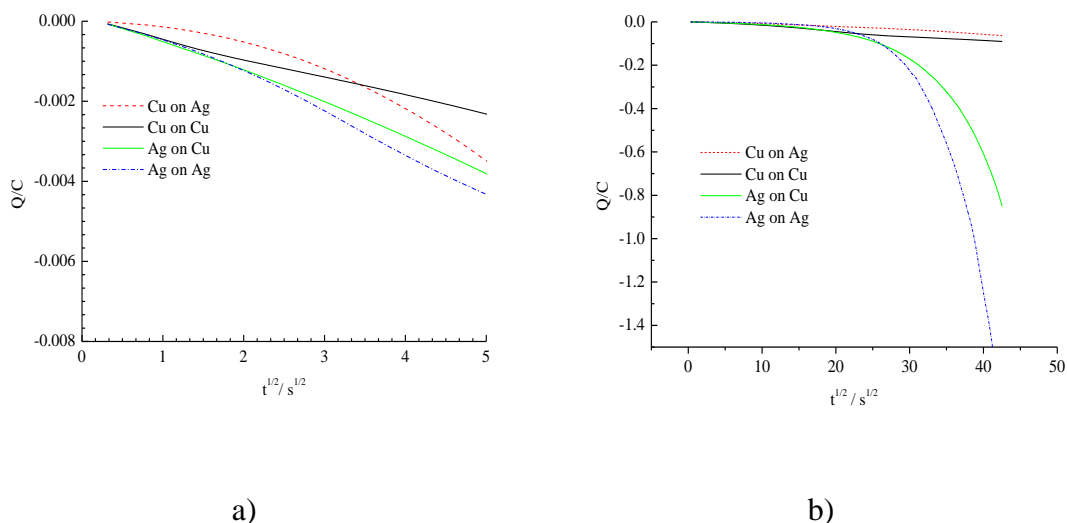
**Figure 3.5** *Chronocoulometry for a) 0.05 mol dm$^{-3}$ CuCl$_2$·2H$_2$O and 0.05 mol dm$^{-3}$ AgNO$_3$ b) 0.15 mol dm$^{-3}$ CuCl$_2$·2H$_2$O and 0.15 mol dm$^{-3}$ AgNO$_3$ from Ethaline at -0.75 V using Cu and Ag disc as working electrode, Ag as reference electrode and Pt flag as a counter electrode.*





a) Copper on copper                                    b)Silver on silver
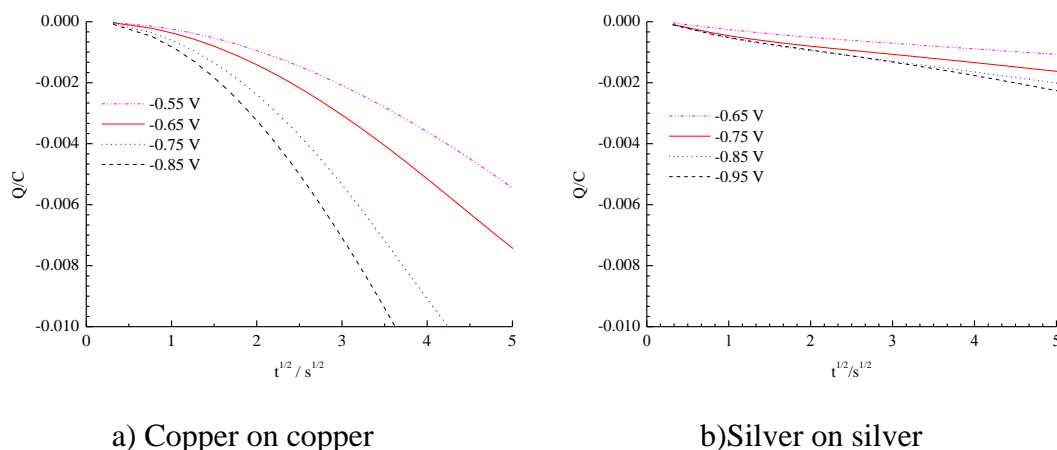
**Figure 3.6** *Chronocoulometry for a) 0.05 mol dm$^{-3}$ CuCl$_2$·2H$_2$O using Cu disc as a working electrode b) for 0.05 mol dm$^{-3}$ AgNO$_3$ using Ag disc as a working electrode from Ethaline at different potentials, Ag as reference electrode and Pt flag as a counter electrode.*

Chronocoulometry plots at different negative electrodeposition potentials -0.55 to -0.95 V are shown in the two **Figures 3.6a and b**, from two systems (0.05 mol dm$^{-3}$ CuCl$_2$·2H$_2$O or 0.05 mol dm$^{-3}$ AgNO$_3$) in Ethaline onto a copper electrode. The chronocoulometry response for the deposition of Cu and Ag shows that the change in charge density for copper on copper is larger than for silver on copper and it is also more potential dependent. This suggests that the copper content of the alloy will be dependent not only on the solution composition but also

57

larger than for silver on copper and it is also more potential dependent. This suggests that the copper content of the alloy will be dependent not only on the solution composition but also on the metal which has already been deposited. This leads to a very complex model of alloy deposition.

**3.6 Analysis of Cu-Ag deposit using SEM, EQCM and EDAX**

In this section electrochemical acoustic impedance EQCM is used to study the deposition of alloys. It is shown for the first time that this technique can be used effectively as an in-situ probe of alloy composition during electrolytic deposition from ionic liquids and that the compositions determined in this way agree well with SEM (EDAX) analysis of the same samples.

The electrochemical quartz crystal microbalance (EQCM) uses the piezoelectric properties of a quartz crystal to measure mass changes at the electrode surface. When an electric field is applied to a quartz crystal it causes strain or shear deformation. This strain results from the realignment of dipoles in the crystal structure with the electric field. Alternating the electric field, at the characteristic frequency of the quartz makes the crystal resonate. The deposition of a mass on the crystal surface shifts the resonant frequency, which can then be measured.

In practice the change in mass of the crystal changes the resonant frequency of the crystal, $\Delta f$, from its fundamental value, $f_0$. The change in mass, $\Delta m$, can therefore be calculated from the change in resonant frequency using the Sauerbrey equation, **Equation (3.4)**

$$\Delta f = -\frac{2f_0^2}{\rho v}\frac{\Delta m}{A} \tag{3.4}$$

where $\rho$ is the density of quartz and $v$ the wave velocity and $A$ is the surface area of the resonator. The Sauerbrey equation can only be used for the determination of mass changes if the deposited mass acts like a rigid resonator.

**Figure 3.7** shows the change in mass as a function of the charge passed for the deposition of pure Ag at a fixed potential of -0.55 V for a time of 1805 s. The slope of the graph in **Figure 3.7** is 1.12 x $10^{-3}$ g $C^{-1}$, which is the same as that calculated from Faraday's law (i.e., r.a.m / nF) showing that the current efficiency of Ag deposition is $\approx$ 100 %. Deposition of pure Cu also gives a current efficiency of 99 %.

In addition, the mole fraction of Cu in Cu-Ag alloy can be calculated from the slope of the $\Delta m$ *vs*. $Q$ plots using Faraday's law in **Equation (3.5).**

$$\frac{dm}{dQ} = \frac{X_{Cu}.ram_{Cu} + (1-X_{Cu}).ram_{Ag}}{F(X_{Cu}+1)} \qquad (3.5)$$

Where $X_{Cu}$ is the mole fraction of Cu, and $X_{Ag}$ is the mole fraction of Ag. The relative atomic masses for Cu and Ag are 63.5 g mol$^{-1}$ and 107.87 g mol$^{-1}$ respectively
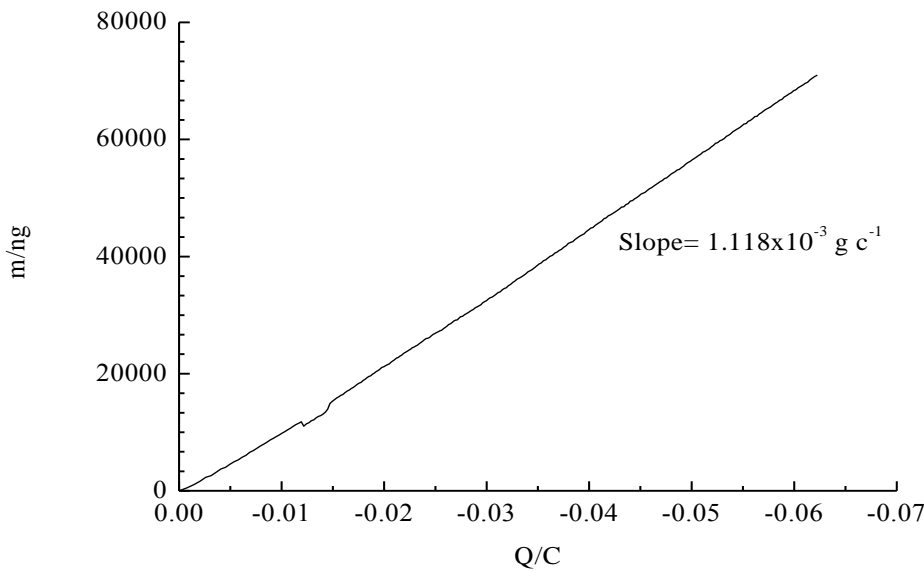


***Figure 3.7*** *Electrochemical acoustic impedance (EQCM) data for Ag deposition on a Au coated quartz crystal using Ag as a reference electrode over a time period of 1805 s; The potential was stepped from O.C.P and held at -0.55 V*

**Figure 3.8** shows the $\Delta m$ vs. $Q$ plots for the three mixed metal systems. The slope of the linear best fit for the 3: 1 $CuCl_2 \cdot 2H_2O$: $AgNO_3$ is 4.52 x 10$^{-3}$ g C$^{-1}$. It follows that the experimental slope, $\frac{d(\Delta m)}{dQ}$ , of the $\Delta m$ *vs.* $Q$ plots is a measure of the average composition according to **Equation (3.6).**
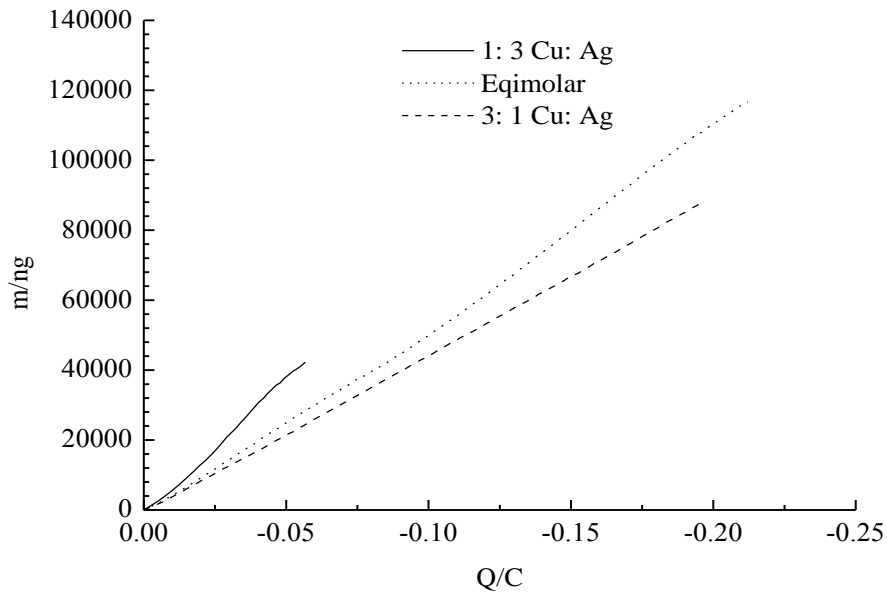
**Figure 3.8** *Mass versus charge plots for Cu/ Ag alloy deposition using EQCM; The electrolyte contained CuCl$_2$·2H$_2$O: AgNO$_3$ in different mole ratios. The potential was stepped from O.C.P and held at -0.75 V, using Ag/AgCl as a reference electrode.*
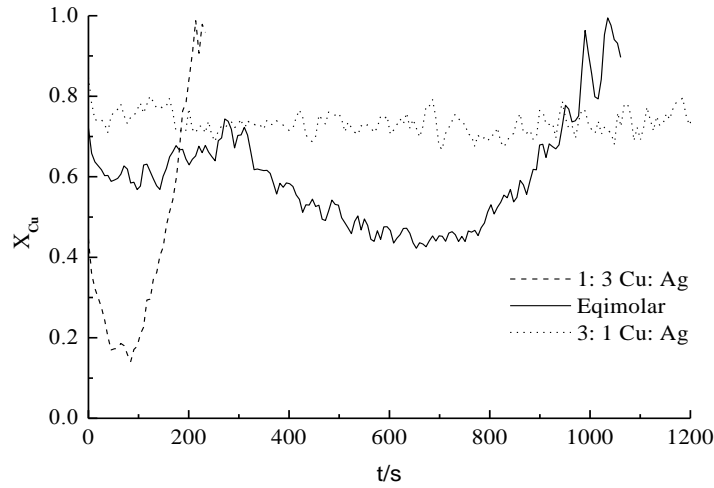


**Figure 3.9** *The mole fraction vs time plot for Cu in three metal mixtures 1:1 CuCl$_2$·2H$_2$O: AgNO$_3$, 1: 3 CuCl$_2$·2H$_2$O: AgNO$_3$ (dash line), (solid), and 3: 1 CuCl$_2$·2H$_2$O: AgNO$_3$ (dot line) from Ethaline. The potential was stepped from O.C.P and held at -0.75 V*

$$X_{Cu} = \frac{ram_{Ag} - \left( \frac{d(\Delta m)}{dQ} \right) . F}{\left( \left( \frac{d(\Delta m)}{dQ} \right) \right) . F - ram_{Cu} + ram_{Ag}} \qquad (3.6)$$

This analysis was carried out on the data shown in **Figure 3.8** and the results are shown in **Figure 3.9.**

The data presented in **Figure 3.9** show the equivalent differential plots expressed as a composition of the alloy ($X_{Cu}$), using **equation (3.6)**. The Cu rich data produces a linear fit as shown in **Figure 3.8** and this corresponds to a noisy but stable composition of copper at around $X_{Cu} = 0.75$. From equimolar $CuCl_2 \cdot 2H_2O$: $AgNO_3$ solutions the copper content in the alloy is initially higher than the solution concentration. This is surprising since silver is thermodynamically easier to reduce than copper; however it suggests that there is a kinetic effect from the substrate on the rate of metal growth. As copper is depleted from the solution the silver content increases and then reverts as the silver is depleted.

The solution containing predominantly silver starts with a high silver content and then reverts to all copper. This suggests that silver in copper forms a solid solution whereas copper in silver forms a two phase alloy. As will be seen below in **Table 3.2**, the results from the average mole fraction calculated using EQCM were very close with the metal ratios determined using EDAX.

The relative compositions of the deposits obtained during this experimental investigation were also analysed using EDAX and SEM. A comparison between the copper content of the deposits estimated using **Equation 3.6** and the copper content measured by EDAX is presented in **Table 3.2.** The alloy composition analysis using both experimental EQCM and EDAX produce consistent values. However, it is clear from the SEM image in **Figure 3.10** that at 1:3 Cu: Ag deposition formation gives a rough surface. The clear change in deposit morphology as Ag content is increased is illustrated in **Figure 3.10**.

In the Ag rich solution, the deposit obtained has a crystalline appearance with branched structures of almost pure silver on the surfaces. Nodules with relatively constant dimensions of approximately 1μm are produced from a solution of equimolar metal salt concentration.

|  | Solution composition | | |
|---|---|---|---|
|  | $X_{Cu} = 0.5$ | $X_{Cu} = 0.25$ | $X_{Cu} = 0.75$ |
| $X_{Cu}$ by EDAX | 0.46 | 0.23 | 0.71 |
| $X_{Cu}$ by EQCM | 0.54 | 0.24 | 0.73 |

**Table 3.2** *Cu mole fractions of the deposits obtained by deposition at -0.75 V from the EQCM technique compared with EDAX analysis of the same deposits.*
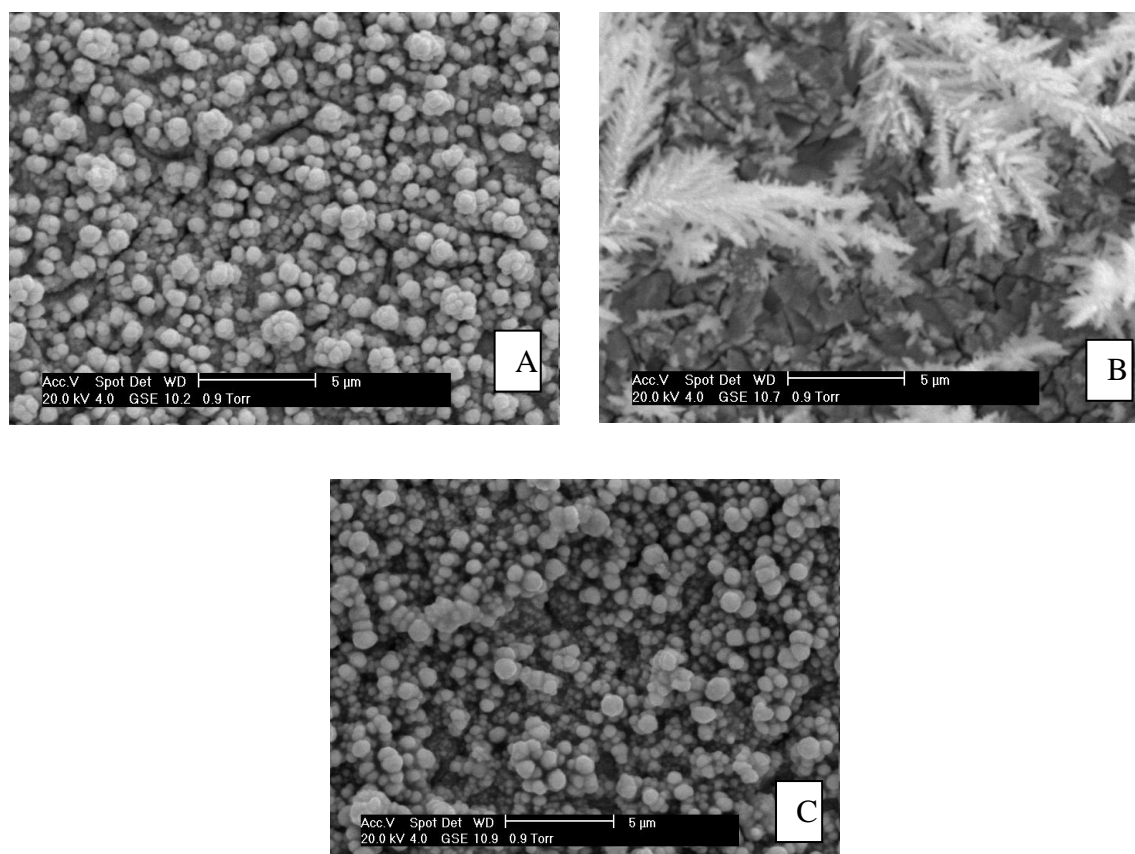
**Figure 3.10** *Representative scanning electron micrographs of Cu-Ag alloys electrodeposited from (**a**) 1:1 CuCl$_2$·2H$_2$O: AgNO$_3$ (**b**) 1:3 CuCl$_2$·2H$_2$O: AgNO$_3$ (**c**) 3:1 CuCl$_2$·2H$_2$O: AgNO$_3$ in Ethaline. Deposits are made on a gold covered quartz crystal. The potential was stepped from O.C.P and held at -0.75 V*

The deposit obtained from the Cu rich solution was similar in appearance to that obtained from the equimolar solution, with a very similar grain size. This is consistent with the data obtained from EDAX and EQCM as discussed later.

The phase composition of the Cu-Ag alloys deposited from Ethaline was determined using EDAX and was found to be strongly affected by the current density. An increase in the

current density leads to an increase in the ratio of Cu:Ag in the deposited layer as shown in **Figure 3.11**. The current density at different positions across the Hull cell was calculated using **Equation 3.7**.

$$C = i(5.1 - 5.24log_{10}X) \tag{3.7}$$

$C$ = current density

$i$ = current applied

$X$ = distance from high current density end of the panel.
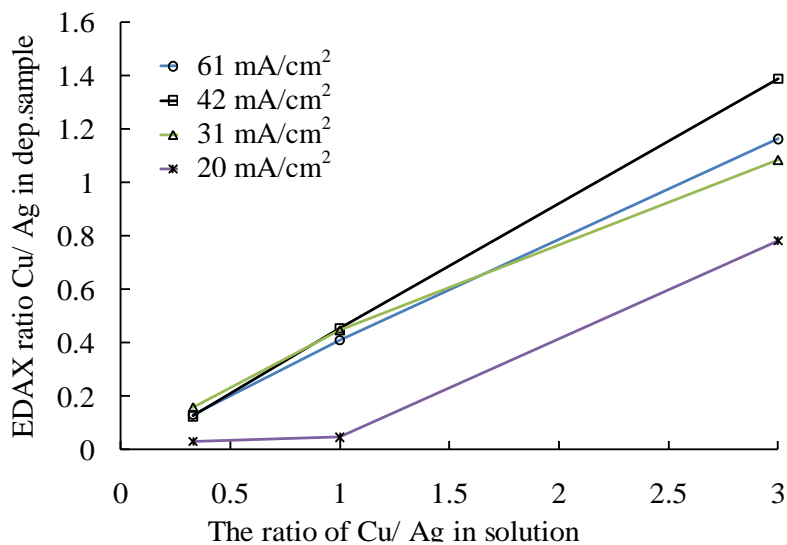


***Figure 3.11*** *EDAX result for the deposits using a Hull cell, obtained at three different concentrations (equimolar, 1: 3 and 3: 1) of CuCl$_2$·2H$_2$O: AgNO$_3$ from Ethaline ionic liquid.*

It was, however, found that the morphology of the surface layer was dependent on the current density, as will be shown later in this chapter.

**Figures 3.12** shows the raw impedance data for the three systems of Cu-Ag alloys deposited and from this data the influences of the surface roughness on the resonance behaviour of a quartz crystal can be seen. The frequency, *f*, and peak shape, *Q*, of the crystal both change substantially during metal deposition, as shown in **Figure 3.12a**. The frequency losses in the Ag rich system are probably the result of surface roughening.
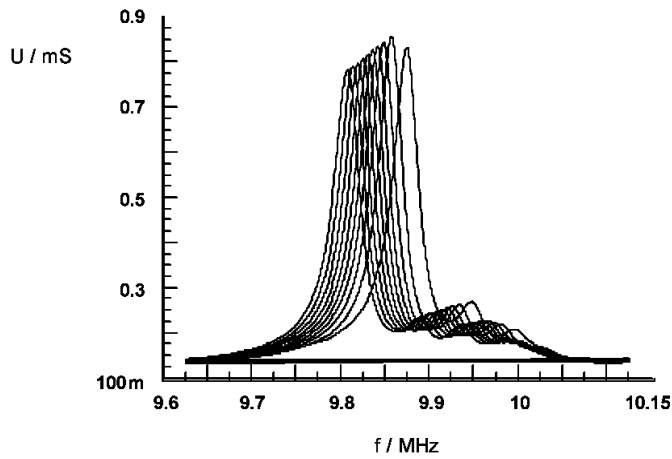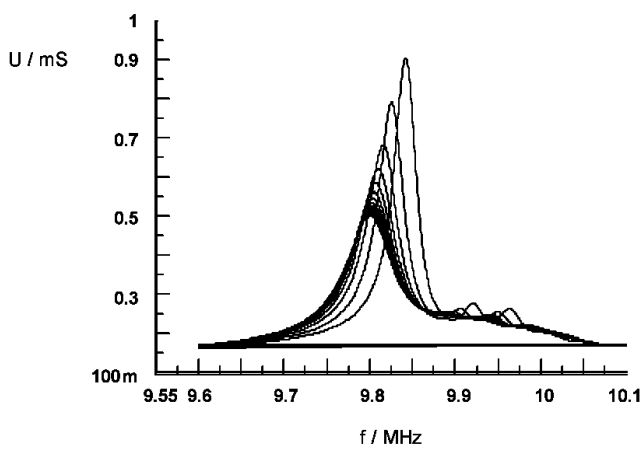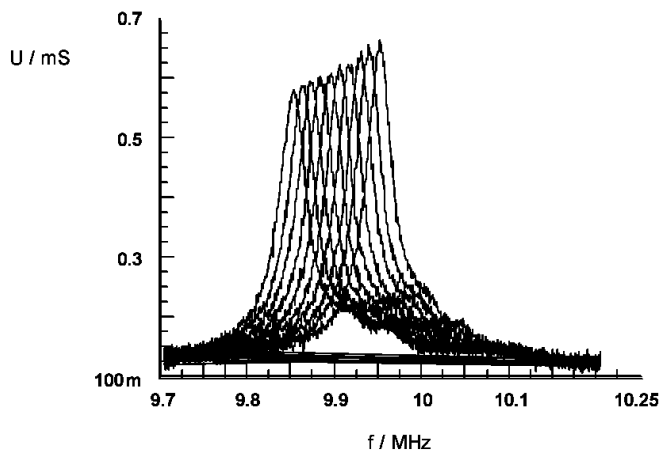
***Figure 3.12*** *Acoustic impedance plot (U = 1/ Z) for deposition of a) 1: 1*
*CuCl$_2$·2H$_2$O: AgNO$_3$, b) 1: 3 CuCl$_2$·2H$_2$O: AgNO$_3$, and c) 3: 1 CuCl$_2$·2H$_2$O: AgNO$_3$ on*
*a gold crystal in Ethaline. Every 10,15 and 25 spectrum respectively is shown, with ca*
*6 s between spectra*

In this case, during the deposition of Ag rich phase the resonance curve shifts to lower values
and broadens. This is confirmed from the SEM image, as shown in **Figure 3.10b**. During the

Cu/Ag deposition, the resonance curve shifts to lower frequencies but does not change its form (**Figure 3.12a and c**).

**Figure 3.13** shows SEM images of four samples; (A) pure Ag with cubic crystallites (B) pure Cu with an amorphous deposit suggesting nanocrystalline growth. The mixed $CuCl_2 \cdot 2H_2O/AgNO_3$ solution produced deposits with different morphologies depending on whether the substrate was copper or silver.
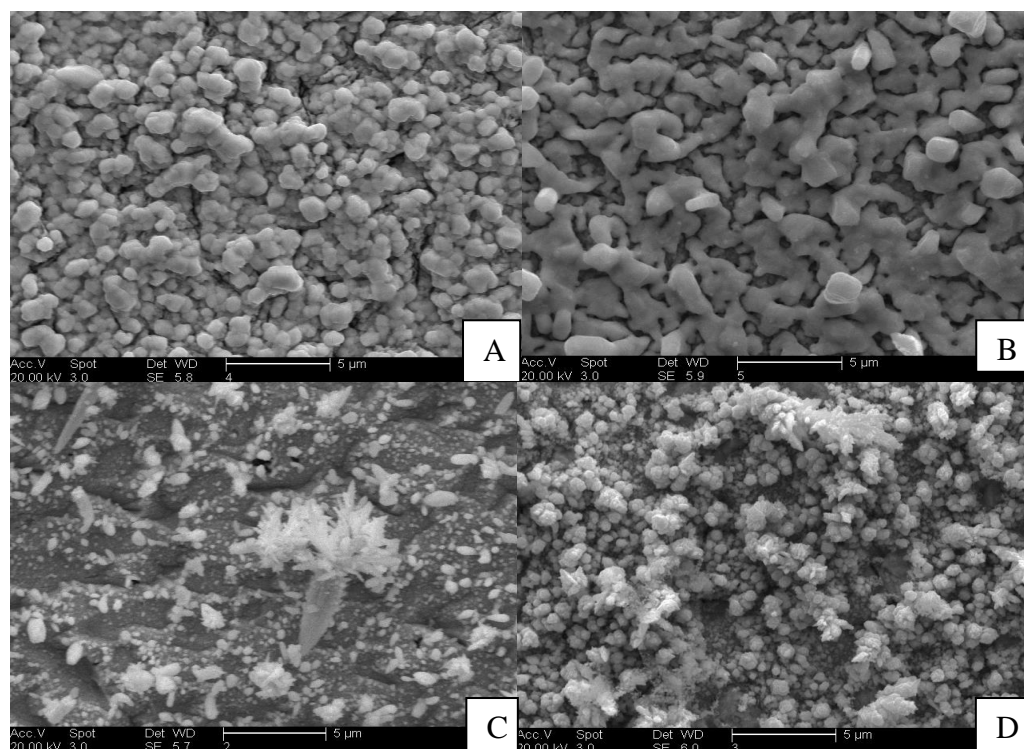


*Figure 3.13* SEM images of (A)Ag deposited from 0.2 mol $dm^{-3}$ $AgNO_3$ and (B) Cu deposited from 0.2 mol $dm^{-3}$ $CuCl_2 \cdot 2H_2O$ deposit both on a Au coated QCM crystal at -0.55V and -0.75V respectively from Ethaline. (C) Cu-Ag alloy deposited on an Ag coated QCM crystal and (D) Cu-Ag alloy deposited on a Cu coated QCM crystal both from a 1: 3 $CuCl_2 \cdot 2H_2O$: $AgNO_3$ solution in Ethaline at -0.75V.

**Figure 3.14** shows the raw impedance data for the deposition of Cu/ Ag alloy on the Au crystal. In this Figure it can be seen that both the frequency and $Q$ shape of the crystal resonance change substantially during the increase of alloy deposition. In addition, the peak of the frequency becomes broader as the resonance frequency drops. The trend shown in this Figure is the same as in **Figure 3.15**.

From the data presented in **Figure 3.15** it can be seen from the plot $I(Q,t)$ that the $Q$ factor rapidly drops with the initial current, I, then after 400 s the current starts to increase, and the

$Q$ factor is shown to be stable at 90. This is good indication of Cu-Ag alloy formation on the Au surface.
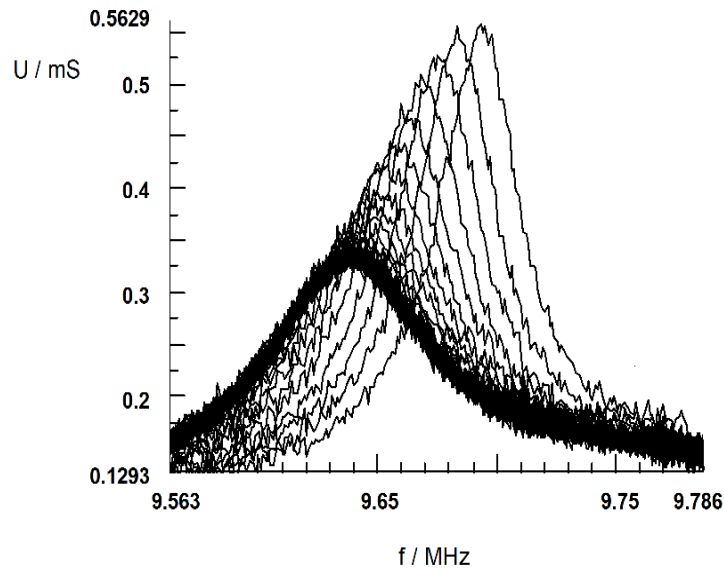


*Figure 3.14 Acoustic impedance plot (U = 1/ Z) for deposition of 1: 3 CuCl$_2$.2H$_2$O: AgNO$_3$ on a gold crystal in 1:2 ChCl: ethylene glycol. Every 5$^{th}$ spectrum is shown, with ca 6 s between spectra.*

In this case the silver rich alloy (similar to that shown in **Figure 3.12b**), 1: 3 CuCl$_2$.2H$_2$O: AgNO$_3$ is plated onto an Ag coated crystal. The small change of the impedance is seen in **Figure 3.16**, as a result the type of substrate gives a different nucleation mechanism. The raw impedance data are presented in **Figure 3.16**, with the corresponding $I(Q,t)$ plot shown in **Figure 3.17**.

It can be seen from the data present in **Figure 3.17** that the rapid drop in $Q$ factor is related to the initial decay in current, $I$, but that after 300 s, when the current starts to increase, the $Q$ factor is stable between 135 and 140.
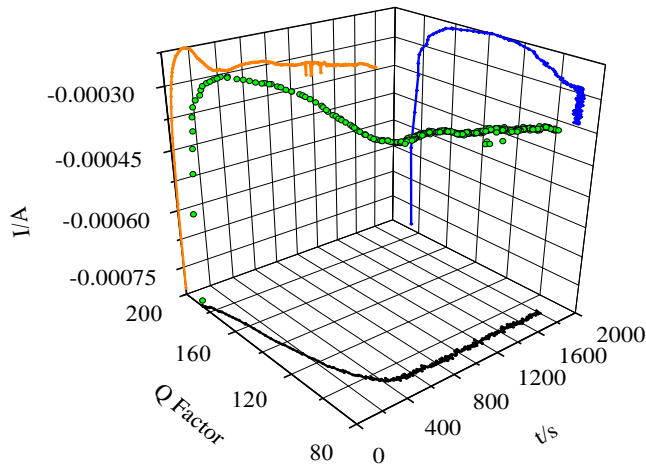
***Figure 3.15*** *3D plot of I(Q,t)(green circles) for deposition of 1: 3 $CuCl_2 \cdot 2H_2O$: $AgNO_3$ on a Au coated QCM crystal from Ethaline solution.2D projections are also shown for clarity, Q(t) (black), I(t) (orange), I(Q) (blue).*

**Figure 3.18** shows the raw impedance data for the alloy (Cu-Ag on Cu coated crystal) and the corresponding *I(Q,t)* plot is present in **Figure 3.19**. Here the raw spectra show sharper peaks compared with the alloy (Cu-Ag on Ag coated crystal).
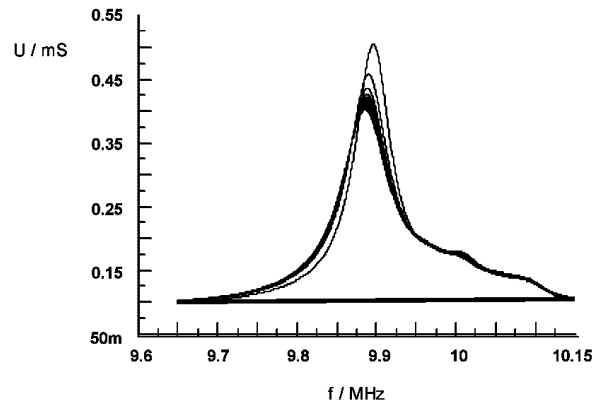


***Figure 3.16:*** *Acoustic impedance plot (U = 1/ Z) for deposition of 1: 3 $CuCl_2 \cdot 2H_2O$: $AgNO_3$ on a Ag coated crystal in Ethaline. Every 20th spectrum is shown, with c.a. 6 s between spectra.*
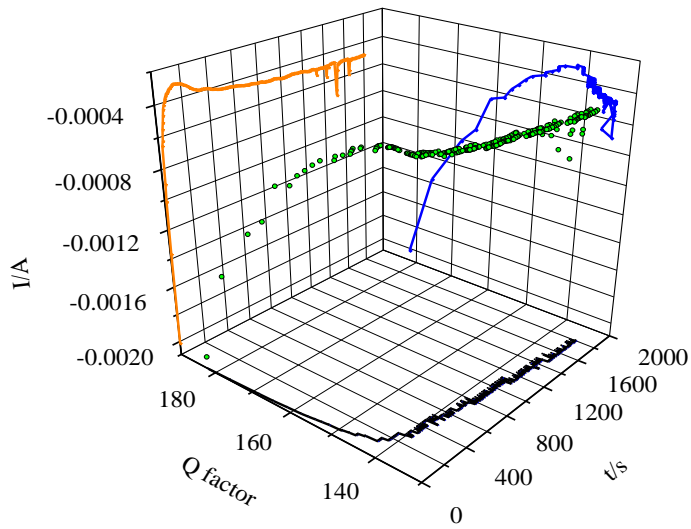
**Figure 3.17** *3D plot of I(Q,t)(green circles) for deposition of 1: 3 $CuCl_2 \cdot 2H_2O$: $AgNO_3$ on a Ag coated QCM crystal from Ethaline. 2D projections are also shown for clarity, Q(t) (black), I(t) (orange), I(Q) (blue).*
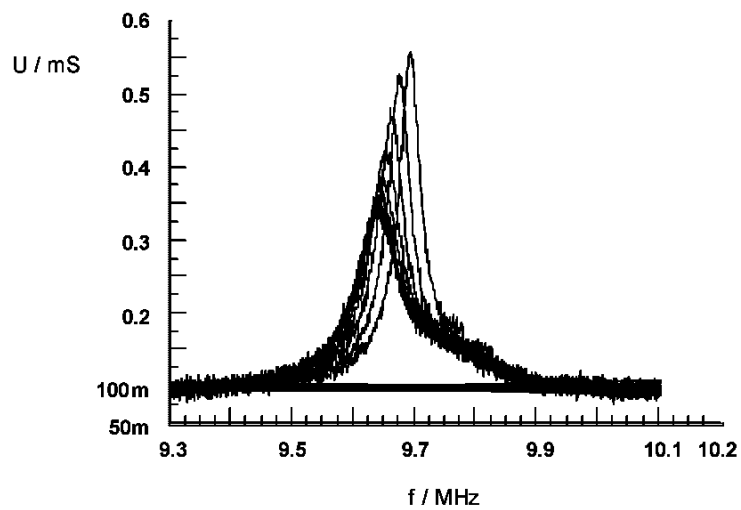


**Figure 3.18** *Acoustic impedance plot (U = 1/ Z) for deposition of 1: 3 $CuCl_2 \cdot 2H_2O$: $AgNO_3$ on a Cu coated crystal from Ethaline. Every 20$^{th}$ spectrum is shown, with ca 6 s between spectra.*
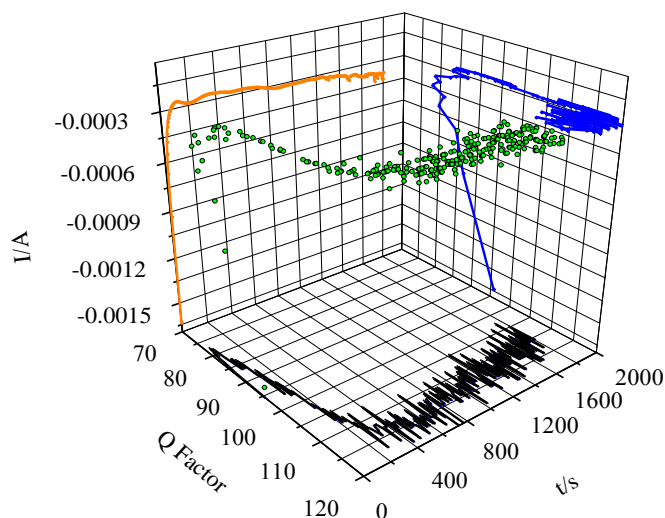
***Figure 3.19:*** *3D plot of I(Q,t) for deposition of 1: 3 CuCl$_2$·2H$_2$O: AgNO$_3$ on a Cu coated QCM crystal from Ethaline. 2D projections are also shown for clarity, Q(t) (black), I(t) (orange), I(Q) (blue).*

**Figure 3.19** shows the rapid noisy drop in *Q* factor with initial decay in current, *I*, but after 400 s, when the current starts to grow, the *Q* factor is constant at 120. This is a strong indication for Cu-Ag deposition on Cu, as a different morphology deposit was observed in **Figure 3.13d**.

A Hull cell test was carried out to determine the effect of current density on the Cu/ Ag alloy composition at different Cu/Ag concentrations in solution, using SEM and EDAX. The appearance of the samples is also recorded using optical photographs. It can be seen from **Figures 3.20, 3.21 and 3.22** that the surface morphologies are homogeneous and adherent.

At a current density of 61 mA cm$^{-2}$ a homogenous deposit is formed for equimolar Cu-Ag alloys as shown from the SEM image in **Figure 3.20**. Decreasing the current density to 20 mA cm$^{-2}$ yields a similar underlying deposit with a larger crystal grain size and an amorphous surface coating that is Ag rich (65% Ag and 3% Cu) (**Figure 3.20D)**.
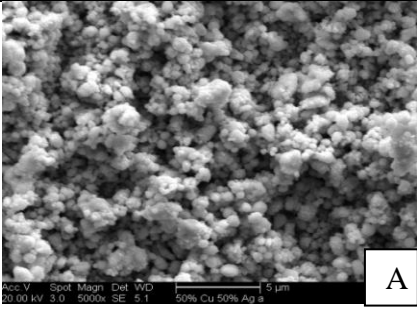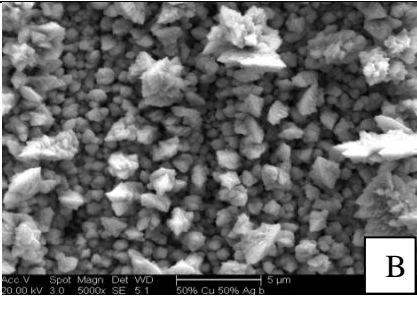
| ESEM | 1:1 CuCl$_2$·2H$_2$O: AgNO$_3$ | | |
| --- | --- | --- | --- |
| | $I$ / mA cm$^{-2}$ | Cu % | Ag % |
| | 61 | 29 | 71 |
| | 42 | 31 | 69 |
| | 31 | 31 | 69 |
| | 20 | 4 | 96 |
| | | | |

***Figure 3.20*** *SEM, EDAX and photograph are showing different regions of a Hull cell panel coated with Cu-Ag alloys deposit grown of  1: 1 CuCl$_2$·2H$_2$O: AgNO$_3$ from Ethaline.*

The Ag content in the deposits could be controlled from 42 to 96 mol % by changing the bath composition and current densities. It does, however, show that the morphology of the surface layer is dependent on the current density. According to, the data of equimolar Cu-Ag alloys depositions from Ethaline is presented in **Figure 3.20 (A, B, C and D)**. The SEM images show that the surface morphology is dependent on the current density.

In **Figure 3.21 (A)**, the crystal growth is not uniform from the equimolar solution of Cu and Ag, the deposit having slightly smaller crystal sizes, but when the current density is decreased, the deposited crystals become larger (**Figure 3.21 (B,C,D)**. At a high current density in the rich Cu solution, a homogenous deposit is formed, as shown in **Figure 3.22 (A)**. Decreasing the current density yields a less crystalline deposit with an amorphous surface coating that is Cu rich (49% Cu and 36 % Ag), as shown in **Figure 3.22 (B)**. At low current densities 42, 31 mA cm$^{-2}$ the Cu percentage is increased and produces a homogeneous morphology (51 % Cu and 47% Ag) **Figure 3.22 (C)**.

At even lower current density the deposits are found on the surface (44 % Cu and 56% Ag) increase the percentage of Ag **Figure 3.22 (D).** These coalesce to give nodular and sharp deposits. Also the colour of the electrodeposits changed from red, to white-brown, to grey-brown as the Cu content decreased. SEM images and photographs of the deposit obtained from the three systems of Cu-Ag alloys showed a non-uniform arrangement of the crystals size and hence gave a dull deposit (**Figures 3.20, 3.21 and 3.22**)
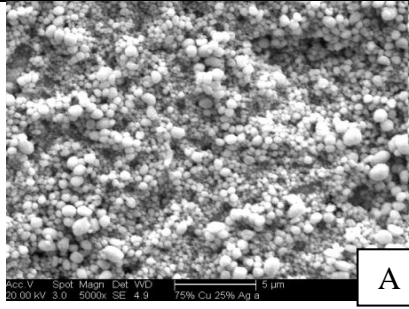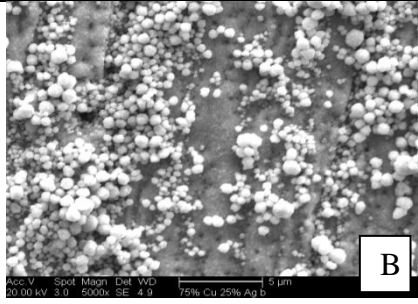
| ESEM | 1:3 CuCl$_2$·2H$_2$O: AgNO$_3$ | | |
|---|---|---|---|
| | $I$ / mA cm$^{-2}$ | Cu % | Ag% |
| | 61 | 12 | 88 |
| | 42 | 11 | 89 |
| | 31 | 14 | 86 |
| | 20 | 33 | 67 |
| | | | |

*Figure 3.21* SEM, EDAX and photograph are showing different regions of a Hull cell panel coated with Cu-Ag alloys deposit grown of 1: 3 CuCl$_2$·2H$_2$O: AgNO$_3$ from Ethaline.
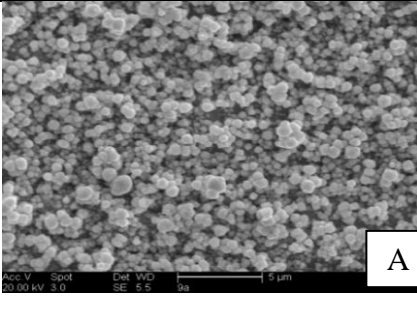
| ESEM | 3:1 $CuCl_2 \cdot 2H_2O$: $AgNO_3$ | | |
| --- | --- | --- | --- |
| | $I$ / mA cm$^{-2}$ | Cu % | Ag% |
| A | 61 | 54 | 46 |
| B | 42 | 58 | 42 |
| C | 31 | 52 | 48 |
| D | 20 | 44 | 56 |
| D    C    B    A | | | |
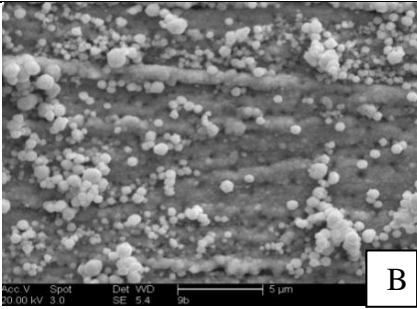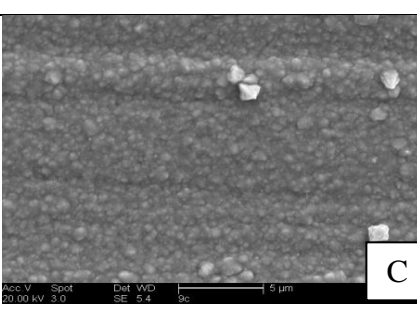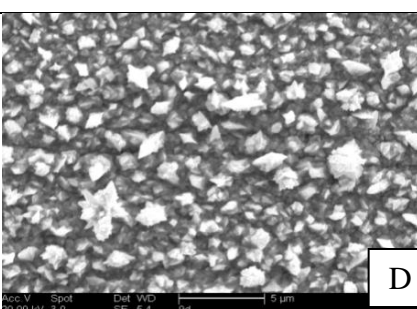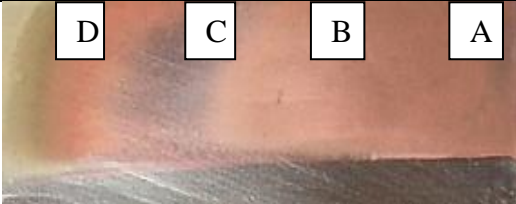
*Figure 3.22* SEM, EDAX and  photograph  are showing different regions of a Hull cell panel coated with Cu-Ag alloys deposit grown of 3: 1 CuCl₂·2H₂O: AgNO₃ from Ethaline.

## 3.7 Phase formation XRD

For determination of the phases that appeared in the alloys, XRD analysis was carried out. **Figure 3.23** shows the profiles of XRD patterns for the Cu-Ag alloys deposited from Ethaline ionic liquid on Ni substrate at (A) position.
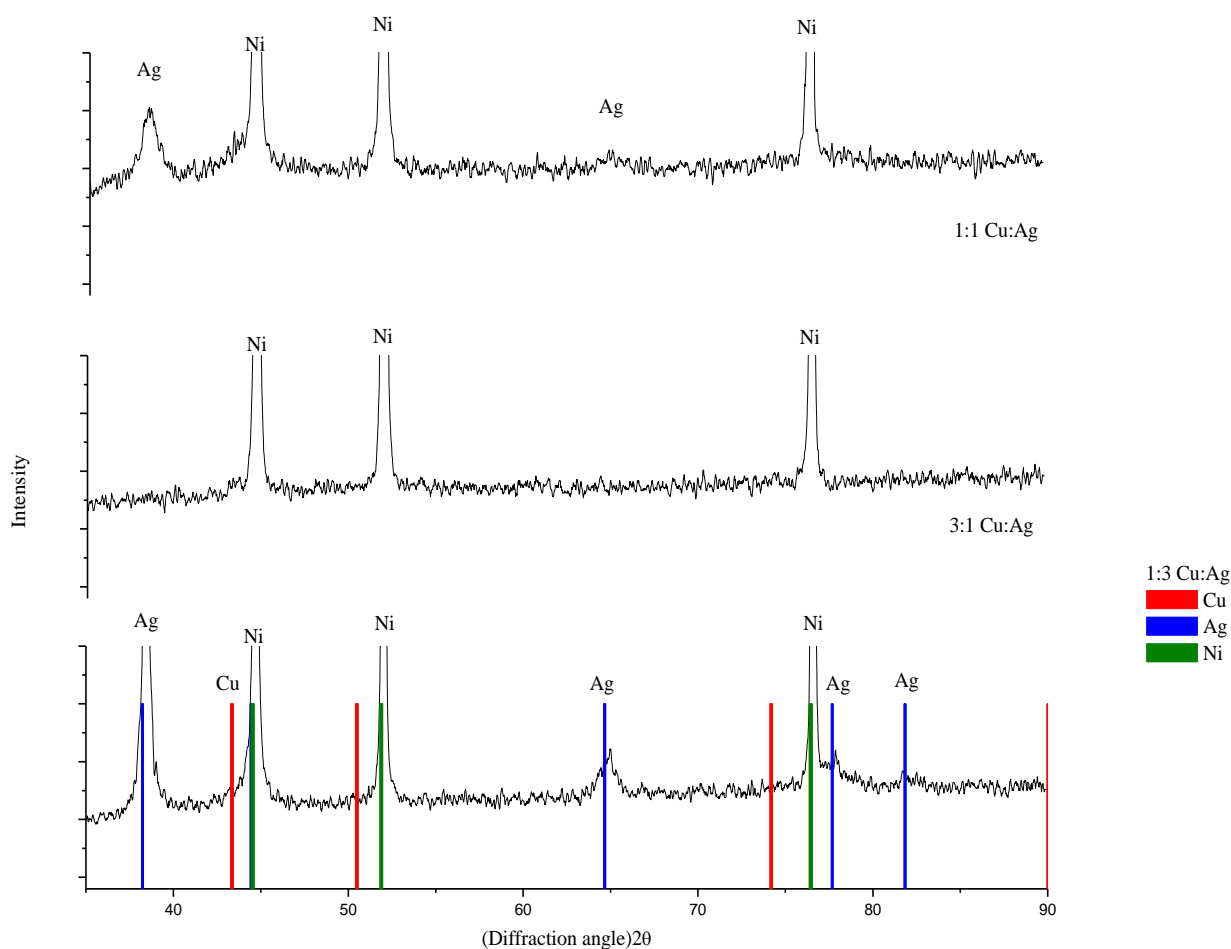


***Figure 3.23*** *XRD results of the Cu–Ag samples deposited on nickel substrate from 1ChCl : 2 EG ionic liquid at different concentrations a) 1: 1 CuCl₂·2H₂O: AgNO₃  b) 1: 3 CuCl₂·2H₂O: AgNO₃, and c) 3: 1 CuCl₂·2H₂O: AgNO₃*

As illustrated in **Figure 3.23**, the pure Cu disappears upon the formation of Cu–Ag alloy, and the characteristic 2θ of the Cu–Ag alloys varied with increasing Cu percentage in the electrodeposited alloys.   The peak intensity of Ag decreases with an increase in Cu

74

concentration. The characteristic signal of pure Cu and Ag disappeared upon the formation of Cu–Ag alloys, with increasing of Cu percentage in the electrodeposited alloys.

## 3.8 Immersion process

Immersion plating is an electroless deposition process, where metal oxidation and metal reduction proceed simultaneously. The process depends upon an autocatalytic effect whereby the metal ions in solution are reduced to the metal, only on the surfaces on which the coating is required.

In addition, electroless deposition of metals can be divided into two categories; catalytically activated deposition and immersion coatings. The former uses a chemical reducing agent in solution, whereas the latter relies on the galvanic potential difference between the ions in solution and the substrate.

The introduction of ionic liquids as a new plating technology for electroless or electrolytic plating offers a new opportunity to investigate non-electrolytic methods of depositing alloys. Previous work has shown the first example of electroless coating of silver on to a Cu surface from a non-aqueous solution. [21, 53] Firstly, the process is particularly designed for silver coating on multi-track circuit boards using DESs, under the same conditions as aqueous systems.[31]

This is the first time that the electroless deposition of a Cu-Ag alloy has been studied from Ethaline on a Ni substrate. For the purposes of this experiment a new way of reducing the metal was developed. The galvanic potential difference between Ni and Cu or Ag is relatively small and nickel is a poor sacrificial metal as it exhibits a low solubility in Ethaline. Therefore in this case a sacrificial metal was connected to the Ni plate. The requirements for this sacrificial metal are that it should dissolve rapidly, but not contaminate the plating solution by re-depositing with the copper alloy. For this reason aluminium was chosen and a simple aluminium foil was connected with a crocodile clip. This allowed thick adherent deposits to be obtained on the Ni substrate. These depositions were analysed using AFM, SEM and EDAX. The results are shown in **Figure 3.24** for three different Cu: Ag compositions. It can be seen that similar compositions are achieved to those using electrolytic deposition.

| ESM | AFM | EDAX |
|------|-----|------|
| 1:1 CuCl$_2$·2H$_2$O: AgNO$_3$ | | |
|  |  | %Cu = 28%<br><br>%Ag = 72% |
| |  | |
| 1: 2 CuCl$_2$·2H$_2$O: AgNO$_3$ | | |
|  |  | %Cu = 6%<br><br>%Ag = 94% |
| |  | |
| 2: 1 CuCl$_2$·2H$_2$O: AgNO$_3$ | | |
|  |  | %Cu = 73%<br><br>%Ag = 27% |
| |  | |
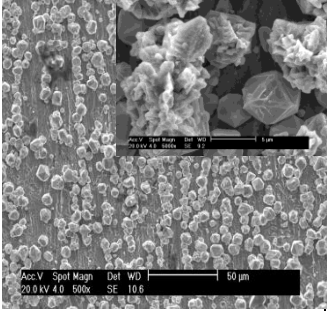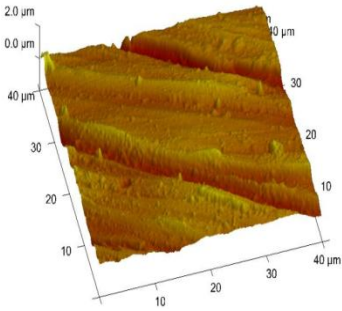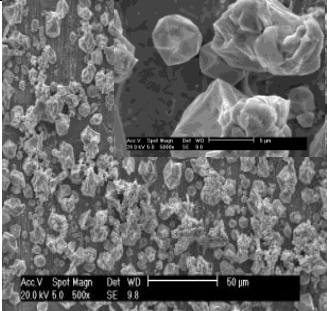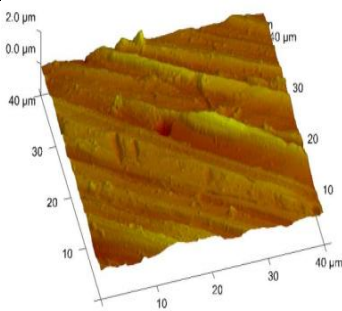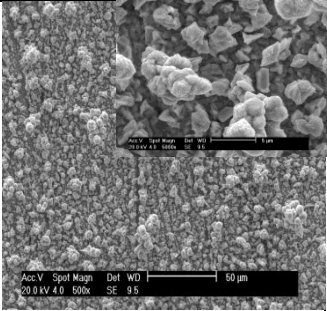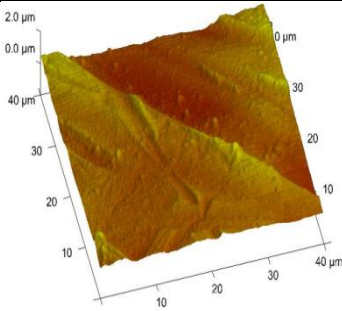
*Figure 3.24* SEM, EDAX, AFM and photographs for different Cu:Ag alloys coated onto Ni using a sacrificial Al foil anode using Ethaline.

Equimolar (1: 1) 0.1 mole $dm^{-3}$ $CuCl_2\cdot 2H_2O$: 0.1 mole $dm^{-3}$ $AgNO_3$ solutions produced a similar 70: 30 Ag: Cu ratio, as was observed in **Figure 3:20**. Both electrolytic and electroless processes show crystallites that are different in dimension. The electroless deposits are more similar in morphology to the high current density results in **Figure 3.20**. Those deposits containing more silver than copper tend to be more crystalline, whereas the higher copper content favours more amorphous morphologies. This section has shown that a sacrificial anode can be used for the deposition of metal alloys and the composition is similar to that obtained via electrolytic deposition.

## 3.9 Conclusions

This work shows that ionic liquids based on eutectic mixtures of choline chloride, with ethylene glycol or urea can be used as electrolytes for the electrodeposition of metals and alloys. It has been found that the most feasible Ethaline and Reline ionic liquids for successful electrodeposition of Ag and Cu-Ag alloys. It is shown here that the current efficiency of Ag deposition is close to 100%. Cyclic voltametry, chronocoulometry and chroamperometry have been used as electrochemical experiments to establish the different behaviour of these three systems of alloys.

It is also shown that the nucleation process is the main factor to control the deposition behaviours, such as morphology and composition change, and depends on the high chloride activity in the solvent and metal substrate. Also the growth mechanism nucleation changes completely from progressive at 0.05 mol $dm^{-3}$ of copper concentration, to instantaneous when the copper concentration is increased to o.15 mol $dm^{-3}$.

*In –situ* QCM has been effectively applied for the first time to report the mass *vs* charge for three systems (Cu-Ag alloys) in ChCl based deep eutectic solvents. A new process has been developed for the electroless (immersion) deposition of copper-silver alloys onto nickel. It has been found that the DESs Ethaline is a suitable medium for (electroless) galvanic coating. The resulting morphological studies showed a very different crystal size of Cu-Ag deposits. These observations may be of interest in the electroless coating industry, particularly the decorative manufacturing.

## 3.10 References

1.  P. Cofré and A. Bustos, *Journal of Electroanalytical Chemistry and Interfacial Electrochemistry*, 1983, **154**, 155-169.

2.  M. B. Davies, R. J. Mortimer and T. R. Vine, *Inorganica Chimica Acta*, 1988, **146**, 59-63.

3.  D. KrznariÄ, *Analytica Chimica Acta*, 1994, **293**, 67-76.

4.  L. M. Abrantes, L. V. Araújo and M. D. Levi, *Minerals Engineering*, 1995, **8**, 1467-1475.

5.  S. Goldbach, W. Messing, T. Daenen and F. Lapicque, *Electrochimica Acta*, 1998, **44**, 323-335.

6.  F. Gobal and R. Arab, *Journal of Electroanalytical Chemistry*, 2010, **647**, 66.

7.  S. S. A. ElRehim, N. F. Mohamed, N. H. Amin and L. I. Ali, *Journal of Applied Electrochemistry*, 1997, **27**, 1385-1389.

8.  F. H. Assaf, S. S. A. Elrehim, A. S. Mohamed and A. M. Zaky, *Indian Journal of Chemical Technology*, 1995, **2**, 147-152.

9.  S. Abd El Rehim, S. Abd El Wahab, S. M. Rashwan and Z. M. Anwar, *Transactions of the Institute of Metal Finishing*, 1999, **77**, 242-245.

10. S. S. Abd El-Rehim, S. M. Abd El-Wahab, S. M. Rashwan and Z. M. Anwar, *Journal of Chemical Technology and Biotechnology*, 2000, **75**, 237-244.

11. A. Brenner, *Electrodeposition of Alloys*, Vol.1, Acadimic Press edn., New York, 1963.

12. C. G. Fink, and J. L. Hutton, *Trans Electrochem Soc*, 1944, **85**, 119.

13. K. Ignatova and L. Petkov, *Journal of the University of Chemical Technology and Metallurgy*, 2009, **44**, 133.

14. R. T. Carlin, H. C. De Long, J. Fuller and P. C. Trulove, *Journal of the Electrochemical Society*, 1998, **145**, 1598-1607.

15. B. J. Tierney, W. R. Pitner, J. A. Mitchell, C. L. Hussey and G. R. Stafford, *Journal of the Electrochemical Society*, 1998, **145**, 3110-3116.

16. C. Nanjundiah and R. A. Osteryoung, *Journal of the Electrochemical Society*, 1983, **130**, 1312-1318.

17. F. Endres and A. Schweizer, *Physical Chemistry Chemical Physics*, 2000, **2**, 5455-5462.

18. P. Y. Chen and I. W. Sun, *Electrochimica Acta*, 1999, **45**, 441-450.

19. K. Murase, K. Nitta, T. Hirato and Y. Awakura, *Journal of Applied Electrochemistry*, 2001, **31**, 1089-1094.

20. S. Z. El Abedin and F. Endres, *Accounts of Chemical Research*, 2007, **40**, 1106-1113.

21. A. P. Abbott, S. Nandhra, S. Postlethwaite, E. L. Smith and K. S. Ryder, *Physical Chemistry Chemical Physics*, 2007, **9**, 3735-3743.

22. A. P. Abbott, J. C. Barron, K. S. Ryder and D. Wilson, *Chemistry-a European Journal*, 2007, **13**, 6495-6501.

23. A. P. Abbott, G. Capper, B. G. Swain and D. A. Wheeler, *Transactions of the Institute of Metal Finishing*, 2005, **83**, 51-53.

24. A. P. Abbott, G. Capper, K. J. McKenzie and K. S. Ryder, *Electrochimica Acta*, 2006, **51**, 4420-4425.

25. A. P. Abbott, G. Capper, K. J. McKenzie, A. Glidle and K. S. Ryder, *Physical Chemistry Chemical Physics*, 2006, **8**, 4214-4221.

26. J. H. Liao, P. C. Wu and Y. H. Bai, *Inorganic Chemistry Communications*, 2005, **8**, 390-392.

27. A. P. Abbott, G. Capper, D. L. Davies, R. K. Rasheed and P. Shikotra, *Inorganic Chemistry*, 2005, **44**, 6497-6499.

28. A. P. Abbott, G. Capper, D. L. Davies, K. J. McKenzie and S. U. Obi, *Journal of Chemical and Engineering Data*, 2006, **51**, 1280-1282.

29. A. P. Abbott, G. Capper, K. J. McKenzie and K. S. Ryder, *Journal of Electroanalytical Chemistry*, 2007, **599**, 288-294.

30. A. P. Abbott and K. J. McKenzie, *Physical Chemistry Chemical Physics*, 2006, **8**, 4265-4279.

31. A. P. Abbott, K. S. Ryder and U. Konig, *Transactions of the Institute of Metal Finishing*, 2008, **86**, 196-204.

32. N. V. Plechkova and K. R. Seddon, *Chemical Society Reviews*, 2008, **37**, 123-150.

33. B. G. Pollet, J.-Y. Hihn and T. J. Mason, *Electrochimica Acta*, 2008, **53**, 4248-4256.

34. A. P. Abbott, K. El Ttaib, G. Frisch, K. J. McKenzie and K. S. Ryder, *Physical Chemistry Chemical Physics*, 2009, **11**, 4269-4277.

35. K. El ttaib, PhD, University of Leicester, 2011.

36. J. Murray, *Metallurgical and Materials Transactions A*, 1984, **15**, 261-268.

37. J. William D. Callister, *Materials Science and Engineering An Introduction*, seventh edn., John Wiley & Sons, 2007.

38. Z. Castro-Dettmer and C. Persad, Electromagnetic Launch Technology, 2004. 2004 12th Symposium on, 2004.

39. F. H. Assaf, A. M. Zaky and S. S. A. El-Rehim, *Applied Surface Science*, 2002, **187**, 18-27.

40. J. C. Barron, PhD, University of Leicester, 24- Mar-2010.

41. A. P. Abbott, J. C. Barron, G. Frisch, S. Gurman, K. S. Ryder and A. F. Silva, *Physical Chemistry Chemical Physics*, 2011, **13**, 10224-10231.

42. A. P. Abbott, G. Frisch, H. Garrett and J. Hartley, *Chemical Communications*, 2011, **47**, 11876–11878.

43. P.-Y. Chen and C. L. Hussey, *Electrochimica Acta*, 2007, **52**, 1857-1864.

44. P. Y. Chen, M. J. Deng and D. X. Zhuang, *Electrochimica Acta*, 2009, **54**, 6935-6940.

45. C. S. Barin, A. N. Correia, S. A. S. Machado and L. A. Avaca, *Journal of the Brazilian Chemical Society*, 2000, **11**, 175-181.

46. P. He, H. Liu, Z. Li, Y. Liu, X. Xu and J. Li, *Langmuir : the ACS journal of surfaces and colloids*, 2004, **20**, 10260-10267.

47. M. Azam, PhD, University of Leicester, 2011.

48. G. de Oliveira and I. Carlos, *Journal of Applied Electrochemistry*, 2009, **39**, 1217-1227.

49. M. Jayakumar, K. A. Venkatesan, T. G. Srinivasan and P. R. V. Rao, *Electrochimica Acta*, 2009, **54**, 6747-6755.

50. G. Scherb and D. M. Kolb, *Journal of Electroanalytical Chemistry*, 1995, **396**, 151-159.

51. B. Scharifker and G. Hills, *Electrochimica Acta*, 1983, **28**, 879-889.

52. D. Grujicic and B. Pesic, *Electrochimica Acta*, 2002, **47**, 2901-2912.

53. A. P. Abbott, J. Griffith, S. Nandhra, C. O'Connor, S. Postlethwaite, K. S. Ryder and E. L. Smith, *Surface & Coatings Technology*, 2008, **202**, 2033-2039.

**Chapter 4: The Electrodeposition of Copper-Tin Alloys using Deep Eutectic Solvents**

**4.1 Introduction**

4.1.1 Cu-Sn alloy deposition in ionic liquids

**4.2 Results**

4.2.1 Cu-Sn phase diagram

4.2.2 The electrodeposition of Cu-Sn alloys

4.2.3 Cyclic voltammetry

4.2.4 Chrono amperometry

4.2.5 Analysis of Cu-Sn deposit using acoustic impedance (EQCM)

4.2.6 Phase formation XRD results

4.2.7 Large scale Cu-Sn deposition with brightener

4.2.8 Bronze dissolution/ electropolishing

**4.3 Conclusions**

**4.4 References**

## 4.1 Introduction

Electroplating of alloys from a solution containing different metal salts is relatively straight forward. In principle solid-solution phases (alloys) can be obtained by co-deposition where the composition of the alloy is determined by the ratio of metal ions in solution and the difference in redox potential. Copper–tin alloy electrodepositions are widely used in manufacturing and are being used in the development of new materials. They are suitable for producing high energy outputs, such as can be found in rechargeable lithium batteries.[1, 2] The majority of the literature about the coating and dissolution of this alloy was collected in the early stages of alloy development. One issue associated with the electrodeposition of these alloys from aqueous solution is the very toxic and corrosive species, such as thiocyanate or pyrophosphate.

In the previous chapter the deposition of a simple alloy was studied in which simple solid solutions were studied; either copper in silver or silver in copper. In this section the deposition of Cu-Sn alloys is studied in which separate distinct phases can be formed. It is the aim of this chapter to use the same complex combination of analytical techniques to elucidate the causes for the formation of different phases.

## 4.1.1 Cu-Sn Alloy Deposition in Ionic Liquids

The majority of Cu alloy research to date has focused on the imidazolium chloride ionic liquids. Sun and co-workers have carried out most of the work on copper alloys and the work was started with Cu-Zn alloy deposited from equimolar 1-ethyl-3-methylimidazolium: $ZnCl_2$ liquids.[3] The composition of the Cu-Sn alloy layers were investigated using a stable, non-flammable ionic liquid, trimethyl-n-hexylammonium bis[(trifluoromethyl)sulfonyl]amide, as a solvent for an electrolytic solution[4]. In addition, the temperature makes the deposition of alloys in ionic liquid faster than in aqueous solution. Also, Murase *et al.*[5, 6] demonstrated the deposition of a Cu-Sn alloy deposited on a non-conductive polymer substrate using the ionic liquid 1-ethyl-3-methylimidazolium bis (trifluoromethylsulfonyl) imide ([EMIM][$Tf_2N$]) at 150 ˚C in two baths, each containing one of the two different metal ions, $Cu^{2+}$ and $Sn^{2+}$. Murase *et al.* also discussed the formation mechanism of the inter-metallic phases and their reduction potential. In practice, these coatings are usually applied by controlling the cathode potential at a value that is substantially negative of the metal ion with the most cathodic reduction potential. This is intended to ensure that mass-transport is rate limiting for both

metal ions. Alternatively, it is possible to control the composition of the deposit by carefully controlling the applied potential to produce differential deposition kinetics but this method of kinetic control is however, notoriously unreliable. Despite the seductive simplicity of this approach the compositions of alloys and mixed phase deposits often bears no resemblance to the composition of the electrolyte from which they were deposited. This is often because of large differences in the redox potentials of the two metal ions, disparate electrode kinetics (slow ligand exchange or electron-transfer) or side reactions from the solvent or electrolyte.

It has been previously shown that the range of metal ion redox potentials is compressed in ionic liquids compared to the equivalent species in aqueous solution, and also that the potential window within ionic liquids is often much larger that aqueous electrolytes[7]. One example of this is the co-deposition of Al and Pt. In aqueous solutions these two metals would be separated by 2.86 V whereas in a mixture of $AlCl_3$, BTMACl and $PtCl_2$ the difference in redox potentials for the two metals of alloy was found to be 500 mV.[8] These combined observations have led to the expectation that ionic liquids can be used effectively for the electrolytic deposition of alloys from binary metal ion mixtures that would not be possible in conventional aqueous electrolytes. The electrodeposition of Cu using 1: 2 ChCl: EG or urea has been proven to be feasible.[9] It is possible to electrodeposit Cu-Sn alloy coatings in ionic liquids. Higher current efficiencies can be expected from depositing Zn-Sn alloy as demonstrated by Abbott and co-workers.[10]

## 4.2 Results

### 4.2.1 Cu-Sn phase diagram

Shim *et al.* [11] studied the phase behaviour of the Cu-Sn system and found good agreement between the thermodynamic data and phase equilibrium achieved experimentally. The phase diagram for the Cu-Sn system is shown in **Figure 4.1**.
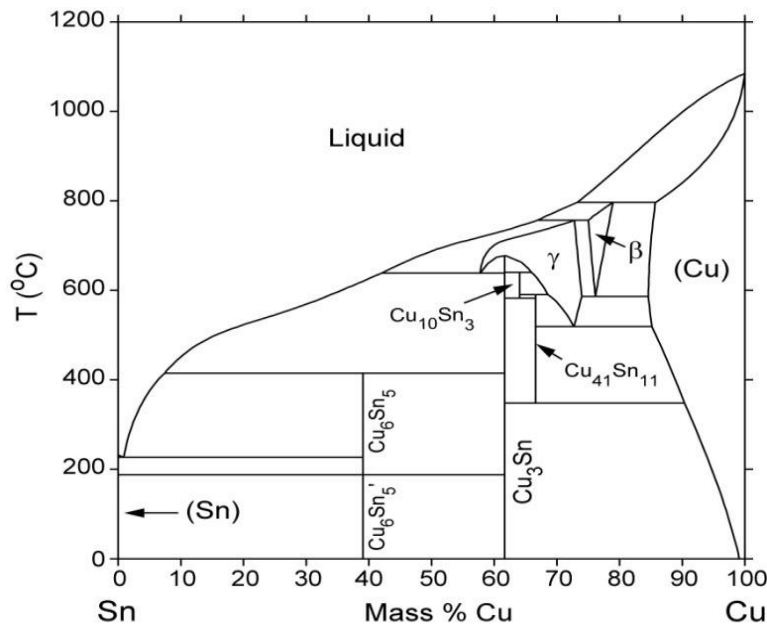
***Figure 4.1*** *The phase diagram for the Cu-Sn system. Image taken from ref.* [11]

In the Cu rich region the intermediate phases decompose in eutectoid reactions at temperatures above 350 °C. The eutectic reaction at 227 °C decomposes from a liquid into $Cu_6Sn_5$ and (Sn), while the equilibrium between the high (unstable stage) and low (stable stage) temperature transformation of $Cu_6Sn_5$ is 186 °C. If the temperature is close to room temperature, transformation does not happen quickly, because of kinetic constraints. However, when the temperature is around 150 ˚C, the transformation occurs relatively rapidly. [12]

### 4.2.2 The electrodeposition of Cu-Sn alloys

Copper and Cu-Sn alloys have received increasing interest in recent years due to their use in microelectronic applications and the development of the use of anodic materials in specific electrochemical reactions such as that found in lithium batteries. It is also a prevalent material in industrial applications primarily for its improved mechanical properties, alloy characterisation and corrosion resistance. The presence of tin is changes ductility, solderability, and low surface tension. The tensile properties of the resultant materials of copper tin are shown in **Table 4.1** below after heat treatment at 500 °C for 150 min in order to improve the yield strength and ductility.[13]

| | Cu / % | Sn / % | Impurities | 0.2% Yield strength / kPa | Tensile strength / kPa | Elongation / % |
|---|---|---|---|---|---|---|
| Cu-Sn alloys | 92.6 | 5.8 | 1.6 | 372 | 510 | 38 |
| | 95.5 | 4.4 | 0.1 | 186 | 331 | 48 |
| | 94.7 | 5.2 | 0.1 | 165 | 352 | 51 |

***Table 4.1*** *the properties of Cu-Sn alloys as a function of tin composition. Ref.* [13]

**4.2.3 Cyclic voltammetry**

The electrochemistry of both Cu and Sn have been studied independently in both ionic liquids. **Figures 4.2 a and c** show cyclic voltammograms of pure $CuCl_2 \cdot 2H_2O$ and $SnCl_2 \cdot 2H_2O$ in 1: 2 ChCl: ethylene glycol (Ethaline) mixture. **Figures 4.2 b and d** show the corresponding voltammograms in 1: 2 ChCl: urea (Reline). The voltammogram recorded in Ethaline show only a single reduction peak, arising from the reduction of $Sn^{2+}$ to Sn metal and a single oxidation peak of the metal being oxidised back to $Sn^{2+}$. The peak potentials for these two processes are at around -0.4 V and -0.2 V, respectively. Whereas in **Figure 4.2d** similar peaks are shown for the reduction and oxidation of tin, but these peaks are shifted to negative values of around -0.45 V and -0.25 V, respectively when using 1: 2 ChCl: urea. In addition, the voltammogram of copper in **Figures 4.2 (a and b)** shows four waves in Ethaline or Reline according to $Cu^{2+}/ Cu^{+}$ and $Cu^{+}/ Cu$, as mentioned in **Chapter 3**.

In order to determine the average cathodic and anodic peaks charge as shown in **Figures 4.2** are listed in **Table 4.2** and the ratio $Q_a/Q_c$ in **Figure 4.3**. The total cathodic and anodic charge of the pure $CuCl_2 \cdot 2H_2O$ in Reline is larger than pure $SnCl_2 \cdot 2H_2O$, whereas the total cathodic and anodic charge peak of pure $SnCl_2 \cdot 2H_2O$ in Ethaline is higher than $CuCl_2 \cdot 2H_2O$. In order to probe the effect upon kinetics and composition of the Cu-Sn deposit during growth, three different mixed metal compositions have been examined have been examined in addition to the pure Cu and Sn metals solution. These three cases are in molar ratios as follows; 1: 1, 0.3: 1 and 1: 0.3. Hence one case is a Cu rich system, one Sn rich and the 1: 1 equimolar amounts of $Cu^{2+}$ and $Sn^{2+}$ ions are present in the third Ethaline solution. The cyclic voltammograms of

various molar ratios of $CuCl_2 \cdot 2H_2O$ and $SnCl_2 \cdot 2H_2O$ dissolved in Ethaline and Reline are presented in **Figure 4.2.**
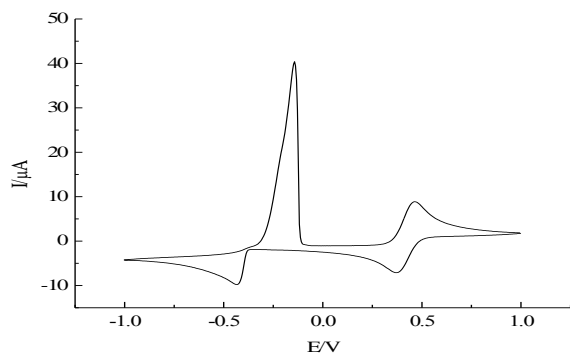
a) 0.1 mole dm$^{-3}$ CuCl$_2 \cdot$2H$_2$O in Ethaline
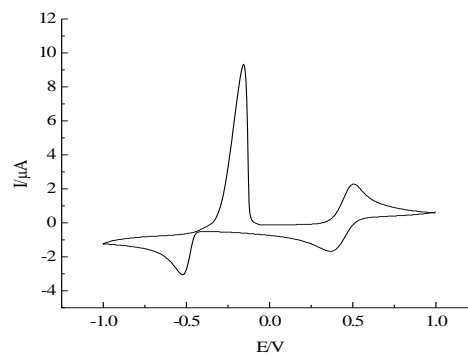
b) 0.1 mole dm$^{-3}$ CuCl$_2 \cdot$2H$_2$O in Reline
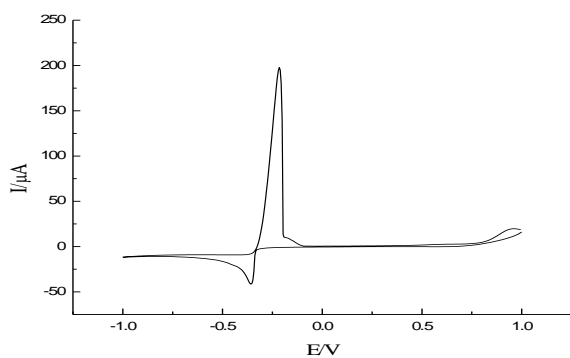
c) 0.1 mole dm$^{-3}$ SnCl$_2 \cdot$2H$_2$O in Ethaline
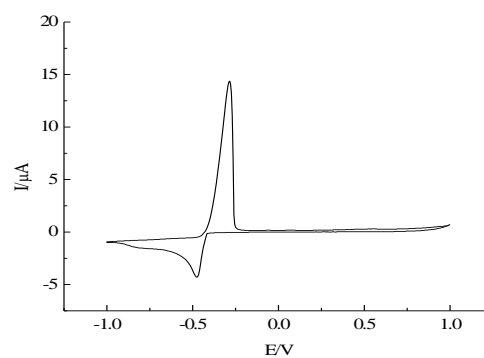
d) 0.1 mole dm$^{-3}$ SnCl$_2 \cdot$2H$_2$O in Reline

**Figure 4.2** *Voltammogram scan rate 5 m V s$^{-1}$ for a Pt as a working electrode (dia. 0.5 mm) using a silver wire pseudo reference electrode immersed in both Ethaline and Reline containing a and c) 0.1 mole dm$^{-3}$ CuCl$_2 \cdot$2H$_2$O and b and d) 0.1 mole dm$^{-3}$ SnCl$_2 \cdot$2H$_2$O.*

|  | Ethaline | | Reline | |
| --- | --- | --- | --- | --- |
|  | $Q_c$ (mC) | $Q_a$(mC) | $Q_c$ (mC) | $Q_a$ (mC) |
| 1: 1Cu: Sn | 11.10 | 10.10 | 3.46 | 3.06 |
| 0.3: 1 Cu: Sn | 8.37 | 8.64 | 4.07 | 3.40 |
| 1: 0.3 Cu: Sn | 4.47 | 4.61 | 1.84 | 1.92 |
| Pure Cu | 1.33 | 1.80 | 0.37 | 0.46 |
| Pure Sn | 2.35 | 1.96 | 0.32 | 0.30 |

**Table 4.2** *Total cathodic and anodic charge density of the three systems Cu-Sn alloys with pure Cu and Sn in two ionic liquids Ethaline and Reline.*
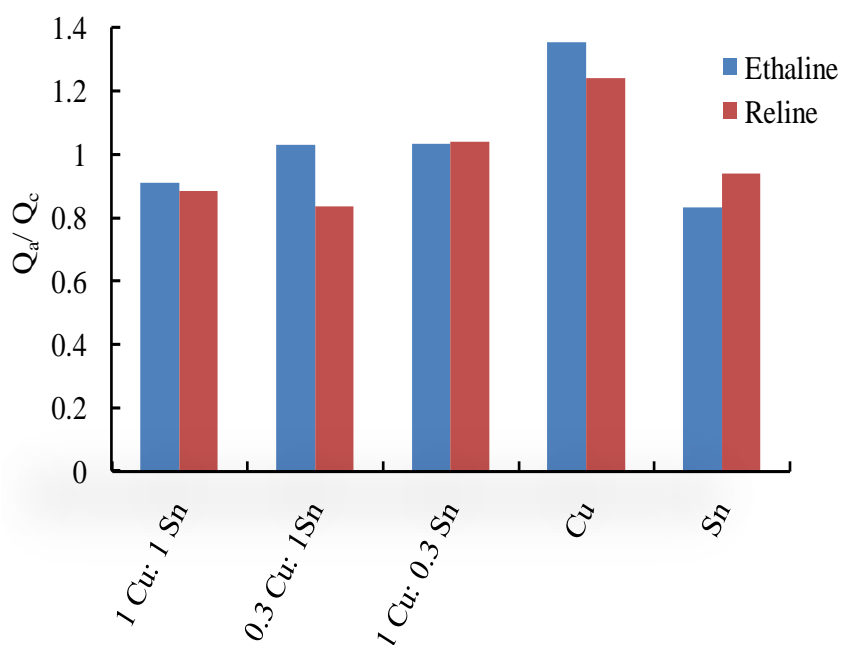


**Figure 4.3** *Ratio of the anodic and cathodic total charge peak of pure Cu, Sn and 1: 1 Cu: Sn, 0.3: 1 Cu: Sn and 1: 0.3 Cu: Sn in Ethaline and Reline ionic liquids. The results were obtained from data presented in **Figures 4.2 and 4.4***
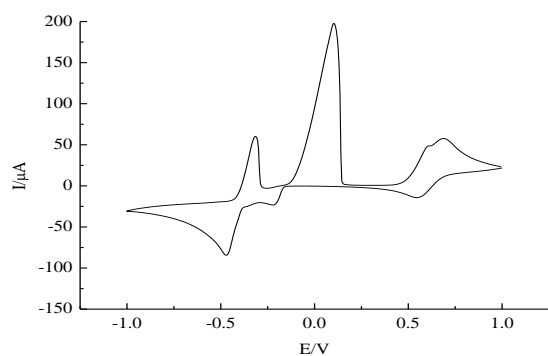
*a)  1 Cu: 1 Sn Ethaline*
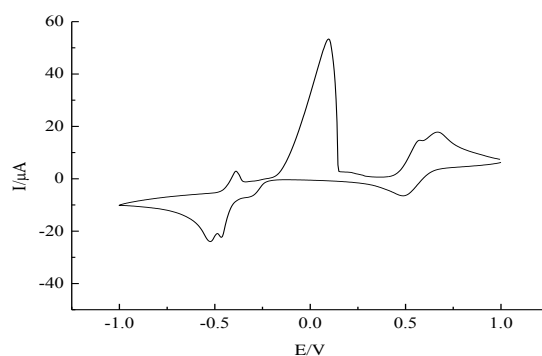
*b)  1 Cu: 1 Sn Reline*
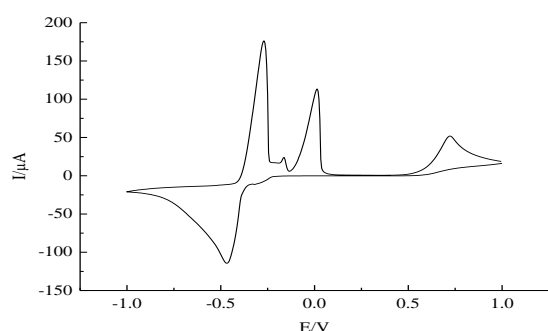
c)  *0.3 Cu: 1 Sn Ethaline*
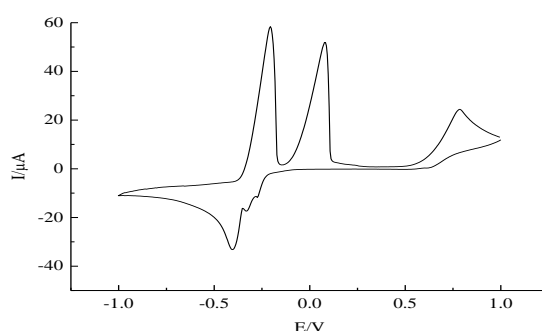
d)  *0.3 Cu: 1 Sn Reline*
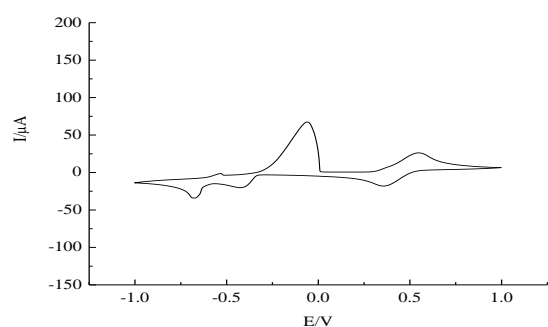
*e)   1 Cu: 0.3 Sn Ethaline*
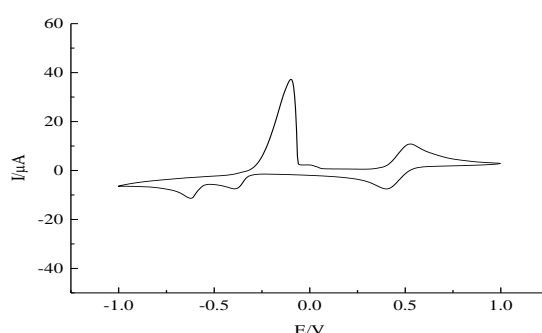
*f)   1 Cu: 0.3 Sn Reline*

**Figure 4.4** *Cyclic voltammograms of a, b) equimolar 1 $CuCl_2 \cdot 2H_2O$: 1 $SnCl_2 \cdot 2H_2O$, c, d) 0.3 $CuCl_2 \cdot 2H_2O$: 1 $SnCl_2 \cdot 2H_2O$, e, f) 1 $CuCl_2 \cdot 2H_2O$: 0.3 $SnCl_2 \cdot 2H_2O$, in different bath Ethaline and Reline at a Pt disk working electrode (dia. 0.5 mm) using a silver wire pseudo reference electrode.  Potential scan rates, v, at 5 mV s$^{-1}$.*

Due to the limited solubility of $SnCl_2$ in Ethaline concentrations of 0.10 mole dm$^{-3}$ and 0.03 mole dm$^{-3}$ were chosen to achieve these molar ratios. Unlike the Cu/Ag alloy studied in the preceding chapter the redox potentials of both metals were almost identical.  This contrasts with the standard aqueous redox potentials for $Cu^{2+}$/ Cu and $Sn^{2+}$/ Sn which are 0.35 V and - 0.14 V verses saturated hydrogen electrode (SHE).

88

Cyclic voltammetry data for the three Cu-Sn mixtures on a Pt wire substrate in Ethaline is presented in **Figure 4.4**. In Ethaline the voltammogram of the equimolar mixture ($1CuCl_2 \cdot 2H_2O$: $1SnCl_2 \cdot 2H_2O$) shows that separate redox processes can be clearly seen (**Figure 4.4a**). Deposition and stripping of Cu occurs at a potential centred about - 0.10 V, while deposition and stripping of Sn occurs at a potential centred about - 0.40 V. The reversible solution couple $Cu^{2+/+}$ is seen at a potential of + 0.65 V. This voltammogram clearly shows two anodic stripping peaks, Sn - 0.35 V and Cu, + 0.10 V. Hence it is clear that both metals are deposited but there is no evidence of a single alloy phase, although there is a separate peak on the $Cu^{2+/+}$ anodic wave that also appears more clearly in the voltammogram of the 1 $SnCl_2 \cdot 2H_2O$: 0.3 $CuCl_2 \cdot 2H_2O$ mixtures (**Figure 4.4c**).

The CV presented as **Figure 4.4c** for the Sn rich mixture also shows a two phase stripping response for both ionic liquids, although there is an additional anodic stripping peak at -0.15 V that is probably a mixed (alloy) phase in 1: 2 ChCl: ethylene glycol only. This is, however, very small by comparison. The significance of the irreversible wave at +0.75 V is unresolved. In contrast the voltammogram presented as **Figure 4.4e** shows a single dominant anodic stripping peak. Furthermore, in **Figure 4.4a, c and e** when those voltammogram is compared with that of the pure Cu system (**Figure 4.2a**) (using the reversible $Cu^{2+/+}$ couple as an internal reference), **Figure 4.4a, c and e** shows that these anodic responses are at a potential that does not correspond to the pure Cu stripping as mentioned above. At this point it should be noted that the shift in the $Cu^{2+/+}$ potential is larger than that would be predicted using the Nernst Equation. It has recently be shown that the $Cu^{2+/+}$ couple shows an ideal Nernstian behaviour up to 1 mol $kg^{-1}$. This would mean that a change in $Cu^{2+}$ concentration from 0.03 to 0.1 mol kg should result in a shift in redox potential of 26 mV. The shift in redox potential observed in **Figure 4.5** is larger than that predicted and could result from a number of causes, the most likely being a difference in the concentration of $Cu^{+}$.

Interestingly the relative peak heights of the cathodic deposition waves for both $Sn^{2+}$ and $Cu^{2+}$ do not follow an intuitive trend (**Figure 4.4e**). This is probably because of the disparity between the kinetics of deposition for Cu on Sn and Sn on Cu. For example, it is known that Cu is not very soluble in Sn metal, whilst Sn, on the other hand, is very soluble in Cu. This is discussed in more detail later in this chapter.
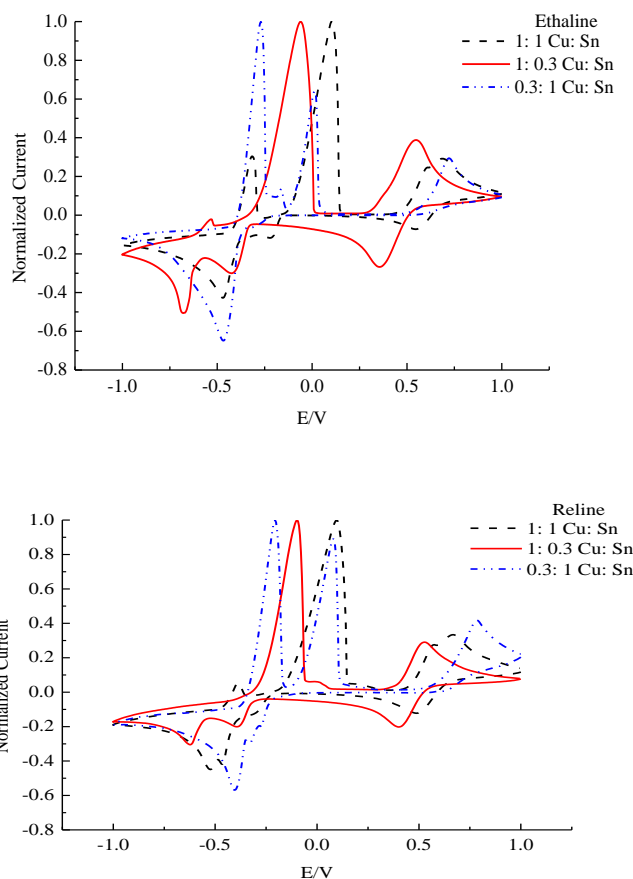
**Figure 4.5** *Normalized CVs of the same samples in* **Figure 4.4.**

The CV data for Cu-Sn mixtures on a Pt wire substrate in Reline is presented in **Figure 4.4b, d and f**. In the voltammogram of the equimolar mixture ($1CuCl_2 \cdot 2H_2O$: $1\ SnCl_2 \cdot 2H_2O$) in Reline, all the redox processes can be clearly seen in the Ethaline based ionic liquid. The deposition and stripping of Cu occurs at a potential centred about - 0.10 V, while the deposition and stripping of Sn occurs at a potential centred about - 0.40 V. The reversible solution couple $Cu^{2+/+}$ is seen at a potential of + 0.65 V. This voltammogram clearly shows two anodic stripping peaks, Sn - 0.35 V and Cu, + 0.10 V. The voltammogram of the Cu rich solution using Reline has two peaks in the reduction wave, with one peak on the oxidative wave, indicating that not all of the deposited Sn could be stripped during the anodic scan. This behaviour is different from that which was observed for the electrodeposition and stripping of the Cu rich solution with Ethaline.

All the plots in **Figure 4.4** have been normalized and these are shown in **Figure 4.5** where it is clear to see that the maximum current occurs at different potentials even taking into account the shift in the reference potential. It can be seen that the overall voltammetric behaviours are strongly dependent on the metal composition in both solutions. In the Cu rich

solutions the reduction and oxidation peaks move to more negative whereas in the Sn rich solutions the potentials move to more positive potentials in both ionic liquids.

In addition, the total charge of the Cu rich system is $Q_c$ = 4.47 mC and $Q_a$ = 4.61mC in Ethaline and $Q_c$ = 1.84 mC and $Q_a$ =1.92 mC in Reline as shown in **Table 4.1**. Comparing these total charge values, as shown in **Figure 4.4**, with the total charge of pure Cu in two systems, it is clearly found that pure Cu system has a lower charge than the Cu-Sn alloys with sharp stripping peak as shown in **Figure 4.2**, also for pure tin. The ratio $Q_a/Q_c$ of Cu and Sn rich in Ethaline are equal but at Reline the Cu rich is higher than Sn rich as shown in **Figure 4.3.** Also for pure Cu shows the highest ratio in both solutions compared with the pure Sn and the other three Cu/ Sn composite. **Figure 4.6** shows the charge cathodic ($Q_c$) versus charge anodic ($Q_a$) plot, found the highest value for equimolar Cu-Sn alloy at Ethaline but the highest value for Sn rich in Reline.

Tin, copper and tin–copper alloys were electrodeposited from a methanesulfonic acid electrolyte containing a perfluorinated cationic surfactant at room temperature was studied by Low.[14] The electrolyte composition was containing $SnSO_4$, $CuSO_4$, $CH_3SO_3H$, hydroquinone and perfluorinated cationic surfactant.
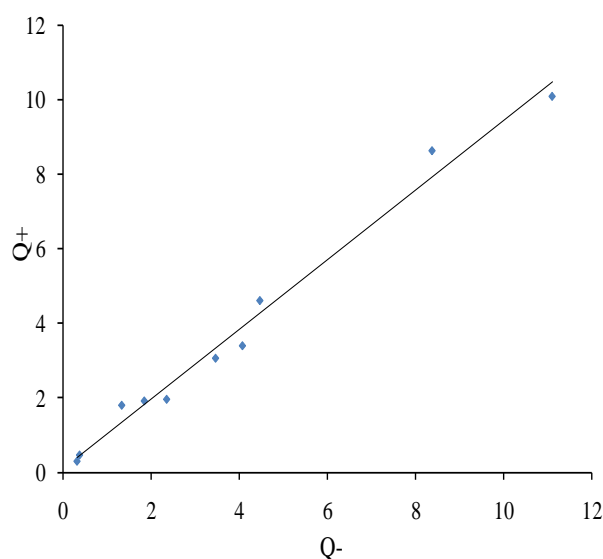


*Figure 4.6 The total charge of cathodic for pure Cu, pure Sn and the three systems (equimolar 1 CuCl₂·2H₂O: 1 SnCl₂·2H₂O, 0.3 CuCl₂·2H₂O: 1 SnCl₂·2H₂O, and 1 CuCl₂·2H₂O: 0.3 SnCl₂·2H₂O, verses the total charge of anodic for the same three systems in both systems Ethaline and Reline.*

Cyclic voltammetry and linear sweep voltammetry were used to examine the current-potential relationships at static and rotating disc electrodes. Sn-Cu alloys were deposited over a wide range of operating conditions. From the cyclic voltammetry of Cu-Sn alloy the two

peaks of reduction were clearly shown when the alloy was deposited on the 316 stainless steel disc electrode.Compare this result to cyclic voltammograms of Cu-Sn using ionic liquids presented in Figure 4.4 was achieved very close but with low potential window in aqueous solution.[15] Also shown the same idea the peaks of Cu-Sn alloy were moved to more negative potential compare to Cu and Sn deposition as shown in Cu-Sn alloy deposition from Ethaline or Reline. According to [2], the electrodeposition of copper, tin and Cu-Sn alloys has been studied by cyclic voltammetry chronoamperometry, scanning electron microscopy and energy dispersive X-rays in the solution containing metallic ions with 0.3 mol dm$^{-3}$ Na$_4$P$_2$O$_7$ and 2.3 mol dm$^{-3}$ HCl. The voltammograms shows the three systems reduction processes was under diffusion controlled. At rich copper, the results were similar to the ones obtained for copper, only that now the second current peak has no dependence on the potential inversion.

### 4.2.4 Chronoamperometry

The current–time transients obtained for pure SnCl$_2$·2H$_2$O deposition from Ethaline are shown in the Appendix **Figure 7.3**. In this case, the first changes to the current are attributed to the double layer charge then immediately afterward, the typical response of nucleation and growth takes place. The data were fitted to the Sharifker-Hills [16] model shown in **Equations 3.2** and **3.3**. The dimensionless plot for the nucleation of tin in **Figure 4.7a** is almost identical to the plot for copper shown in **Figure 3.4a** in the previous chapter. There are few systems to compare this result to in ionic liquids but a study of tin nucleation in aluminium chloride -1-methyl-3-ethylimidazolium chloride gave a very similar response.[17] The results are slightly different when tin is deposited from aqueous solutions, where the nucleation and growth mechanisms stay at instantaneous, as reported in a previous study.[2] This aspect of the chronoamperometry of Cu-Sn alloys is discussed in greater detail later in this chapter.

Abbott and co-workers recently analysed all of the nucleation reports for metals in ionic liquids.[18] They found that electronegative metals such as Zn & Al always tended to show progressive nucleation, and metals such as silver and that of Cu & Sn was somewhere in between. This was ascribed to the structure of the double layer and that, particularly, the presence of bulky cation below the potential of zero charge.

### *Chrono amperometry of copper-tin alloys*

**Figure 4.7** (raw data are given in the Appendix **Figure 7.4**) shows the current–time transients for three systems of copper-tin alloys electrodeposited from Ethaline at different potentials.
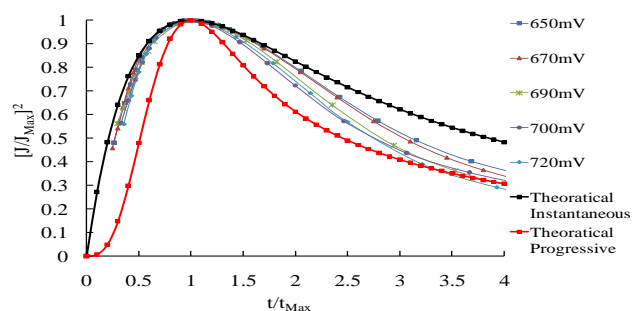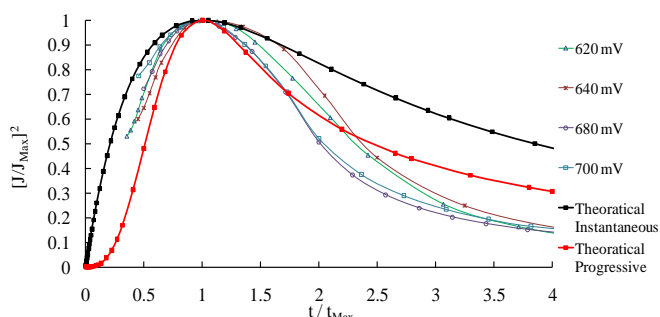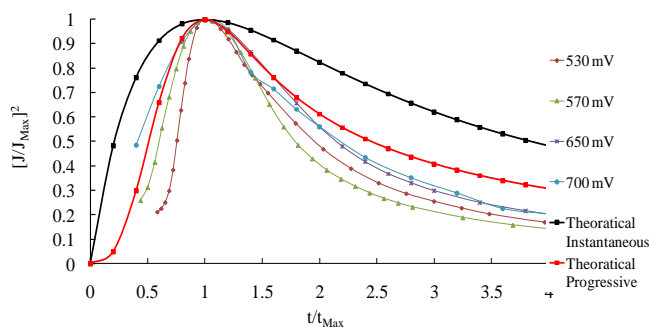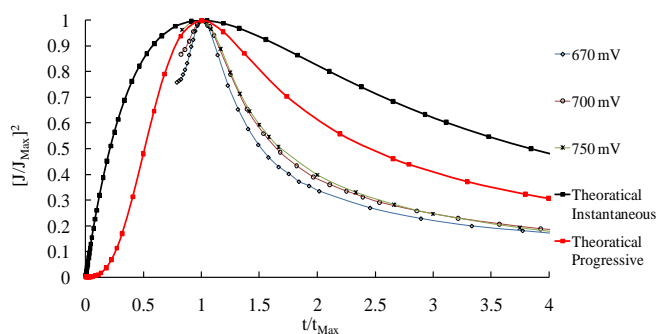
***Figure 4.7*** *Comparison of the dimensionless and theoretical chronoamperometric curves of*
***a)*** *0.1 mole dm$^{-3}$ SnCl$_2$·2H$_2$O **b)** equimolar 1 CuCl$_2$·2H$_2$O: 1 SnCl$_2$·2H$_2$O, **c)** 0. 3
CuCl$_2$·2H$_2$O: 1 SnCl$_2$·2H$_2$O and **d)** 1 CuCl$_2$·2H$_2$O: 0.3 SnCl$_2$·2H$_2$O from Ethaline. Applied
potentials all negative.*

Firstly, at equimolar concentrations the nucleation corresponds to an instantaneous
mechanism, followed by a progressive mechanism at the end. In the other two cases, the
transients recorded using Cu$^{2+}$ rich solutions could be reproduced but with poorly fitting

nucleation curves, while for the rich $Sn^{2+}$ solutions, the best fittings correspond to a progressive nucleation process.

**Figure 4.7** shows theoretical plots and experimental curves for three systems Cu-Sn alloy nucleation on Pt at different of potentials. Given that the two individual metals nucleate by a similar mechanism it could be expected that a combination of the two metals, particularly if they form a solid solution should grow nuclei by a similar mechanism. It can be seen that at 0.3 Cu: 1 Sn and 1 Cu: 0.3 Sn, the experimental curves deviate quite significantly from either nucleation mechanism. Comparing the results with those in **Figure 3.4**: in silver-copper alloys increasing the copper composition changes the mechanism from progressive to instantaneous whereas with copper-tin it is only when the metal concentrations are roughly equal that the mechanism resembles either nucleation mechanism

## 4.2.5 Analysis of Cu-Sn deposit using (EQCM)

In the previous chapter it has been shown that EQCM can be used to determine alloy composition during deposition. In the case of Cu/ Sn clearly both metals are in the M(II) state but fortunately these metals have very different molar masses.

Electrochemical acoustic impedance, EQCM, data were gathered from deposition of the pure metals phases together with those from the three different mixtures. The raw and processed data for pure Cu and pure Sn deposition at a fixed potential of - 0.75 V are shown in **Figure 4.8a and b**. The centre frequency of the admittance (admittance is the reciprocal of impedance) spectra, **Figure 4.8a and b** moves to a lower value as Cu or Sn is deposited. This is indicative of increased mass. In addition, and most importantly, the shape and intensity of the spectrum remains mostly unchanged. Under these circumstances the frequency change can be converted to an equivalent mass, $\Delta m$, using the Sauerbrey equation[19]. A plot of deposited mass, $\Delta m$, *versus* Faradaic charge, $Q$, passed during electrolysis is presented in **Figure 4.8c**. Comparing the slope (linear regression) of these data with the Faradaic ratio, *ram*$_{Cu}$/ *2F,* gives a current efficiency of 99.9 % for Cu deposition.

Consequently Cu behaves as a model metal under these circumstances. Deposition of pure Sn also yielded essentially quantitative current efficiencies but over smaller time scales. For example at an applied potential of -0.75 V for 246 s the current efficiency (from the plot of *Δm verus Q*) was determined as 94.5 % as shown in **Figure 4.8c**. At longer time scales, however, the *Δm (Q)* plots were no longer linear.
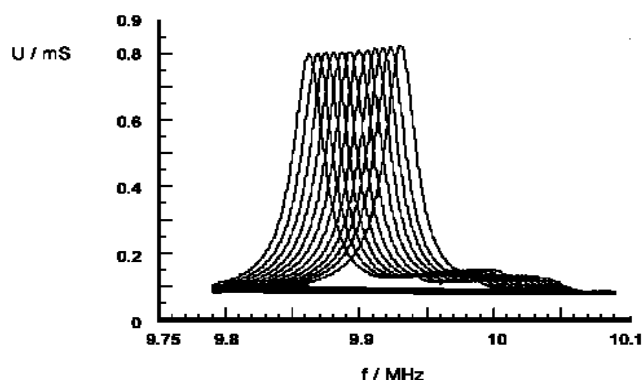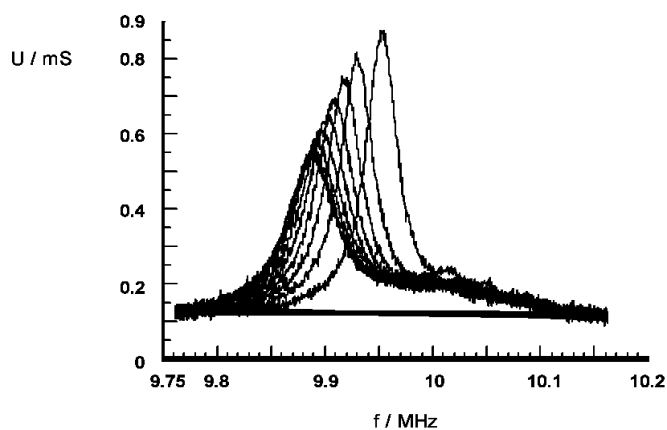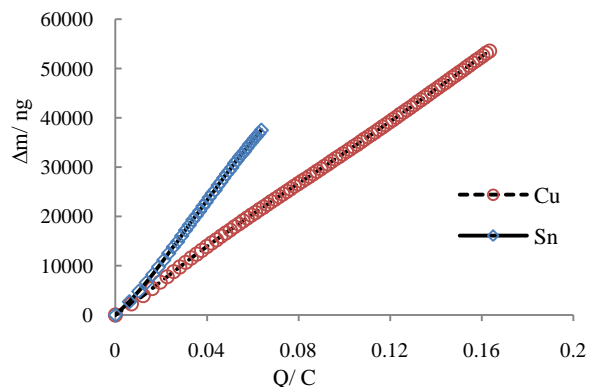
**Figure 4.8** *Electrochemical acoustic impedance (EQCM) data for Cu & Sn deposition on a Au coated quartz crystal over a time period of 560 s & 246 s respectively; (**a and b**) raw admittance spectra (U = 1/ Z) every $20^{th}$ spectrum is shown, (**c**) processed peak frequency data (obtained by fitting or spectra in part (**a**)) displayed as deposited mass, $\Delta m/ ng$ versus charge, Q/ c. The slope of the best fit linear regressions of Cu (circle) & Sn (square) was $3.291 \times 10^{-4}$ g $c^{-1}$ & $5.846 \times 10^{-4}$ g $c^{-1}$ with $r^2 = 0.999$ & $0.945$ respectively.*

This is because of progressive surface roughening as a consequence of the Sn deposit. This causes damping of the crystal resonance and makes the device less sensitive, or more ineffective, as a gravimetric sensor. For the co-deposition of metals it can easily be shown

that, as a consequence of Faraday's law, the slope of the $\Delta m$ $(Q)$ plots is a linear sum of contributions from both metals present in the deposit. This is shown in for the Cu-Sn system in **Equation 4.1**.

$$\frac{dm}{dQ} = \frac{X_{Sn}.ram_{Sn} + (1 - X_{Sn}).ram_{Cu}}{2F}$$

(4.1)

It follows that the experimental slope, $d(\Delta m)/dQ$, of the $\Delta m$ $(Q)$ plot is a measure of the average composition according to **Equation 4.2** (where $X_{Sn}$ is the mole fraction of Sn and $X_{Cu}$ is the mole fraction of Cu in the alloy such that, $X_{Sn} + X_{Cu} = 1$, $ram_{Sn}$ and $ram_{Cu}$. correspond to the relative atomic masses of Sn and Cu respectively).

$$X_{Sn} = \frac{\left\{\frac{d(\Delta m)}{dQ}\right\}.2F - ram_{Cu}}{ram_{Sn} - ram_{Cu}}$$

(4.2)

Furthermore the sensitivity of such a measurement is maximised where the difference between the relative atomic masses ($ram$) is large. This is clearly the case for the Cu-Sn system where $ram_{Sn}$ and $ram_{Cu}$ are 118.71 and 63.55 g mol$^{-1}$ respectively.

The data for the equimolar mixture, **Figure 4.9** (*black*) show a quasi linear response but it is clear that there is some variation to the slope as a function of charge passed (time). SEM is used to study the morphology of the deposition on gold crystal as shown in **Figure 4.10a**. In addition to this, the data for the Sn rich mixture, **Figure 4.9**(*blue*) are linear only at the very beginning of deposition (*i.e.* small $Q$ and short $t$) but otherwise show a continual drop in mass deposited for a given charge. In order to progress the analysis of these data the equivalent differential plots, expressed as composition of alloy ($X_{Sn}$), using **Equation 4.2**, are presented in **Figure 4.11**.

The data presented in **Figure 4.9** show the $\Delta m$ $(Q)$ plots for the three mixed metal systems; here it is clear that the Cu rich system shows a good linar response. The slope of the best fit linear regression to these data is $3.71 \times 10^{-4}$ g C$^{-1}$, giving a composition of $X_{Sn} = 0.15$, according to **Equation 4.2**.
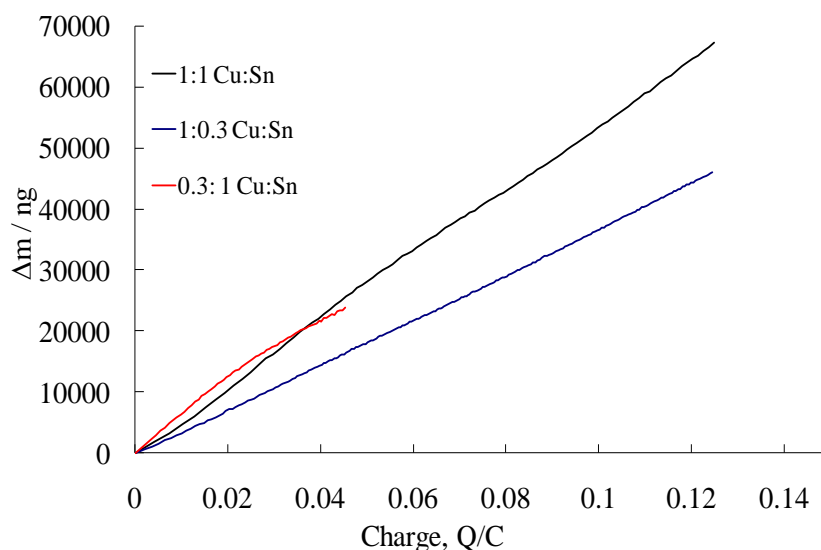
***Figure 4.9** Mass versus charge plots for alloy deposition using acoustic impedance electrochemical QCM; equimolar 1 $CuCl_2 \cdot 2H_2O$: 1 $SnCl_2 \cdot 2H_2O$ (black), 0.3 $CuCl_2 \cdot 2H_2O$: 1 $SnCl_2 \cdot 2H_2O$ (red), 1 $CuCl_2 \cdot 2H_2O$: 0.3 $SnCl_2 \cdot 2H_2O$, (blue) from Ethaline. Time scales, t, for the deposition data shown are 635 s, 440 s and 1607 s respectively. The potential was stepped from O.C.P and held at -0.75 V and Ag wire as a reference electrode*

These plots are quite noisy, as is often the case for differential data; however several important features can be easily determined. First, the good linear fit for the Cu rich data is reflected in **Figure 4.11** (*red*) in a fairly constant value of $X_{Sn}$, centred around $X_{Sn} = 0.15$. This response is reasonably gratifying and represents the first good evidence that a homogeneous composite phase (alloy) is being deposited under these conditions.

In contrast the trace for deposition from the equimolar mixture, **Figure 4.11** (*black*), varies widely between $0.4 < X_{Sn} < 1.0$. Also the response of the Sn rich system, **Figure 4.11** (*blue*), is very variable. In both these cases it seems clear that either the current efficiency of the systems is very low (*i.e.* charge passed without mass deposited) and that the quartz crystal is not functioning as a gravimetric sensor because of mechanical losses due to damping of the crystal resonance.
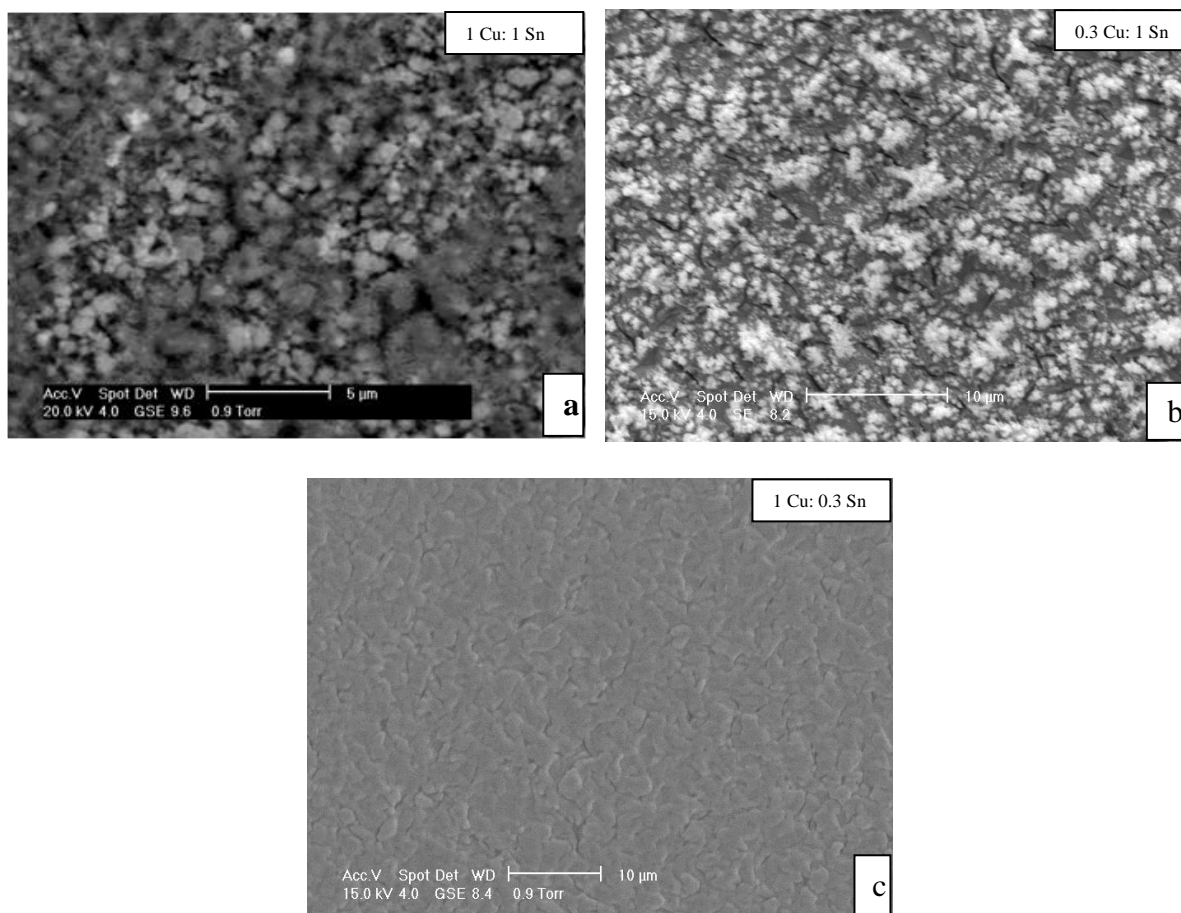
***Figure 4.10*** *SEM of Sn-Cu deposit on a Au coated QCM crystal; plated at – 0.75 V (constant potential) from an Ethaline solution containing at **a**) 1 CuCl$_2$·2H$_2$O: 1 SnCl$_2$·2H$_2$O, **b**) 0.3 CuCl$_2$·2H$_2$O: 1 SnCl$_2$·2H$_2$O, **C**) 1 CuCl$_2$·2H$_2$O: 0.3 SnCl$_2$·2H$_2$O.*

This latter effect is quantified by the Q factor (broadness) of the crystal resonance[20] and is probably caused by roughening of the surface as the metal deposit grows. Having already established (at least for short times) that the current efficiency for both Sn and Cu deposition on the Au substrate are essentially quantitative it is important to understand the deposition of Sn on Cu and similarly, Cu on Sn in an analogous manner to that already done with Cu and Ag in the previous Chapter.
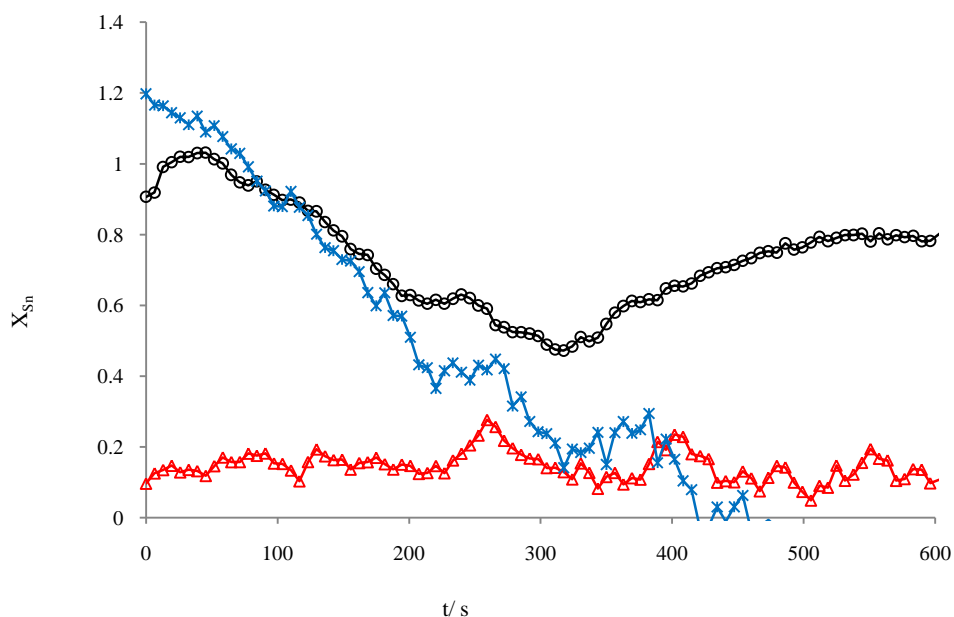
***Figure 4.11*** *The calculated mole fraction of Sn in Cu-Sn deposits obtained from 1 CuCl$_2$·2H$_2$O: 1 SnCl$_2$·2H$_2$O (black circle), 0.3 CuCl$_2$·2H$_2$O: 1 SnCl$_2$·2H$_2$O (blue star) and 1 CuCl$_2$·2H$_2$O: 0.3 SnCl$_2$·2H$_2$O (red triangle) in Ethaline plotted as a function of potential time scale. The depositions were carried out at a constant potential of - 0.75 V (vs. Ag wire) at room temperature.*

|  | **Solution composition** | | |
|---|---|---|---|
|  | $X_{Sn} = 0.5$ | $X_{Sn} = 0.77$ | $X_{Sn} = 0.23$ |
| **% Sn by EDAX** | 25 | 71 | 23 |
| **% Sn by EQCM** | 64 | 83 | 13 |

***Table 4.3*** *Sn mole fractions of the deposits obtained by deposition at -0.75 V from the EQCM technique compared with EDAX analysis of the same deposits.*

The comparative compositions of the alloy deposits obtained during the EQCM experiments were also analysed using EDAX. A comparison between the Sn content of the deposits estimated using **Equation 4.2** and the Sn content measured by EDAX is presented in **Table 4.3.** The co-deposit compositions monitored using the EQCM are quite close at rich Sn to the values obtained by EDX analysis.

The raw impedance data for deposition of Sn on Cu are shown in **Figure 4.12**. In the latter phases, both *f* and *Q* remain more or less constant; hence many of the spectra are overlaid. A more concise representation of the considerable quantity of data acquired during this experiment is presented in **Figure 4.13**. Here both the current data, *i*(*t*), and peak shape data,

$Q(t)$, are represented on the same synchronous 3D axis, $i(Q,t)$. Here it can be seen that a rapid drop in $Q$ corresponds with the initial decay in current, $i$, but that after, $t = 200$ s, when the current starts to grow, corresponding to bulk metal deposition, $Q$ remains fairly constant at around 130. During this time period the frequency of the crystal resonance also remains fairly constant.
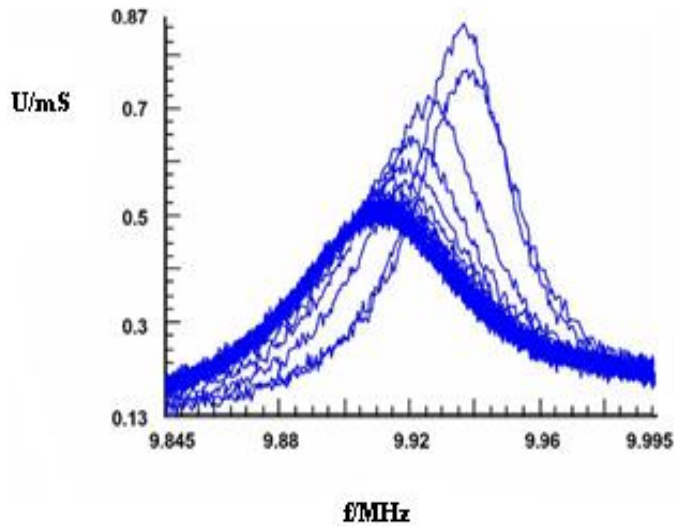


**Figure 4.12** *Acoustic impedance plot (U = 1/ Z) for deposition of Sn metal on a Cu coated crystal in Ethaline. Every 5th spectrum is shown, with ca 6 s between spectra.*
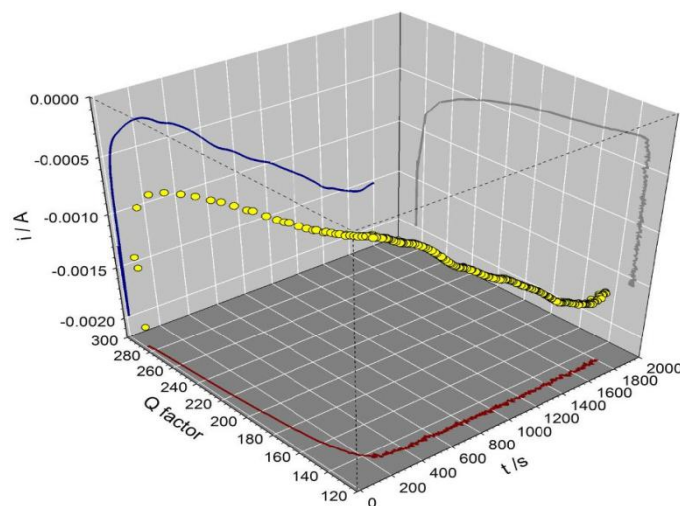


**Figure 4.13** *3D plot of i (Qₛt) (yellow circles) for deposition of Sn metal on a Cu coated QCM crystal from Ethaline. 2 D projections are also shown for clarity, Q (t) (red), i (t) (blue) and i (Q) (grey).*

This is strong indication that surface roughening occurs rapidly during the initial phases of Sn deposition and that as a consequence of the rough surface the outside extrema of the deposit are mechanically decoupled from the quartz crystal. A similar, although less dramatic, picture is seen for the deposition of Cu onto a Sn coated substrate. The raw impedance data are presented in **Figure 4.14**, with the corresponding $i$ $(Q,t)$ plot shown in **Figure 4.15**. Here the frequency trend persists throughout the experiment but the peak continues to become broader as the resonant frequency drops. The trend here is similar to that shown in **Figure 4.12** but the mechanical damping and concomitant losses are less extreme. This is seen clearly in the 3D plot, **Figure 4.15**, where the initial drop in $Q_s$ associated (synchronous) with the transient current decay, is less rapid. Subsequently the value of $Q$ continues to drop during the bulk metal deposition phase where current is increasing. During this period the measured resonant frequency also continues to drop.
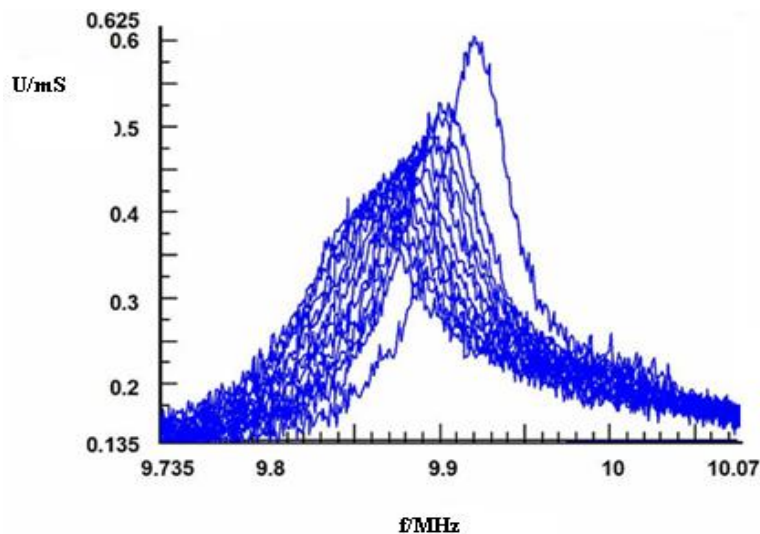


***Figure 4.14*** *Acoustic impedance plot (U = 1/ Z) for deposition of Cu metal on a Sn coated crystal in Ethaline. Every 20th spectrum is shown, with ca 6 s between spectra.*

Whilst the latter observation is consistent with deposition of Cu on the Sn surface the current efficiency cannot be determined from these data because a quantitative relation between frequency and deposited mass is precluded by the increase in $Q$, peak broadening, due to mechanical losses.
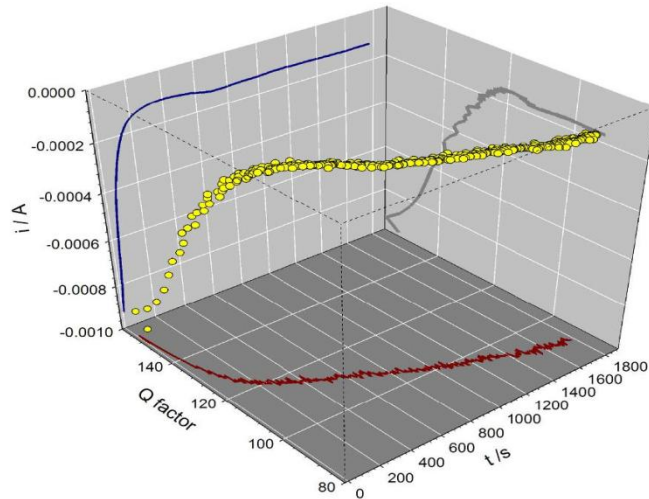
***Figure 4.15*** *3D plot of i (Q,t) (yellow circles) for deposition of Cu metal on a Sn coated QCM crystal from Ethaline. 2D projections are also shown for clarity, Q (t) (red), i (t) (blue) and i (Q) (grey).*

Once again these losses are probably the result of surface roughening, although to a lesser extent than has been observed for Sn on Cu (above). In fact, here it is likely that the initial Sn substrate surface was sufficiently rough to dominate subsequent growth.

This data can be contrasted with the near-ideal behaviour of the Cu rich system. The raw impedance data for Cu rich alloy are shown in **Figure 4.16** and the corresponding *i (Q,t)* plot is presented as **Figure 4.17**. Here the raw spectra show a clear and monotonic peak frequency trend throughout the experiment, whilst the shape of the crystal resonance does not change appreciably. These data are very similar to the pure copper data shown in **Figure 4.8a**.
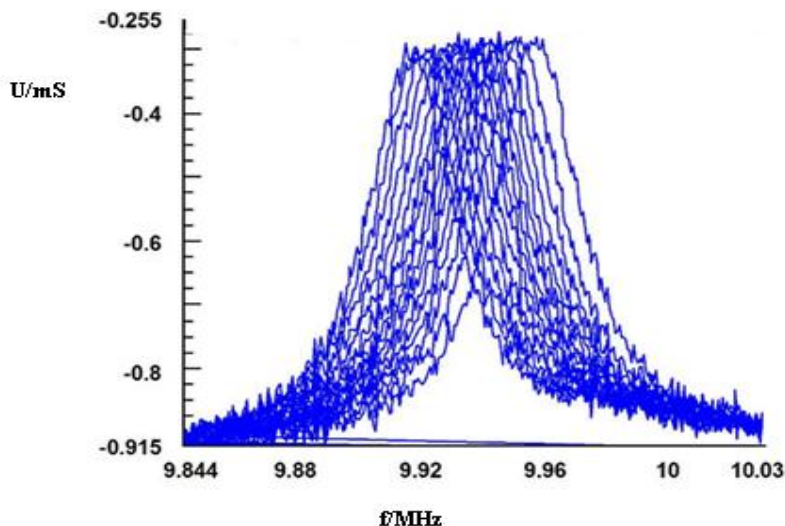


***Figure 4.16*** *Acoustic impedance plot (U = 1/ Z) for deposition of Cu-Sn alloy on a Au coated crystal in Ethaline (1 CuCl$_2$·2H$_2$O: 0.3 SnCl$_2$·2H$_2$O) under potentiostatic control at - 0.75 V versus Ag wire. Every 10th spectrum is shown, with c.a. 6 s between spectra.*

Similarly, a close examination of **Figure 4.17** reveals that the Q factor for this experiment remains essentially independent of current and time throughout the course of the deposition. Consequently this analysis demonstrates that the compositional profiles calculated for alloy deposition, **Figure 4.11**, can only be interpreted in the presence of the raw data and that in these examples gravimetric analysis of both the equimolar mixture and the Sn rich data sets are compromised by peak broadening due to mechanical losses caused by surface roughening.
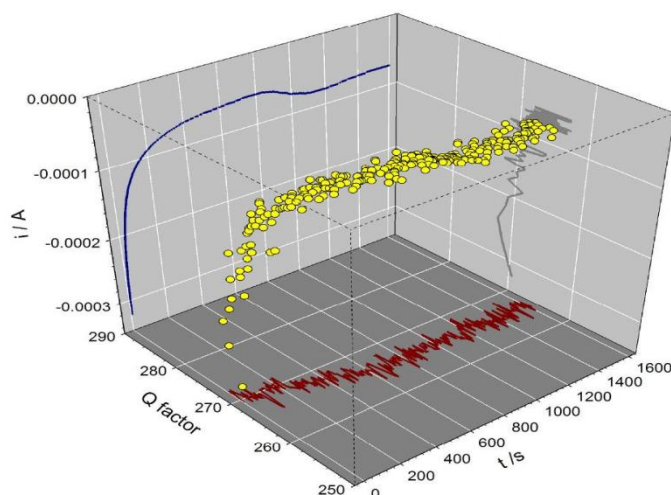


***Figure 4.17*** *3D plot of i ($Q$,t) (yellow circles) for deposition of Cu-Sn alloy on a Au coated QCM crystal from Ethaline (1 CuCl$_2$·2H$_2$O:  0.3 SnCl$_2$·2H$_2$O) under potentiostatic control at -0.8 V versus Ag wire. 2D projections are also shown for clarity, Q (t) (red), i (t) (blue) and i (Q) (grey).*

On the other hand the data set for the Cu rich alloy is both convincing and reasonably consistent, suggesting that a homogeneous mixed alloy phase is deposited at all times, Finally, despite the apparently quasi linear trend exhibited by the equimolar mixture of Cu and Sn, in fact at longer time scales the trace of mass, $\Delta m$, *versus¸* charge, $Q$, curves off and the slope eventually approaches zero, **Figure 4.18**. This shows that for the passage of a given quantity of charge, less than the equivalent mass of metal is observed at the crystal. As it has seen, this is in fact not a current efficiency issue but a break down in model for mass deposition at the surface.

Nevertheless, the plots in **Figure 4.9** and **Figure 4.18** (backed up by the raw data), appear to suggest that a transition occurs between the deposition of compact mass (at short times) which can be evaluated using a rigid resonator model and a more diffuse mass (at longer times) that causes progressive mechanical losses (peak broadening) where the extrema of the deposit are effectively mechanically decoupled from the rest of the surface. Although it has

not been directly observed such two-phase morphology deposits for Cu-Sn alloys it has been seen very similar behaviour for the deposition of Zn metal from Ethaline.

The SEM for one such $1CuCl_2\cdot2H_2O$: $1SnCl_2\cdot2H_2O$ deposit is shown in **Figure 4.10a**. Here two types of distinct morphology are clearly visible for the Cu-Sn deposit. Whilst the difference in morphology of these two phases is striking, the reason for the change in growth characteristics is far from clear. Under these circumstances, mechanical coupling of the edges of the platelets to the substrate surface would be very poor, such that gravimetric detection of the mass would only extend to the edge of the dense phase.
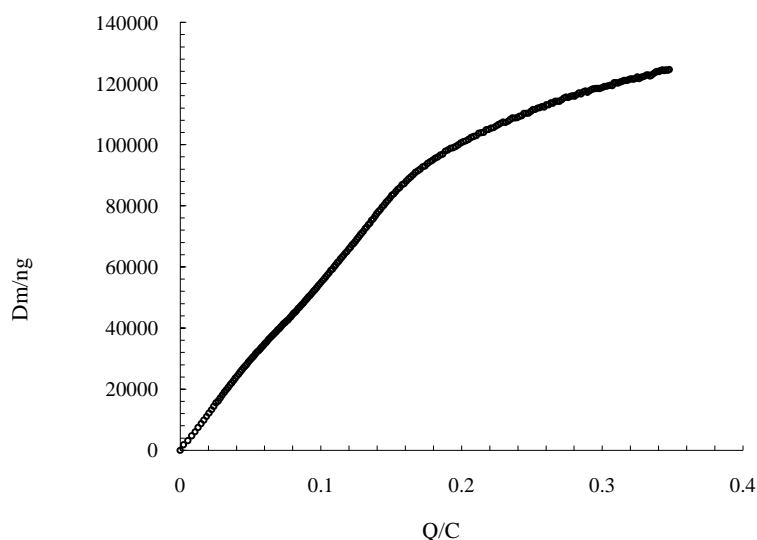


*Figure 4.18* *Mass versus charge plot for alloy deposition using acoustic impedance electrochemical QCM; deposition on a Au coated quartz crystal from Ethaline containing 1 $CuCl_2\cdot2H_2O$: 1 $SnCl_2\cdot2H_2O$. [These data correspond to the full data set from which the trace shown as* *Figure 4.10*(black) is taken.]*

AFM and SEM were used to study the morphology of the alloy deposits using a Hull cell and the results are displayed in **Figure 4.19.** A Hull cell test was also carried out to determine the effect of current density on the Cu, Sn of the film (determined by EDAX) also used the **equation 3.7** in the previous chapter. **Figure 4.19** shows the percentage of each component as a function of high current density ($I = 127.5$ mA cm$^{-2}$) at a region. It was, however, found that the morphology of the surface layer was dependent on the metal composition during 70 min. The current densities for three regions, a, b and c, are $I = 127.5, 64.8$ and $48.5$ mA cm$^{-2}$ respectively were studied by XRD later. It can be seen that a homogeneous and compact deposition is obtained in the equimolar and Cu rich liquids, whereas the Sn rich solution shows big grains on the sample surface.

1 CuCl₂·2H₂O: 1 SnCl₂·2H₂O
AFM                    ESM                    EDAX  Cu: Sn

5.9:1

1 CuCl₂·2H₂O: 0.3 SnCl₂·2H₂O

78.7:1

0.3 CuCl₂·2H₂O: 1 SnCl₂·2H₂O

0.64:1
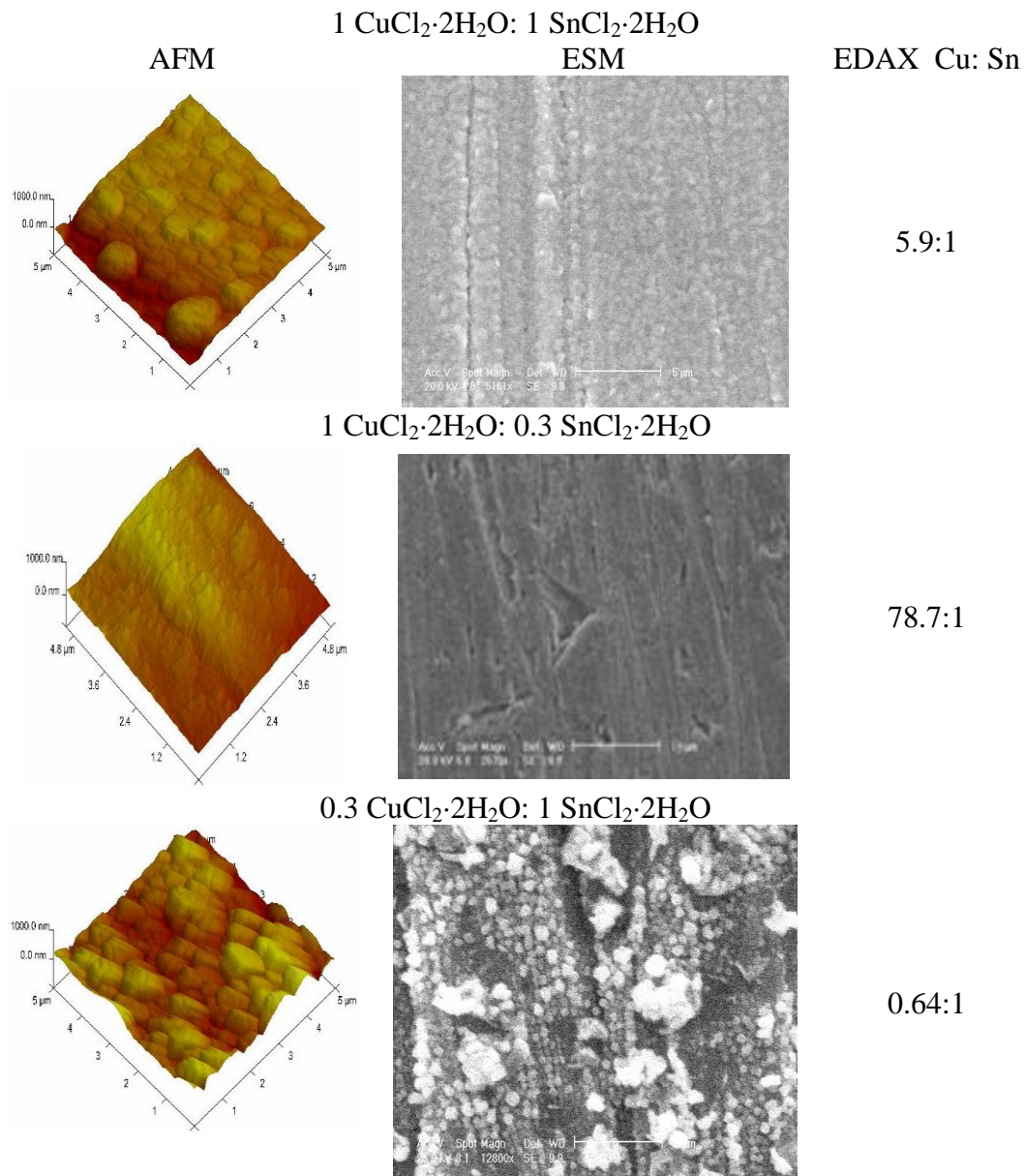
***Figure 4.19** shows SEM images of the Cu-Sn alloy deposited from the Ethaline based liquid and compare with AFM and EDAX results. EDAX analysis confirms the percentage of two components in the alloy at high current density a (I = 127.5 mA cm⁻²)*

AFM results give good agreement when compared with the results of SEM. In addition, many small clusters are found when Cu/ Sn is deposited from the three different mixtures onto gold crystal, as mentioned above in **Figure 4.10**. Additionally, Correia[2] found that morphology of Cu-Sn alloy when deposited from pyrophosphate-based electrolyte solution, the grains are distributed with different sizes, that is similar as shown in **Figure 4.10,** where a Cu–Sn alloy is deposited from Ethaline, an ionic liquid.

## 4.2.6 Phase formation XRD results

Alloy layers were deposited onto nickel from the three Cu: Sn ratios from Ethaline ionic
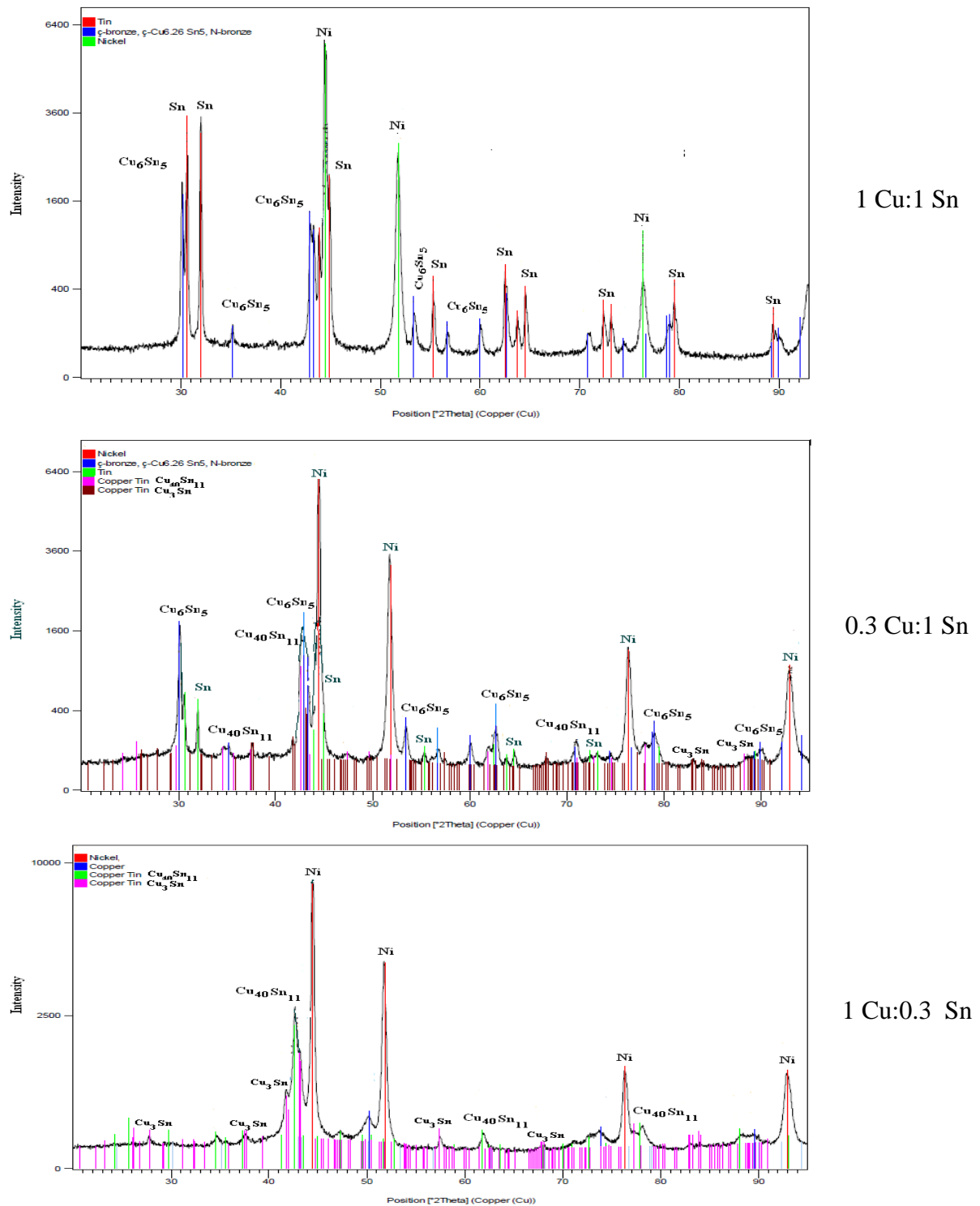


**Figure 4.20** *XRD patterns of thin layer Cu-Sn alloy after electrolysis at low current density (48.5 mA cm$^{-2}$) i) equimolar 1 CuCl$_2$·2H$_2$O: 1 SnCl$_2$·2H$_2$O ii) 0.3 CuCl$_2$·2H$_2$O: 1 SnCl$_2$·2H$_2$O iii) 1 CuCl$_2$·2H$_2$O: 0.3 SnCl$_2$·2H$_2$O from Ethaline.*

liquid and the XRD spectra are shown in **Figure 4.20** at low current density (48.5 mA cm$^{-2}$).
A Hull cell test was also carried out to determine the effect of current density on the Cu-Sn alloy structure of the film (determined by XRD) as shown in **Table 4.4**.

**Table 4.4** lists the relative amounts of the different phases present in the three alloys at three different current densities. According to the data from X-ray diffraction (XRD), Cu-Sn alloys consist of a variety of intermetallic phases including $Cu_6Sn_5$, $Cu_3Sn$, and $Cu_{41}Sn_{11}$ as shown in **Figure 4.21 and 4.22**. The relative percentages of these alloys depend upon the current density. At high current density the copper rich and equimolar solutions lead to just pure copper deposition showing that tin containing phases are kinetically slower to deposit. Pure tin is only observed at lower current density which is counter intuitive when analysing **Figures 4.4, 4.13 and 4.15.** These all tend to show that tin deposition results in a larger charge under the deposition voltammograms and the *i-t* curves are larger for Sn on Cu than Cu on Sn.

| 1 $CuCl_2 \cdot 2H_2O$: 1 $SnCl_2 \cdot 2H_2O$ | | | |
|---|---|---|---|
| | $I = 127.5$ mA cm$^{-2}$ | $I = 64.8$ mA cm$^{-2}$ | $I = 48.5$ mA cm$^{-2}$ |
| Copper | 100% | - | - |
| Tin | - | - | 13% |
| Bronze ($Cu_{41}Sn_{11}$) | - | 84% | 56% |
| Bronze ($Cu_3Sn$) | - | 16% | 6% |
| Bronze ($Cu_6Sn_5$) | - | - | 25% |
| 0.3 $CuCl_2 \cdot 2H_2O$: 1 $SnCl_2 \cdot 2H_2O$ | | | |
| Tin | 50% | 77% | 76% |
| Bronze ($Cu_6Sn_5$) | 50% | 23% | 24% |
| 1 $CuCl_2 \cdot 2H_2O$: 0.3 $SnCl_2 \cdot 2H_2O$ | | | |
| Copper | 100% | 100% | 47% |
| Bronze ($Cu_{41}Sn_{11}$) | - | - | 47% |
| Bronze ($Cu_3Sn$) | - | - | 6% |

**Table 4.4** *XRD patterns of the nickel substrate and Cu-Sn alloy samples prepared on nickel substrate from Ethaline ionic liquid containing 1 $CuCl_2 \cdot 2H_2O$: 1 $SnCl_2 \cdot 2H_2O$, 0.3 $CuCl_2 \cdot 2H_2O$: 1 $SnCl_2 \cdot 2H_2O$ and 1 $CuCl_2 \cdot 2H_2O$: 0.3 $SnCl_2 \cdot 2H_2O$.*

In a previous study, the Cu-Sn alloy was deposited using trimethyl-hexylammonium bistriflamide TMHA-Tf$_2$N formed and it was shown that the intermetallic phases, Cu$_6$Sn$_5$, Cu$_3$Sn, and Cu$_{10}$Sn$_3$ were formed.[21] This shows that different alloys can be formed using ionic liquids, however, it should be stressed that this latter study was carried out at 100 °C which possibly favoured the formation of Cu$_{10}$Sn$_3$.[21]
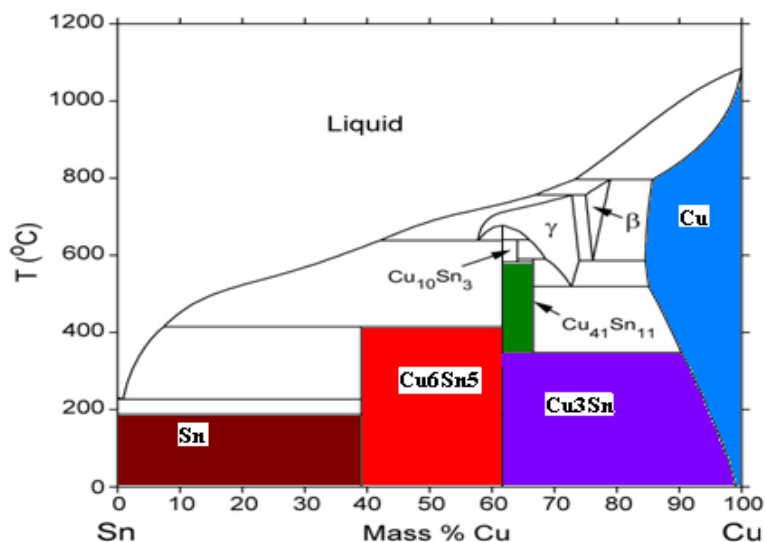


**Figure 4. 21** *The phase diagram of the Sn-Cu system. Image taken from ref* [11]
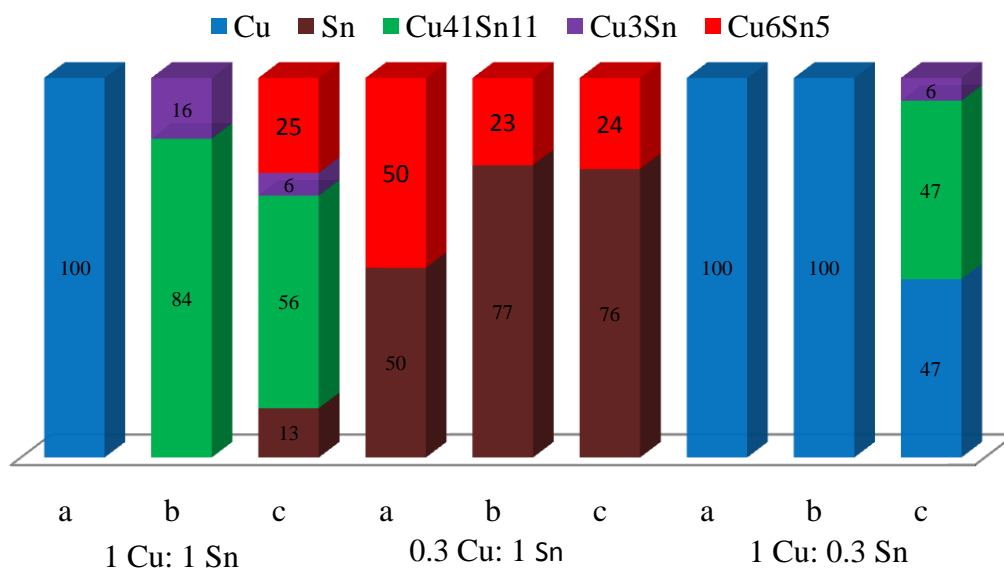


**Figure 4.22** *The percentage of Cu-Sn alloy composition deposition after analysis by XRD for three different systems, equimolar 1 CuCl$_2$·2H$_2$O: 1 SnCl$_2$·2H$_2$O, 0.3 CuCl$_2$·2H$_2$O: 1 SnCl$_2$·2H$_2$O and 1 CuCl$_2$·2H$_2$O: 0.3 SnCl$_2$·2H$_2$O from Ethaline at different current density.*

Clearly there are a lot of variables to consider, most notably the speciation and this is the subject of further study. It was envisaged that it would be possible to correlate speciation to the redox potentials in **Figure 4.4,** however, authoritative assignment cannot be achieved due to the close proximity of the different phases and the shift in the reference potential.

### 4.2.7 Large scale Cu-Sn deposition with brighteners

The presence of organic additives in the electroplating bath can significantly affect the Cu-Sn alloy reduction kinetics, as well as the morphology of the deposit. The electrodeposition of copper-tin alloys from a deep eutectic solvent in Ethaline was studied with a variety of additives classically used in copper plating *viz.* boron trihydride-N,N-dimethylmethanamine, sodium 2-ethylhexyl sulfate and *1,10-phenanthroline*.  The alloy bath of 1 $CuCl_2 \cdot 2H_2O$: 0.3 $SnCl_2 \cdot 2H_2O$ was used and it was found that all three organic additives producing a shinier finish by changing the morphology of the metallic grains.

Barron[22] investigation the effect of organic additive addition such as acetonitrile, ammonia and ethylene diamine on the Zn electrodeposition process in ChCl: ethylene glycol and ChCl: urea. The morphology and growth mechanism of Zn deposition from Ethaline and Reline with brighteners (ammonia and ethylene diamine) were studied.
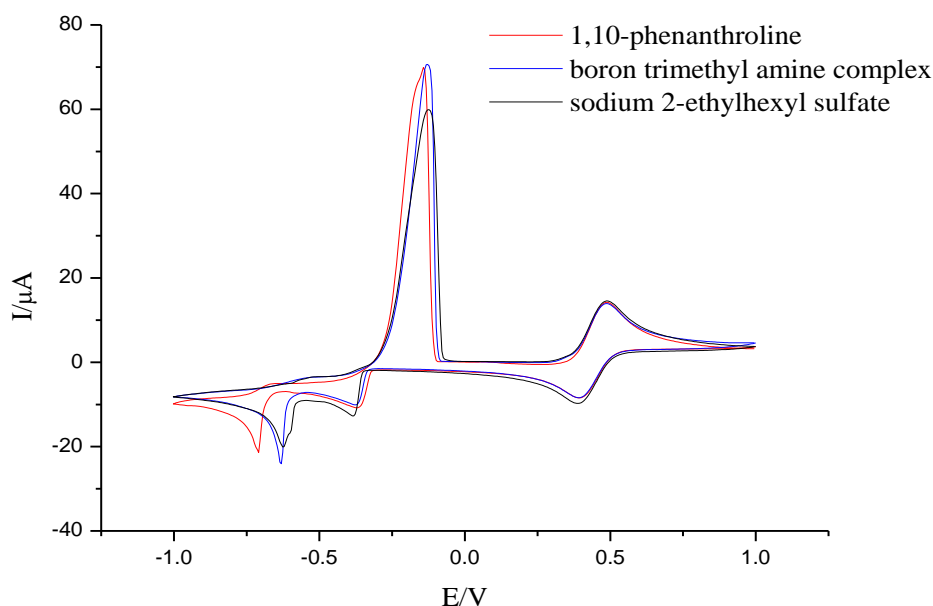


***Figure 4.23*** *Cyclic voltammograms obtained at a Pt disc (0.5 mm dia.) at 5 mV s$^{-1}$ for 1$CuCl_2 \cdot 2H_2O$: 0.3 $SnCl_2 \cdot 2H_2O$ alloy in Ethaline deposit with 1% of a) boron trimethyl amine complex b) sodium 2-ethylhexyl sulfate and c) 1,10-phenanthroline.*

**Figure 4.23** shows the affect of the three additives on the voltammetry of the mixed copper-tin solution. The organic additive do not appear to change the shape and the position of deposition and stripping peaks with the exception of 1,10-phenanthroline which shifts the position and increases the reduction current for the second reduction process.

Several selected samples of Cu-Sn alloy were examined by SEM and micrographs are shown in Figure **4.24**. The electrodeposit that was obtained from the solution containing the boron trimethyl amine complex was dense and homogeneous. A similar response is observed with 1,10-phenanthroline whereas sodium 2-ethylhexyl sulphate leads to a more nodular although ultimately flatter surface than without additive.



| Cu= 97 % Sn = 3% | Cu = 99 % Sn = 1% | Cu = 98 % Sn = 2 % |
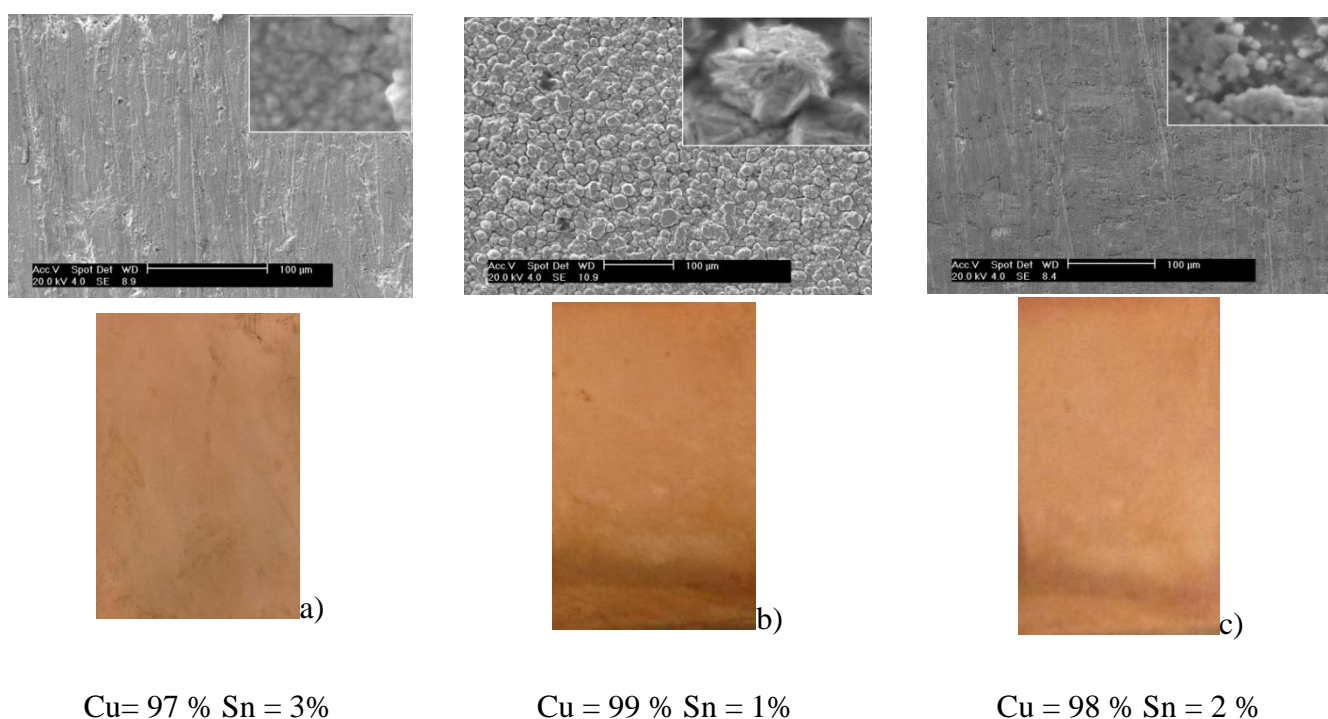
*Figure 4.24* SEM images and photographs of 0.1 mole dm$^{-3}$ CuCl$_2$·2H$_2$O: 0.03 mole dm$^{-3}$ SnCl$_2$·2H$_2$O alloy in Ethaline deposit with 1% of a) boron trimethyl amine complex b) sodium 2-ethylhexyl sulfate and c) 1,10-phenanthroline. All electrodepositions were carried out on mild steel plates with a constant current density of 5.5 mA cm$^{-2}$.

## 4.2.8 Bronze dissolution/ electropolishing

Electropolishing (controlled anodic dissolution) is a common process to control dissolution of a metal surface to obtain a smooth surface, free of contaminants and more passive. Jacquet investigated the first system of the electropolishing effect and pointed out the importance of diffusion in electropolishing.[23] Electropolishing is mostly carried out on stainless steel using

solutions consisting of mixtures of concentrated phosphoric and sulphuric acids. This process is successful but with many limitations which occur during the process, for example they are highly corrosive, toxic, and produce extensive gas evolution with low current efficiency. The wide variety of electrochemical and synthetic applications in ionic liquids have been studied since the 1980s until now.[24] Electropolishing of stainless steel has been demonstrated in DESs based on Ethaline.[24] A selection of the 300 series stainless steel samples were shown to be polished by a different mechanism to aqueous electropolishing. Relatively few studies have been carried out into the electropolishing of copper alloys although Mansour and co-workers studied the rates of electropolishing of single-phase bronze alloys in unstirred $o$-$H_3PO_4$ with some promising results.[25]



c) Polished                    d) unpolished
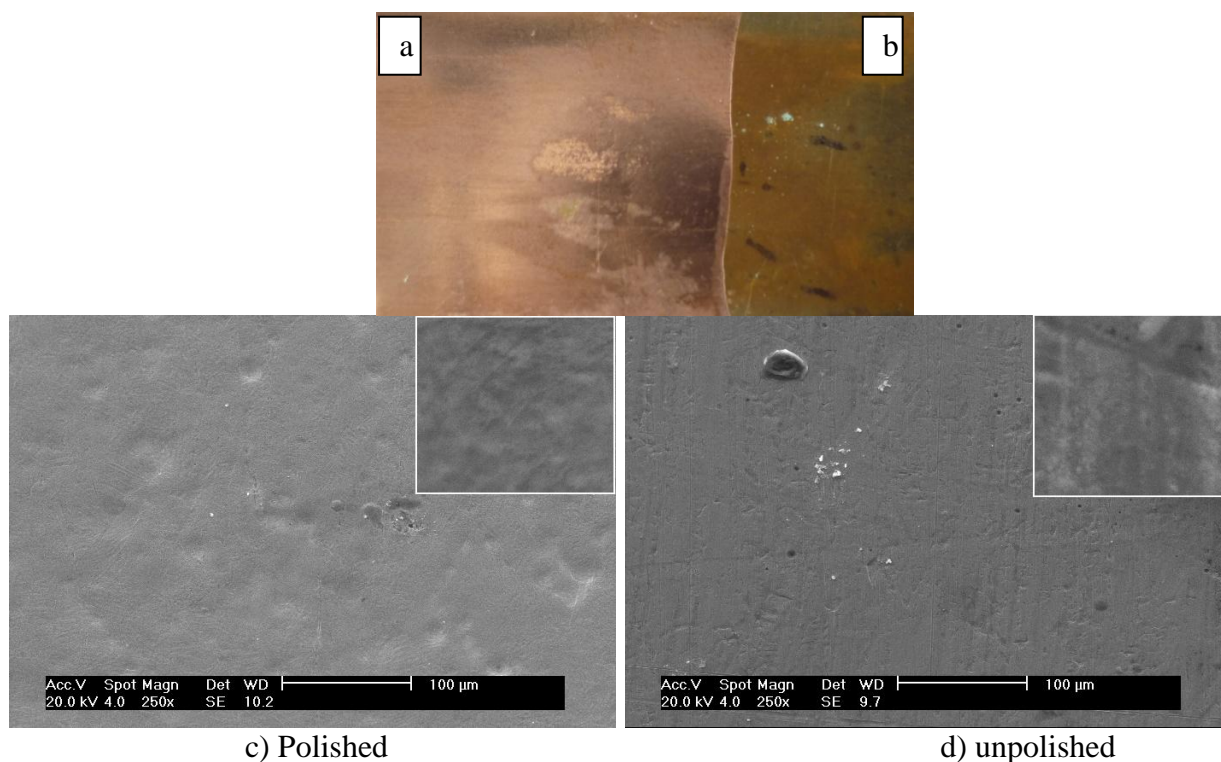
*Figure 4.25 (a and b) Photograph of a sample of Cu-Sn alloy showing polished and unpolished respectively. (c) Scanning electron micrograph of the polished region of the sample shown with high magnification insert in. (d) Scanning electron micrograph showing of the unpolished regions of the sample.*

In this study the surface morphology of polished and unpolished regions of the Cu-Sn alloy etched using Ethaline were studied. **Figures 4.25a** and **b** show an optical photograph of Cu-Sn alloy sample. The polished (a) and unpolished (b) regions are clearly visible. SEM images

were also taken for this sample to study the morphology, as presented in **Figures 4.25 c and d,** where they show the polished and unpolished surface respectively.

The advantage for the commercial electropolishing process is to improve corrosion resistance of the metal and alloy surfaces. It is very important to establish the polishing mechanism of the Cu-Sn alloy in the ionic liquid without changing the elemental composition.

The Cu and Cu-Sn alloy electrodes were immersed into a fresh ionic liquid of Ethaline; **Figure 4.26** shows the cyclic voltammograms for each in separate solution. The Cu sample shows a double sharp anodic peak at a potential from -0.1 to 1.3 V, while the Cu-Sn alloy also shows three broad anodic peaks at the same area of potential.
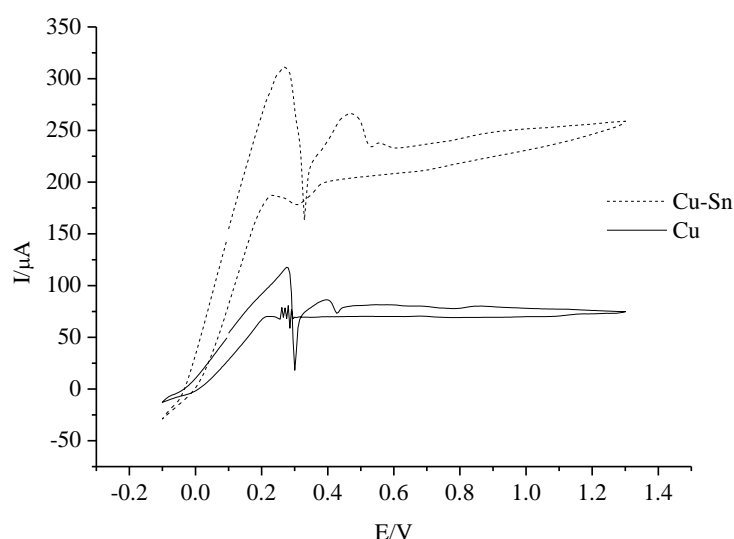


*Figure 4.26* Linear sweep voltammograms recorded for Cu and Cu-Sn alloy in Ethaline ionic liquid. The voltammograms were recorded at a potential scan rate of 5 mV s$^{-1}$ using a silver wire pseudo reference electrode.

The variation in peaks between Cu and Cu-Sn alloy current is quite large; this is due to a variation in surface area and also by metal composite effects resulting in which the electrodes were prepared such as Cu-Sn electrode. According to the lower percentage of Sn (5%) in the Cu-Sn alloy composition is due to a little different in anodic linear sweep voltammogram compared with pure Cu under the same condition.

In order to investigate the surface morphology and roughness of the bronze (Cu-Sn alloy) before and after polishing, AFM was used to study the rate of etching from the surface.
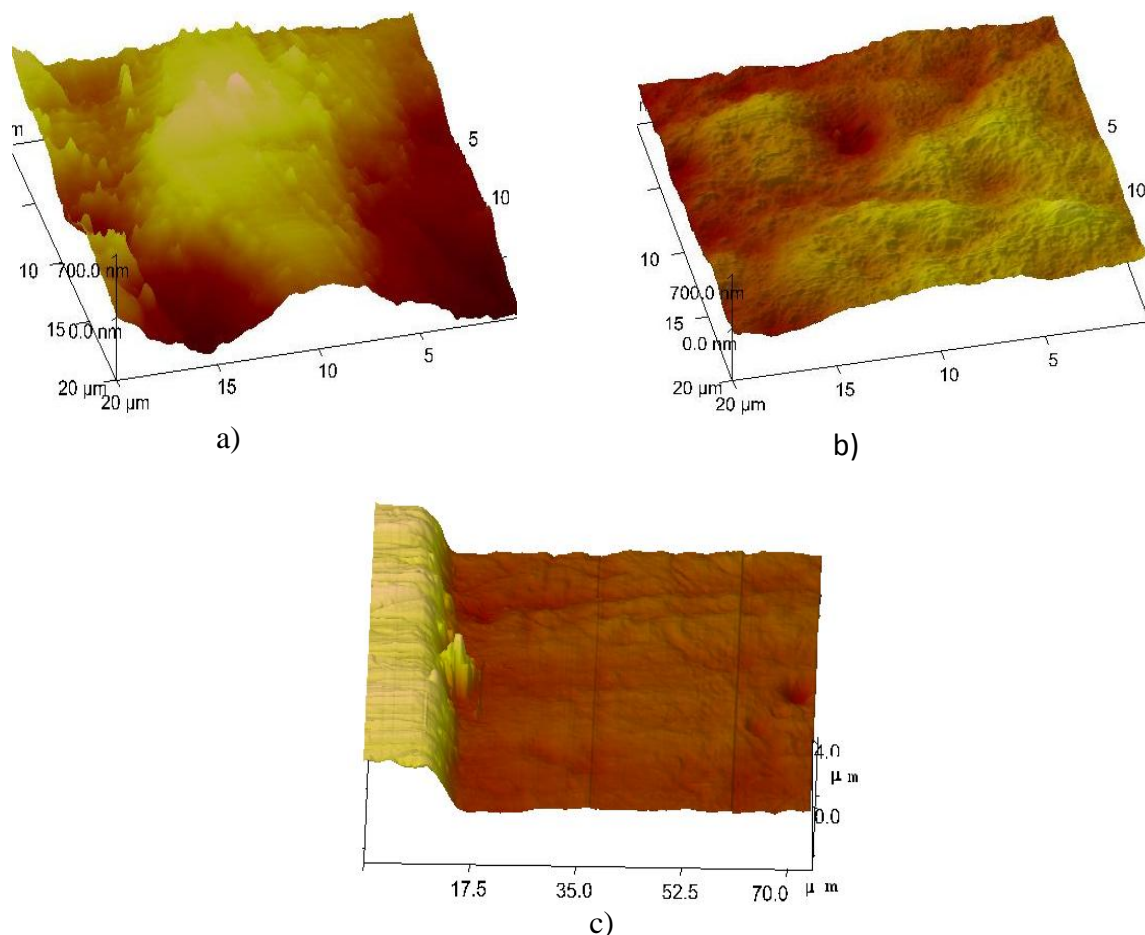
*Figure 4.27* AFM images of bronze before and after dissolution. Topography a) before dissolution. Topography b) after dissolution. Topography c) before and after dissolution from Ethaline an ionic liquid.

**Figure 4.27** shows height contrast images of a sample of Cu-Sn alloy recorded across the boundary between polished and unpolished areas over a length scale of ca. 70 µm. A cross-section of this surface for the unpolished and polished area shows in **Figure 4.27c** the surface roughness and grain boundary structure in unpolished and smooth in polished area.

## 4.3 Conclusions

This study shows the successful electrodeposition of copper-tin alloys from Ethaline and Reline at room temperature. The objectives of these studies have been largely achieved in that a real time in-situ method for probing the mass-composition of mixed metal electrolytic deposits in Ethaline and Reline has been developed. The suite of analytical techniques including cyclic voltammetry, chronoamperometry, SEM, EDAX and AFM have shown that there are significant differences between the responses for multiphase alloys than those for

simple solid solutions although these are not as simple to analyse due to the complexity of the phases formed.

As would be expected the concentration of Cu ion in the solution is a very important factor which influences the composition of the Cu-Sn alloy deposition and the properties of the film. In the previous chapter it was seen that the alloy composition was relatively homogeneous throughout the film, but this was less so in the Cu-Sn alloys. In addition, acoustic impedance electrochemical QCM has also been successfully applied to characterising the formation of a Cu rich Cu-Sn alloy and has been partially validated by SEM (EDAX) analysis of the same samples. The method has been less successful with Sn rich alloys where rough surface morphologies are formed that preclude gravimetric correlation.

**4.4 References**

1.  W. Pu, X. He, J. Ren, C. Wan and C. Jiang, *Electrochimica Acta*, 2005, **50**, 4140-4145.

2.  A. N. Correia, M. X. Façanha and P. de Lima-Neto, *Surface and Coatings Technology*, 2007, **201**, 7216-7221.

3.  P. Y. Chen, M. C. Lin and I. W. Sun, *Journal of the Electrochemical Society*, 2000, **147**, 3350-3355.

4.  A. Ito, K. Murase, T. Ichii and H. Sugimura, *ECS Transactions*, 2009, **16**, 461-468.

5.  T. Katase, R. Kurosaki, K. Murase, T. Hirato and Y. Awakura, *Electrochemical and Solid State Letters*, 2006, **9**, C69-C72.

6.  T. Katase, R. Kurosaki, K. Murase, T. Hirato and Y. Awakura, *Electrochemical and Solid State Letters*, 2006, **9**, L5-L5.

7.  P. Hapiot and C. Lagrost, *Chemical Reviews*, 2008, **108**, 2238-2264.

8.  A. P. Abbott, C. A. Eardley, N. R. S. Farley, G. A. Griffith and A. Pratt, *Journal of Applied Electrochemistry*, 2001, **31**, 1345-1350.

9.  A. P. Abbott, K. El Ttaib, G. Frisch, K. J. McKenzie and K. S. Ryder, *Physical Chemistry Chemical Physics*, 2009, **11**, 4269-4277.

10. A. P. Abbott, G. Capper, K. J. McKenzie and K. S. Ryder, *Journal of Electroanalytical Chemistry*, 2007, **599**, 288-294.

11. J. H. Shim, C. S. Oh, B. J. Lee and D. N. Lee, *Zeitschrift fuer Metallkunde/Materials Research and Advanced Techniques*, 1996, **87**, 205-212.

12. T. Laurila, V. Vuorinen and J. K. Kivilahti, *Materials Science and Engineering: R: Reports*, 2005, **49**, 1-60.

13. B. Mravic, S. Shapiro, D. E. Tyler and A. Khan, *United States Patent*, Dec. 2, 1975, US No 3923558.

14. C. T. J. Low and F. C. Walsh, *Surface and Coatings Technology*, 2008, **202**, 1339-1349.

15. A. P. Abbott, K. S. Ryder and U. Konig, *Transactions of the Institute of Metal Finishing*, 2008, **86**, 196-204.

16. B. Scharifker and G. Hills, *Electrochimica Acta*, 1983, **28**, 879-889.

17. X.-H. Xu and C. L. Hussey, *Journal of the Electrochemical Society*, 1993, **140**, 618-626.

18. A. P. Abbott, J. C. Barron, G. Frisch, S. Gurman, K. S. Ryder and A. F. Silva, *Physical Chemistry Chemical Physics*, 2011, **13**, 10224-10231.

19. G. Sauerbrey, *Z. Physik* 1959, **155**, 206.

20. A. P. Abbott, S. Nandhra, S. Postlethwaite, E. L. Smith and K. S. Ryder, *Physical Chemistry Chemical Physics*, 2007, **9**, 3735-3743.

21. K. Murase, R. Kurosaki, T. Katase, H. Sugimura, T. Hirato and Y. Awakura, *Journal of the Electrochemical Society*, 2007, **154**, D612-D616.

22. J. C. Barron, PhD, University of Leicester, 24- Mar-2010.

23. P. A. Jacquet, *French Patent No. 707526*, 1930.

24. A. P. Abbott, G. Capper, K. J. McKenzie, A. Glidle and K. S. Ryder, *Physical Chemistry Chemical Physics*, 2006, **8**, 4214-4221.

25. I. A. S. Mansour, T. H. El-Sherify, G. H. Sedahmed and S. S. Iskander, *Surface Technology*, 1981, **13**, 325-329.

**Chapter 5: The Electrodeposition of Copper-phosphorus Alloys using Deep Eutectic Solvents**

## 5.1 Introduction

Copper and its alloys are attracting the attention of the electronics industry because they have excellent material properties due to the effect of precipitation hardening. The copper lattice is able to dissolve some other metallic elements in high percentages, e.g. Zn and Sn which are 39% Zn in brass, and 15% Sn in bronze, according to the equilibrium phase diagram.

These atoms take the lattice sites of copper atoms, which is called a solid solution (**Figure 5.1 a** and **b**). The copper lattice can be changed to a non-uniform lattice by adding different large or small atoms to copper atoms, as shown by **Figure 5.1**. In both cases the resistance of the alloy material against deformation is increased compared to pure copper, in other words: changing the mechanical properties.[1] Generally, addition of various atoms into the normal lattice structure is used to change the electronic properties of both compound and elemental semiconductors.
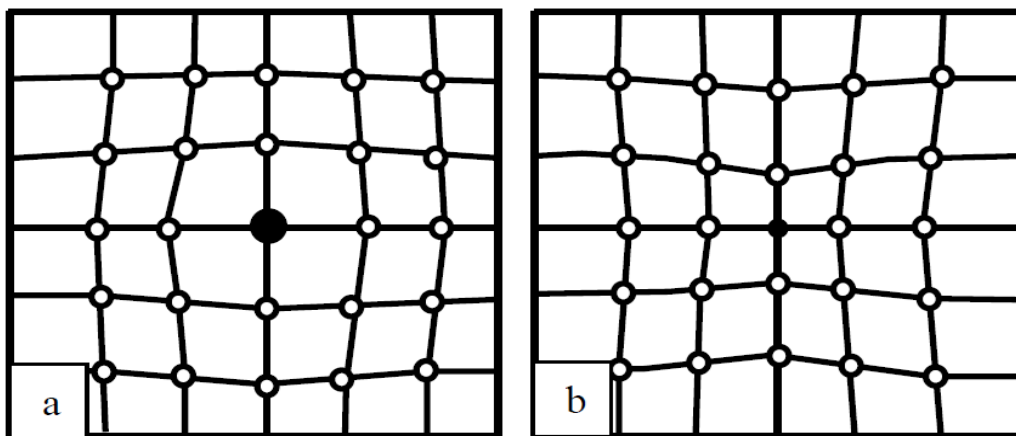


**Figure 5.1** *Solid solution (schematic) of **a**) atoms with bigger size and **b**) atoms with smaller size than the lattice atoms. Image taken from ref [1]*

Generally, metal-phosphorus deposits are important engineering materials for many applications because of their exclusive properties, such as corrosion and wear resistance, and improved micro-hardness properties. Deposition conditions are strongly affected by the phosphorus content, which raises an important issue for their wide spread application. In the past all studies have focused on the deposition of Ni-P alloy from different baths; both chemical (electroless) and electrochemical deposition which use different types of phosphorus complexes.

**Phase diagram**

The copper-phosphorus system shows a simple eutectic and so it could be expected that the results for metal deposition should be similar to those presented in Chapter 3 for Cu-Ag systems.
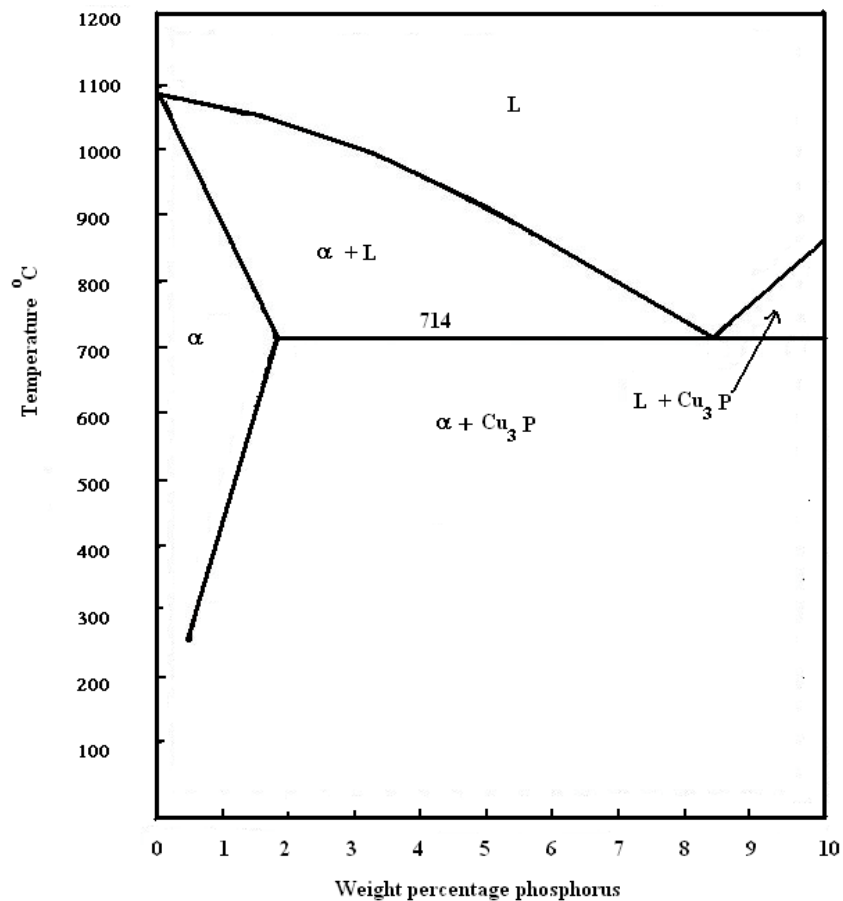


*Figure 5.2 Cu/P phase diagram. Image taken from ref* [2]

The $Cu_{100-x} P_x$ alloys have phosphorus contents ranging from about (x = 4- 8.3 at %), as can be seen in **Figure 5.2**, which is the copper rich end of the copper-phosphorus thermal equilibrium phase diagram, the system contains a eutectic at 8.25% phosphorus. As a result, all the alloys have a solidus temperature of 714 ·C. From this figure, the degree of super saturation increases when the phosphorus concentration increases. In contrast, very few studies to investigate the binary Cu-P system have been reported.[3]

The composition of electroless nickel/phosphorus deposits, as mentioned in the many previous publications, depend on a range of different properties during the coating process, one of which is temperature. The deposition rate and the P content range (0.01 to 0.14 wt%)

in the coating increase with an increasing phosphorus content in the bath under heat treatment. [4-9]

Srinivasan *et al*.[10] have been investigated as a new electroless formula to deposit nickel-phosphorus alloy from a nickel methanesulphonate bath. Using SEM and XRD to probe thin films, the surface morphology and also study the effect of changing pH with temperature. The system is quite complex, however, due to the simultaneous change in pH with temperature, however it is generally acknowledged that the lower the bath pH, the higher the phosphorus content.[11]

In this chapter a new bath formulation was developed, which allowed the deposition of copper-phosphorus alloys in both Ethaline and Reline. Electrodepositon of thin film copper-phosphorus (Cu–P) alloys are very attractive due to the changing behaviour compared to pure Cu deposits. In this section the specific aim was to develop a material which demonstrated greater ductility for the application to electroformed copper cylinders. The properties of these deposits are usually dependent on the crystal structure, which in turn is influenced to a large extent by the copper-phosphorus content. Younan *et al*.[12] have investigated the ternary nickel-copper-phosphorus alloy deposits on aluminium alloys in an alkaline bath containing sodium citrate and lactic acid as complexing agents. Crousier *et al*.[13] carried out the dissolution of copper in a chloride-based solution and they have found the presence of CuCl as a passive layer, which is shows the anodic dissolution of copper to form the complex $CuCl_2^-$. In addition, the electrochemical behaviour of copper in 1-alkyl-3-methylimidazolium bis[(trifluoromethyl) sulfonyl] imide ionic liquid electrolytes were investigated by Peng [14] and co-workers. It shows that the cyclic voltammetry results from the RTIL with EC/ DMC have large oxidation–reduction currents occurring at the copper foil, while a much smaller current appeared in the pure RTIL electrolytes, which decreased gradually, indicating that the copper foil was anodically stable. Electrochemical dissolution of metals in choline chloride based ionic liquids, which are stable in air and moisture, have been investigated extensively. In the case of metal dissolution using the ionic liquid, the mechanism is different and slower than in aqueous solution.[15]

In the previous chapters copper alloys have been electrodeposited from deep eutectic solvents with metals which are larger than copper. In this chapter it is shown that electrodeposition of copper-phosphorus alloys can occur, opening the door to focus on alloys of Cu with a small atom co-deposition in ionic liquids. A combination of electrochemical techniques, including EQCM, cyclic voltammetry and chronoamperometry together with scanning electron microscopy are used to characterise these systems. In addition, the tensile strength was

measured to give an indication of the properties of the deposit and this is compared with pure Cu deposits.

## 5.2 Cyclic voltammetry

**Figure 5.3** shows the influence of increasing sweep rates on the cyclic voltammogram of Cu and Cu-P alloy in Ethaline. **Figure 5.3** contains a representative voltammogram for 0.1 mol $dm^{-3}$ $CuCl_2 \cdot 2H_2O$ in Ethaline upon the addition of 0.2 mol $dm^{-3}$ $NaH_2PO_2$ which has large effect on the voltammetric response. Here, the onset of the two reduction peaks are shifted cathodically by almost 150 mV to E = -0.25 V. The observation that the $Cu^{2+/+}$ response is also shifted suggests that this is due to a shift in reference potential. Given that sodium hypophosphite is a good reducing agent it is probable that the concentration of $Cu^+$ in solution increases.
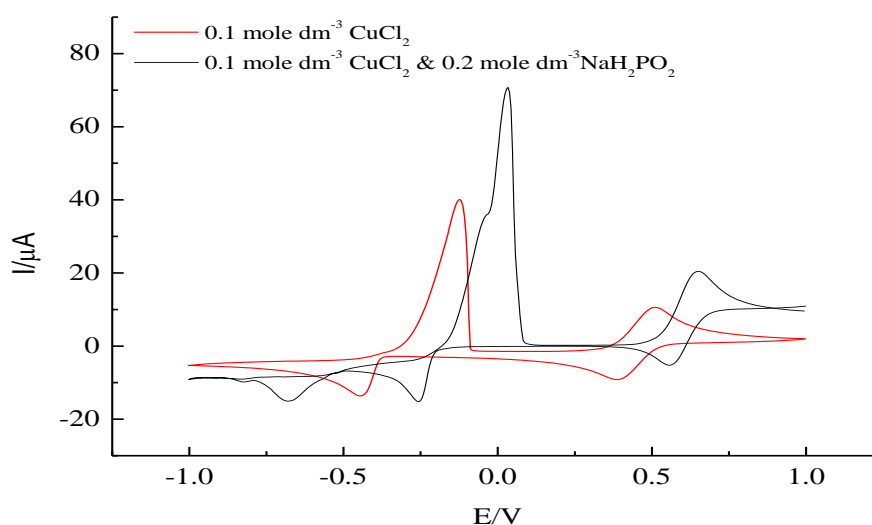


***Figure 5.3*** *Cyclic voltammograms of a) 0.1 mol $dm^{-3}$ $CuCl_2 \cdot 2H_2O$ (Red) b) 0.2 mol $dm^{-3}$ $NaH_2PO_2$ (Black) in Ethaline at a Pt disk working electrode (dia. 0.5 mm) using a silver wire pseudo reference electrode. Potential scan rate at 5 mV $s^{-1}$*

.

This is borne out by the observation that the background current at +1V increase when sodium hypophosphite is added to the solution because the $Cu^+$ in solution is being oxidised. Taking this into account it is evident therefore that the phosphorous species in solution is reduced at -0.7 V.

As seen above, the position of the reduction and oxidation peaks are relatively independent of the concentration of the phosphorus species in the ionic liquids at high phosphorus concentration. This suggests that 1 mole equivalent is sufficient to reduce all the $Cu^{2+}$ to $Cu^+$. At the Cu cathode, in the presence of the copper ions formed during the anodic scan, the co-reduction of copper ions and hypophosphite can be achieved and a Cu-P alloy is obtained, as shown clearly at equimolar concentrations (**Figure 5.4**).
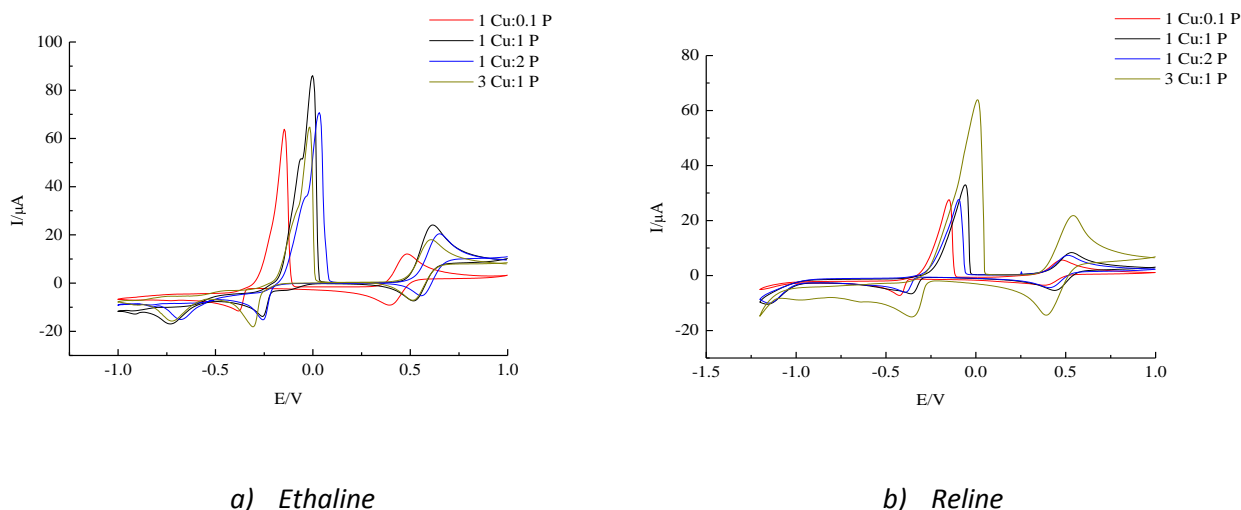


a) *Ethaline*  b) *Reline*

***Figure 5.4*** *Cyclic voltammograms of 1: 0.1, 1: 1, 1: 2 and 3: 1 CuCl₂·2H₂O: NaH₂PO₂ in Ethaline and Reline at a Pt disk working electrode (dia. 0.5 mm) using a silver wire pseudo reference electrode. Potential scan rate at 5 mV s⁻¹.*

At lower concentrations of $NaH_2PO_2$ (0.01 mol dm⁻³, **Figure 5.4 (a)**) the high activity of the free chloride in Ethaline effectively inhibits the reduction of Cu-P. In Reline, the activity of the free chloride is lower. It is interesting to note that the two reduction peaks of Cu-P were shown in Ethaline but in Reline only one peak for reduction is observed.

The oxidative processes observed as two peaks in Ethaline which is probably from rich Cu and Cu-P mixed phases rather than the third peak oxidation of $Cu^+$ to $Cu^{2+}$. The cathodic and anodic peaks are suggesting that the two oxidation processes are both due to the oxidation of Cu.

## 5.3 Chronoamperometry

As a preliminary step, from the characteristic shapes of the current transients presented in **Figure 5.5** (raw data are given in the Appendix **Figure 7.5**), all current transients were

122

presented in a nondimensional form, normalized current versus time plot [$(J/J_{\text{Max}})^2$ versus $t/t_{\text{Max}}$].[16] A comparison of the theoretical lines with the experimental data was often used for the determination of the nucleation mechanism, which is due to either instantaneous processes (**Equation 3.2)** or progressive processes (**Equation 3.3)**.
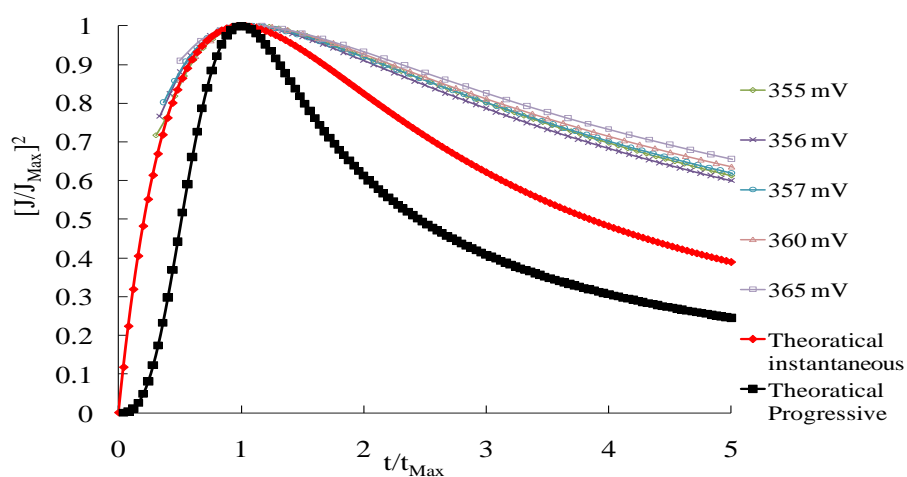


*a)*
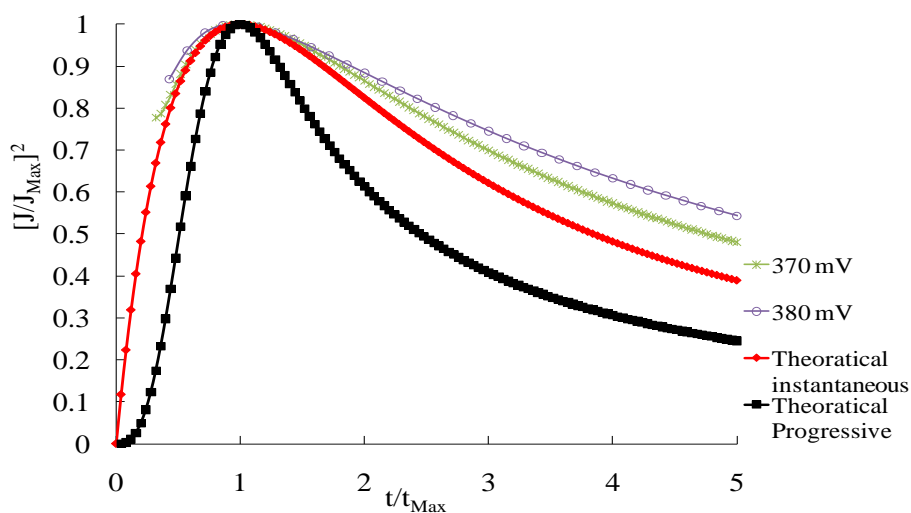


*b)*

**Figure 5.5** *Comparison of the dimensionless and theoretical chronoamperometric curves of 3:1 Cu:P in Ethaline  a) without, and b) with 1% boron trimethylamine complexes from Ethaline. Applied potentials all in negative*

**Figure 5.5** shows the representative nondimensional plots of 3:1 copper-phosphorus and copper-phosphorus with 1% of $(CH_3)_3N \cdot BH_3$ deposition in Ethaline with the theoretical curves for the limiting cases of instantaneous and progressive 3D nucleation with diffusion-controlled growth. At the potential ranges depicted, the analysis of the experimental results under different over potentials showed good agreement with the theoretical lines which fit instantaneous nucleation.

The effect of the additives on the Cu-P nucleation mechanism is shown to be similar to the behaviour of Zn in the same ionic liquid when using ethylene diamine is added as an organic additive.[17] A clear nucleation maximum is seen when boron trimethylamine complexes are introduced to the additive free solution, **Figure 5.5** It is evident that boron trimethylamine complexes acts to inhibit the initiation of Cu nucleation and this is supported by the cyclic voltammetric data discussed in **Figure 5.4a**.
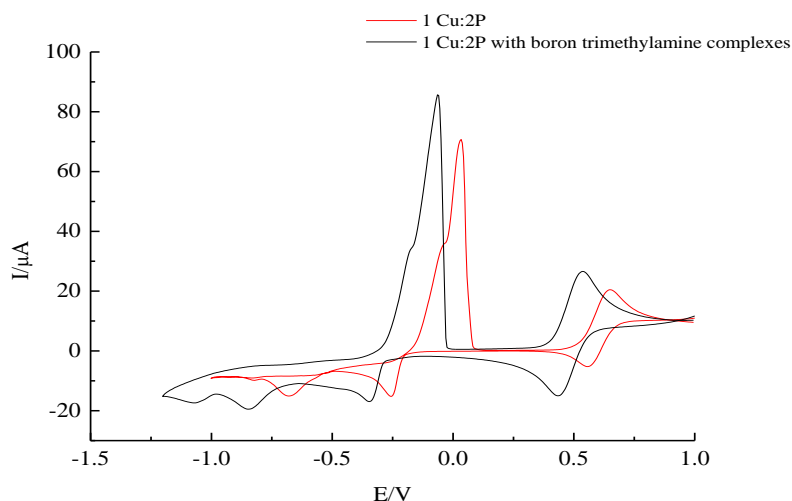


***Figure 5.6*** *Cyclic voltammograms of 1Cu: 2P with and without boron trimethylamine complexes in Ethaline at a Pt disk working electrode (dia. 0.5 mm) using a silver wire pseudo reference electrode. Potential scan rate at 5 mV s⁻¹.*

**Figure 5.6** contains a representative voltammogram for 1:2 Cu: P in Ethaline with and without 1 % of boron trimethylamine complexes. The addition of $BH_3$ trimethylamine complexes has a noticeable effect on the voltammetric response. Here the onset of Cu reduction is shifted cathodicaly by 100 mV to E = -0.350 V, again presumably due to the chemical reduction of $Cu^{2+}$. Additionally it should be noted that the charge passed during Cu-P oxidation and reduction is greatly increased relative to the additive free solution, which is due to an increase in the mass transport.

124

## 5.4 EQCM, SEM and EDAX analysis

In this experiment the change of mass for three mixture Cu/ P and pure Cu ions was studied to determine the current efficiencies, mechanistic information and structure type of the surface. The deposited layers have a different morphology when examined by SEM (**Figures 5.8**).
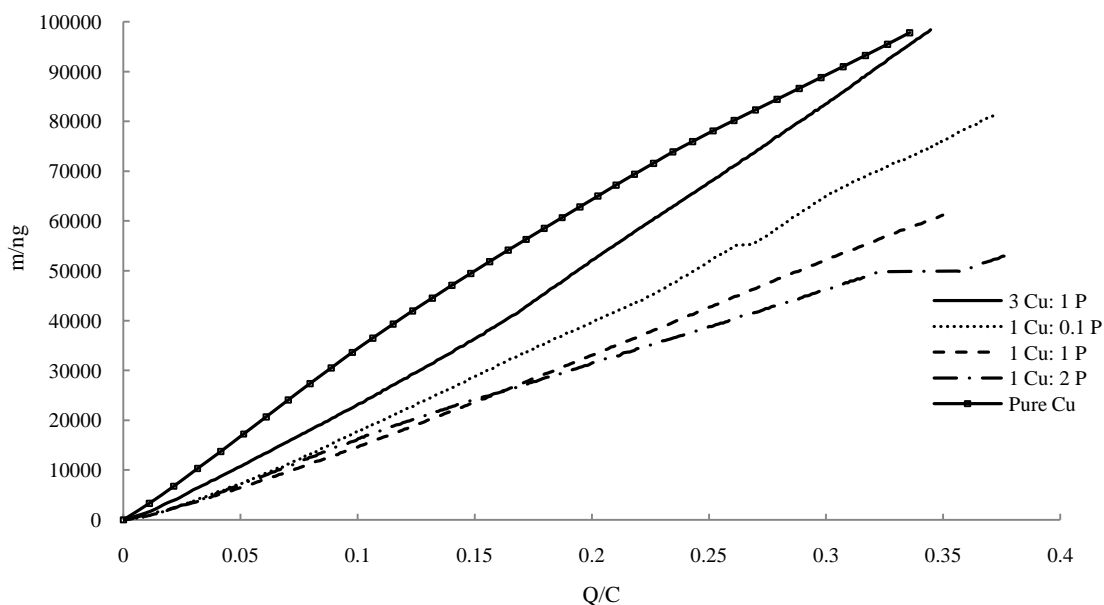


***Figure 5.7*** *Mass versus charge plots for pure Cu and alloy deposition using acoustic impedance electrochemical QCM; of 1: 0.1(dot), 1: 1(dash),1: 2 (dash-dot) and 3: 1(solid) CuCl$_2$·2H$_2$O: NaH$_2$PO$_2$. The potential was stepped from O.C.P and held at -0.9 V, using Ag wire as a reference electrode.*

A relatively dense, amorphous structure is observed. The acidic protons on NaH$_2$PO$_2$ mean that during alloy deposition small, but noteworthy amounts of hydrogen are evolved. This demonstrates the limitation of using EQCM for alloy determination which is only viable for processes with close to 100 % current efficiency. This means that **Figure 5.7** cannot be deconvoluted to determine the phosphorous content of the alloy. **Figure 5.8** shows that the phosphorous content of the alloy can be varied from 0.2 to 2 mol % depending on the NaH$_2$PO$_2$ content.
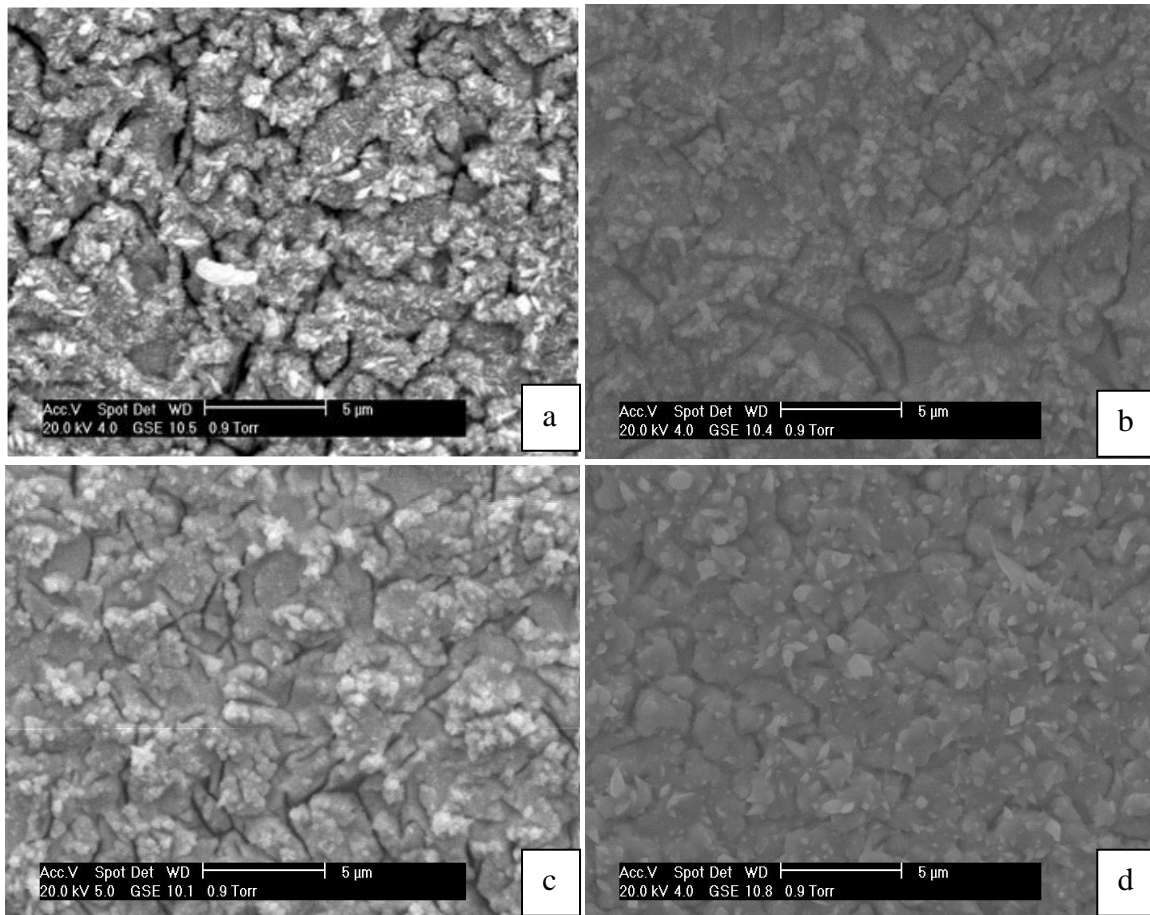
EDAX

a) Cu:P = 55:1

b) Cu:P = 85.6:1

c) Cu:P = 71.3:1

d) Cu:P = 470:1

*Figure 5.8* SEM images and EDAX data for Cu-P alloys deposition using acoustic impedance electrochemical QCM; of a) 1: 0.1, b) 1: 1,c) 1: 2 and d) 3: 1 $CuCl_2 \cdot 2H_2O$: $NaH_2PO_2$. Deposits are made on a gold covered quartz crystal. The potential was stepped from O.C.P and held at -0.9 V

## 5.5 Large scale deposition

Thin film copper and copper-phosphorus alloys were investigated for engineering coatings to increase hardness and corrosion resistance. The aim was to form metal films and then peel then from the substrate to test their tensile strength. This actually proved quite difficult to do as the adhesion was extremely good on most substrates. The conventional method to electroform copper sheet or tube is to electrodeposit onto mild steel. Once a layer of sufficient thickness is formed the sample is rapidly heated and then quenched. The thermal

shock is usually sufficient to separate the two metals. This was attempted with various pre-treatments but the copper adhesion was too good. It is assumed that the reason for this is the crystal structure of the copper. In aqueous solutions the copper deposited is microcrystalline whereas in ionic liquids it is amorphous.
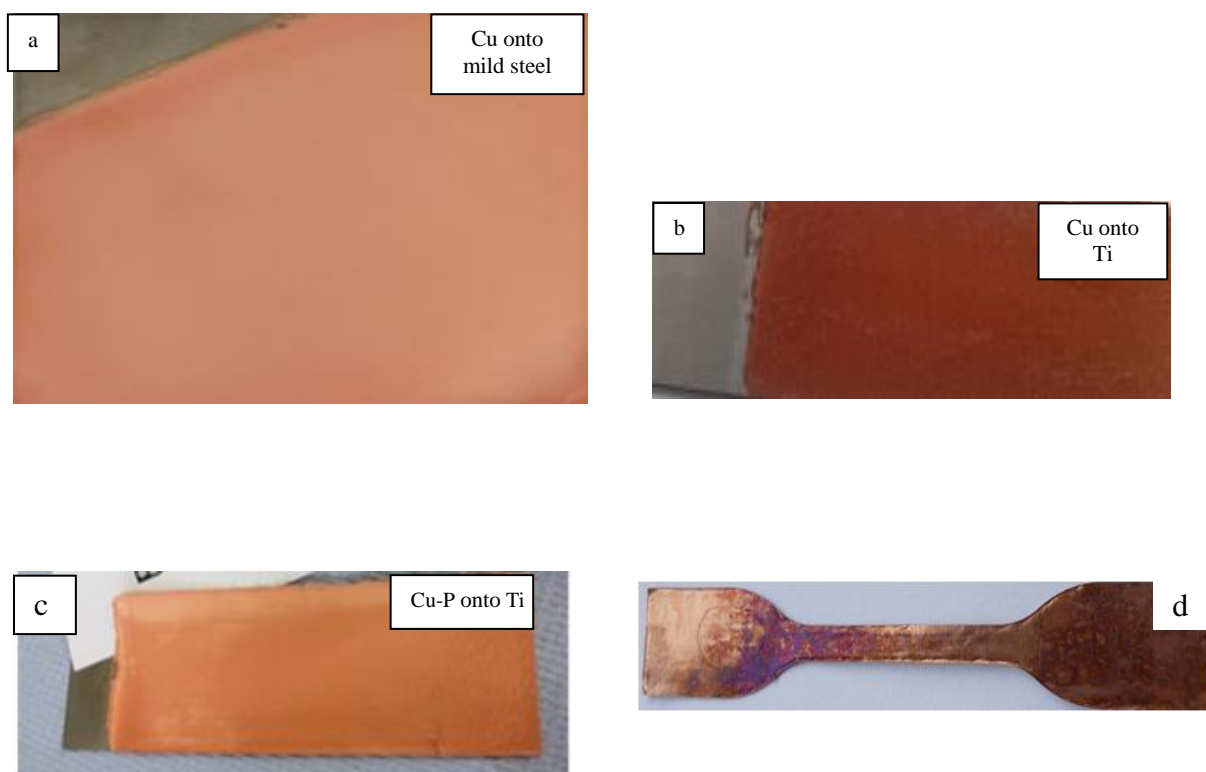


*Figure 5.9* *Photographs of electrodeposited Cu and Cu-P alloy from Ethaline a) 0.3 mol dm$^{-3}$ CuCl$_2$·2H$_2$O deposit on mild steel, b) 0.3 mol dm$^{-3}$ CuCl$_2$·2H$_2$O deposit on Ti, c) 0.3 mol dm$^{-3}$ CuCl$_2$·2H$_2$O with 0.1 mol dm$^{-3}$NaH$_2$PO$_2$ deposit on Ti. d) The dog bone shaped test sample.*

The only substrate which gave suitable separation from the deposited film was titanium sheet. This is interesting from two points: firstly copper can only deposited on a copper substrate through careful substrate etching and secondly the adhesion of the copper film deposited from Ethaline was actually very good and only separated upon thermal shock. **Figure 5.9** shows the Cu and Cu/ P layer deposited on a variety of substrates. **Figure 5.10** shows the samples of copper films once they had been removed from the titanium substrate. The experiments were also carried out on wires and here, it was found that Nichrome was a suitable substrate for this process. SEM photographs of the tube formed by this process are shown in **Figure 5.11**. The average wall thickness was found to be 27 µm
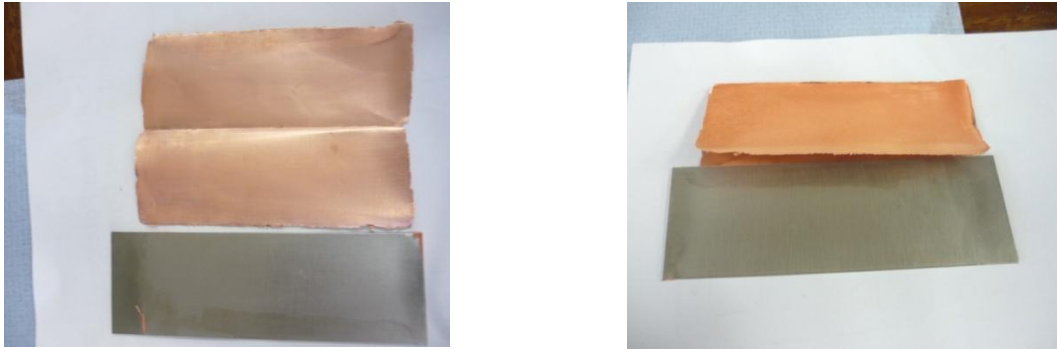
*Figure 5.10* *photographs of the Cu-P alloy film after removal from the Ti substrate*
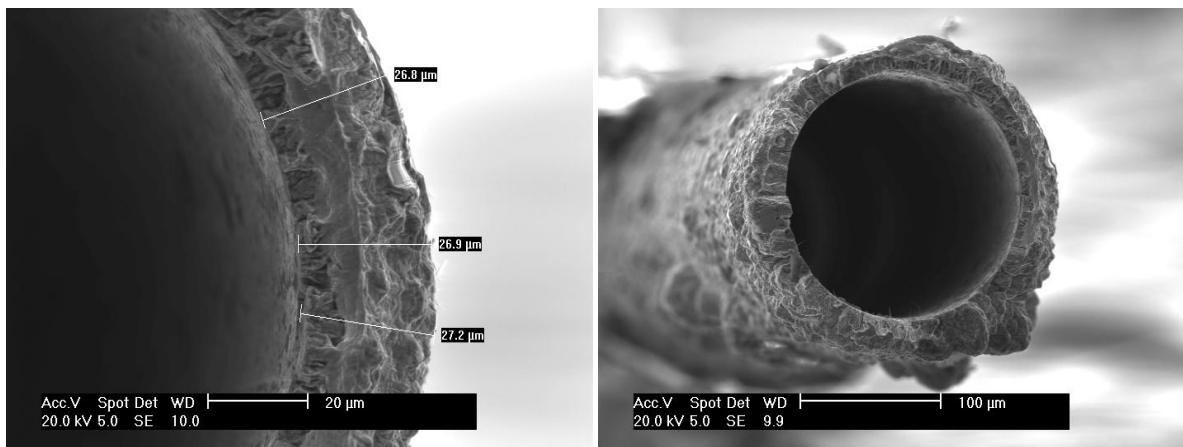


*Figure 5.11* *SEM images of Cu deposition on Ni-Cr wire after peel off*

## 5.6 Mechanical properties

The aim of this investigation was to successfully deposit copper and copper-phosphorus alloys on a Ti substrate from Ethaline and then to peel off the thin film deposition and study the mechanical behaviour of these deposited materials. Two sets of test samples composed of Cu and Cu-P thin films were produced as shown in **Figure 5.9.** These were cut into a standard dog bone shape for tensile testing. From the stress/strain curve, the mechanical strengths of the Cu and Cu-P alloy thin film were determined.

A 78 μm thick Cu and 81 μm thick Cu-P thin film were prepared cut into dog bone-shaped samples with a rectangular gauge section of 4 mm in width and 75 mm in length, as shown in **Figure 5.9 d**. The thickness of the films was determined using a micrometer, however **Figure 5.12** shows that the thickness varied when determined using scanning electron microscopy.

**Figure 5.13** shows the stress–strain curve is non-linear at very low loads, with a small slope that initially increases with increasing strain. It was found that the ultimate tensile strength of the copper-phosphorus alloy was 83 MPa, whereas the ultimate tensile strength of the pure copper film was 67 MPa. Interestingly the ductility of the copper-phosphorous alloy was also higher than the pure copper deposit. From this figure, after the onset of yielding, the stress increases strongly until an almost constant value is reached. The different in those results confirm that it is possible to change the strength and ductility of copper by adding small amounts of phosphorous. These results are considerably less than the values for bulk copper of about 220 MPa and an elongation at break of approximately 45 %.[18] [19] This difference is probably due to the uneven nature of the electroformed test piece and the uncertainty in the material thickness.
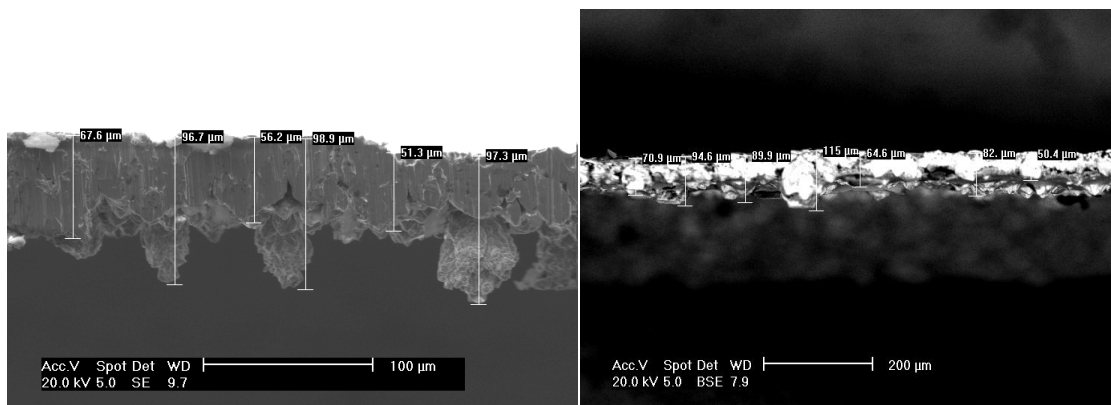


*Figure 5.12 SEM images showing thickness of Cu and Cu-P alloy sheet after peeling off then cut as a dogbone-shape.*
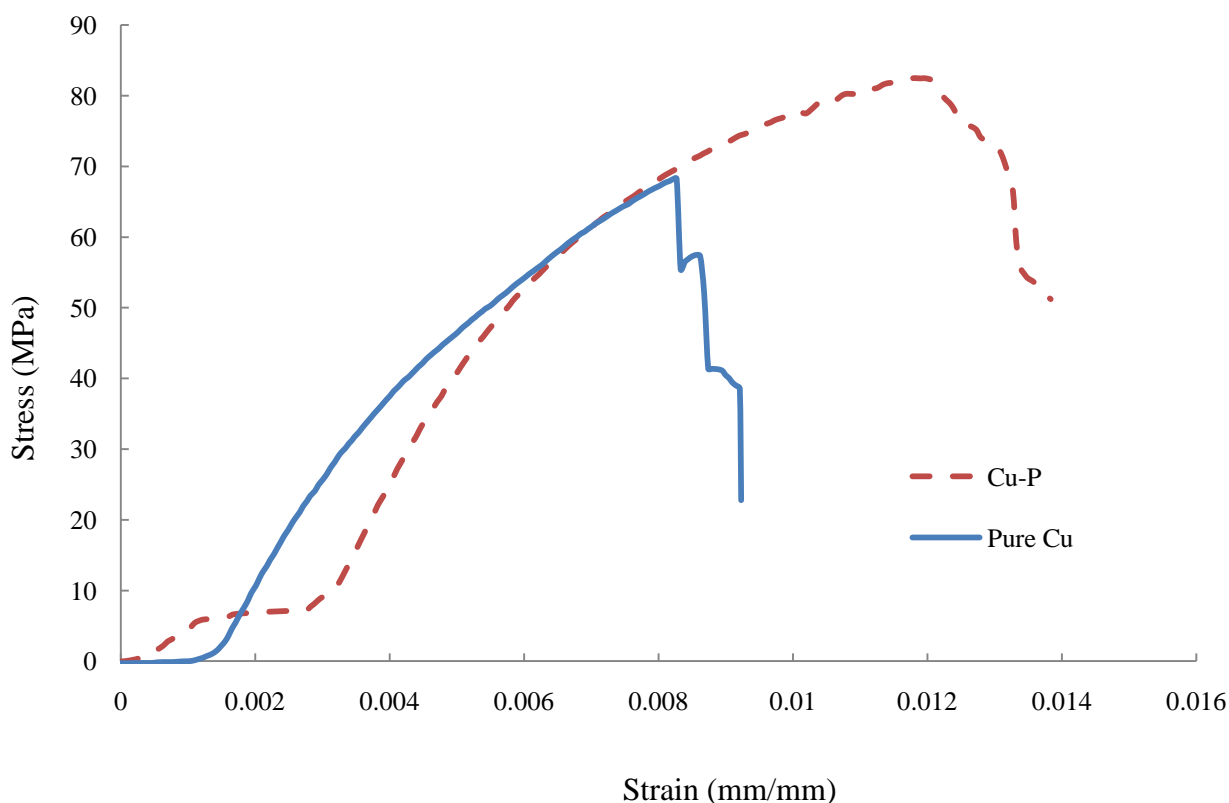
***Figure 5.13*** *Stress vs strain reponse of the pure Cu and Cu-P alloy deposited from 0.3 mol dm$^{-3}$ CuCl$_2$·2H$_2$O  and 0.3 mol dm$^{-3}$ CuCl$_2$·2H$_2$O with 0.1 mol dm$^{-3}$ NaH$_2$PO$_2$ in Ethaline.*

## 5.7 Electrolytic deposition of Cu onto Al

Copper is one of the metals most extensively used in industry, either because of its intrinsic properties or as a base to further formation of metallic films. Copper thin films are used for various applications, particularly for the preparation of interconnections in the semiconductor industry. Electrodeposition of Cu is an attractive technique because of its simplicity, low cost and possibility of coating large areas. One difficulty with electrodeposition is the substrate specificity of process in that metals such as Mg, Al and Ti are difficult to deposit onto using aqueous electrolytes due to the presence of passivating oxide films. This is less of an issue with ionic liquids.

The deposition of copper from a 0.1 mol dm$^{-3}$ CuCl$_2$·2H$_2$O solution in Ethaline was attempted using an Al substrate. While it was possible to achieve, the deposition time was 30 min at very low current density (0.15 mA/cm$^2$). The surface structure of the deposit was more crystalline than on more conducting substrates and this is probably due to the slow growth time. The SEM images shown in **Figure 5.14** show large Cu crystallites which grow

perpendicular to the surface with sharp edges. This shows that DES are able to extend the range of substrates onto which metals can be directly electrodeposited.
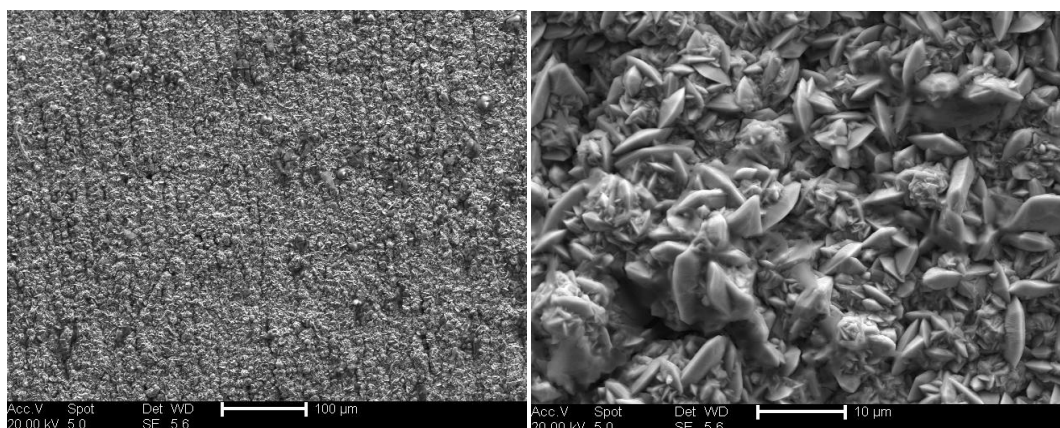


**Figure 5.14** *SEM images of Cu deposited onto an Al substrate at 100 $\mu$m and 10 $\mu$m from a solution containing 0.1 mol $dm^{-3}$ $CuCl_2 \cdot 2H_2O$ with 0.01mol $dm^{-3}$ $NaH_2PO_2$ in Ethaline at 0.15 $mA/cm^2$ current density*

## 5.8 Electrodissolution of copper

In a previous study it has been shown that the anodic dissolution of aluminium is the rate controlling step in the electrodeposition of aluminium. This is counter intuitive since in most aqueous electrodeposition experiments the anodic process is all but ignored. In an ionic liquid, however, it is understandable that the diffusion of a ligand to the anode surface may be rate limiting, particularly if the liquid is not particularly Lewis basic and/or very viscous. Cyclic voltammetry is a suitable method to study the mechanism of formation of any anodic layers or mass transport limited processes.[13]

**Figure 5.15** shows the cyclic voltamograms recorded for a copper disc electrode immersed 0.1 mol $dm^3$ $CuCl_2 \cdot 2H_2O$ in Ethaline. Two <u>reduction</u> peaks are observed at $-0.1$ and $-0.45$ V labelled $c_1$ and $c_2$. The peak at $-0.1$ V (*vs.*Ag) corresponds to Cu underpotential deposition and the peak at $-0.45$ V to bulk deposition. On the anodic scan, two stripping peaks at $+0.25$ V and $+0.4$ V $a_1$ and $a_2$, respectively, are observed. The peak at $a_1$ is classically formed by a passivation process or due to solution super-saturation. The shape of the peak and the appearance of a second maximum at $a_2$ suggests that the process being observed in due to the solution close to the electrode being super-saturated with copper ions. **Figure 5.16** shows a repeat experiment but this time the electrode is immersed in pure Ethaline i.e. no copper in solution. The current is the same as that in the previous figure but the redox potentials of all

the processes are slightly shifted due to the shift in the reference potential. Direct comparison can be made from **Figure 5.17**.
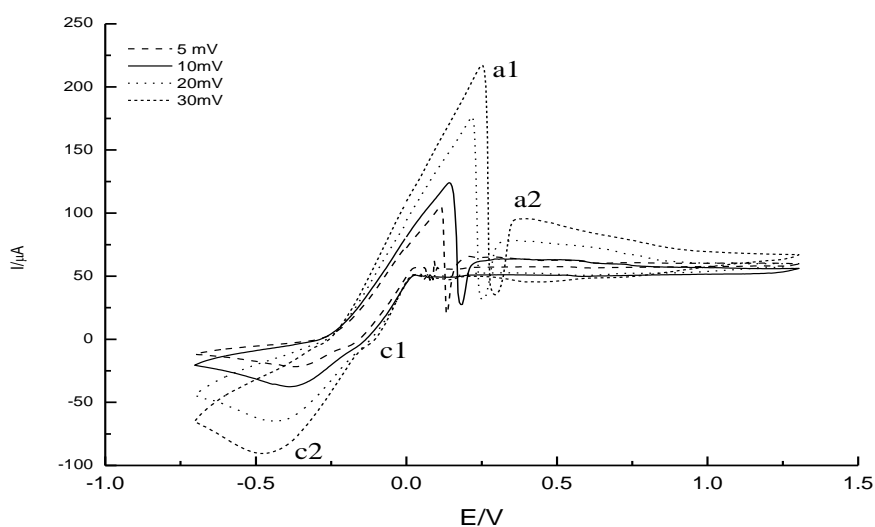


***Figure 5.15*** *Cyclic voltammograms of Cu dissolution in 0.1 mol dm$^{-3}$ CuCl$_2$·2H$_2$O based in Ethaline at a Cu disk working electrode (dia. 0.5mm) using a silver wire pseudo reference electrode at 5, 10, 20 and 30 mV s$^{-1}$ scan rates.*
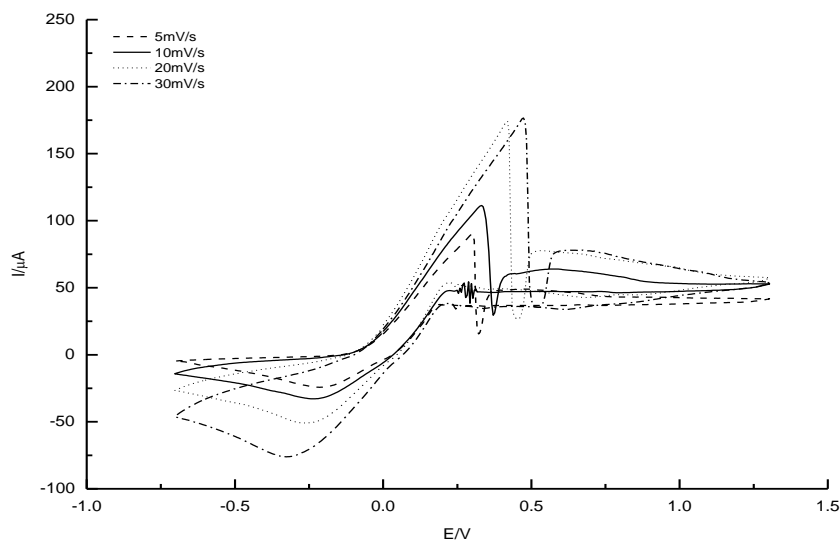


***Figure 5.16*** *Cyclic voltammograms of Cu dissolution in Ethaline at a Cu disk working electrode (dia. 0.5mm) using a silver wire pseudo reference electrode at 5, 10, 20 and 30 mV s$^{-1}$ scan rates.*
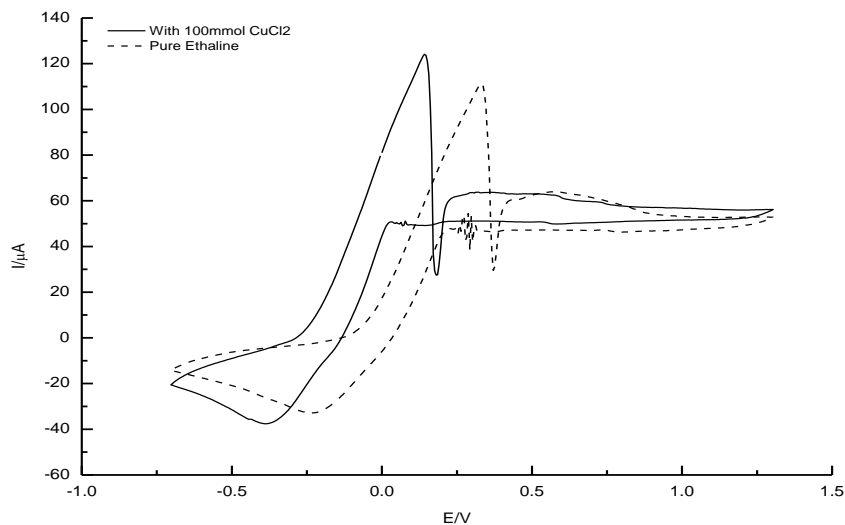
***Figure 5.17*** *Cyclic voltammograms of Cu dissolution in 0.1 mol dm$^{-3}$ CuCl$_2$·2H$_2$O and copper free Ethaline at a Cu disk working electrode (dia. 0.5mm) using a silver wire pseudo reference electrode at 10 mV s$^{-1}$ scan rates.*

Stirring and the use of ultrasound increases the plateau current significantly by increasing the transport away from the electrode surface, as has been seen in **Figure 5.18**.
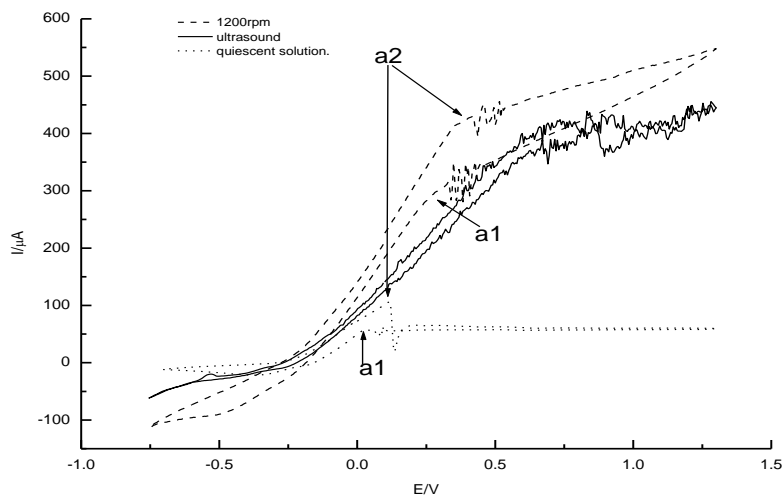


***Figure 5.18*** *Cyclic voltammograms of Cu dissolution in 0.1 mol dm$^{-3}$ CuCl$_2$·2H$_2$O based in Ethaline at a Cu disk working electrode (dia. 0.5mm) using a silver wire pseudo reference electrode at scan rate 5 mV s$^{-1}$, with a) stirrer (1200 rpm) b) ultrasound c) quiescent solution.*

This strengthens the idea that the minimum between a$_1$ and a$_2$ is not due to passivation. The limiting current under ultrasound is over 4 times that in the quiet experiment, indicating that

133

the oxidised product has moved away from the metal surface.[13] **Figure 5.19** shows that the limiting current also increases as the solution stirring rate is increase.
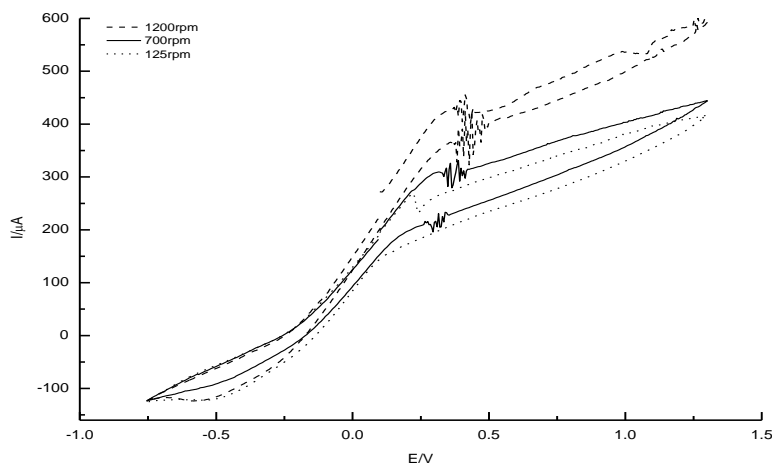


***Figure 5.19*** *Cyclic voltammograms of Cu dissolution in 0.1 mol dm$^{-3}$ CuCl$_2$·2H$_2$O based in Ethaline at a Cu disk working electrode (dia. 0.5mm) using a silver wire pseudo reference electrode with stirrers 1200, 700 and 125 rpm at 5 mV s$^{-1}$ scan rate.*

## Quartz crystal microbalance

Investigation of the dissolution of copper in Ethaline containing no copper ions was carried out on a gold coated quartz crystal onto which copper had been electrodeposited. The electrode potential was from -0.237 to 0.75 V as shown in **Figure 5.20**. In the anodic direction, the corresponding two anodic peaks were at + 0.159 V and + 0.555 V respectively and the main copper dissolution reaction which began at a potential of around -0.235V. The scan rate was 5 mVs$^{-1}$ and the reference electrode was Ag, while the counter electrode was a platinum flag.

From the slope of the mass versus the charge passed, the equivalent weight was estimated for two materials that had been dissolved. The slope of the first line was found to be 90 g/ mole which is very close to the molar mass of CuCl$^+$, **Figure 5.20**. The second line gives a value of 60.7 g/ mole which is also very close to the molar mass of the cuprous ion Cu$^{+1}$, **Figure 5.20**.
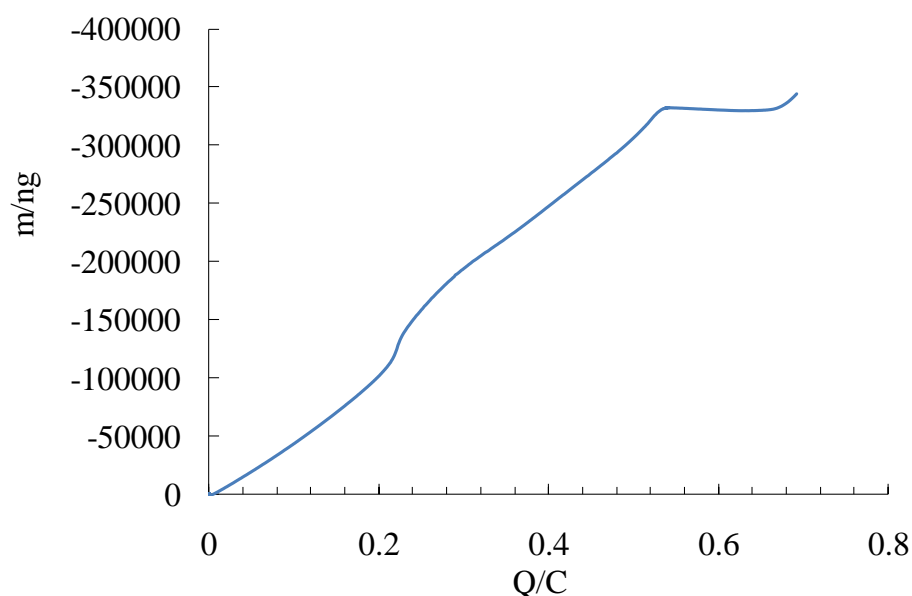
***Figure 5.20*** *Electrochemical acoustic impedance (EQCM) data for Cu dissolution after deposition on gold crystal based in Ethaline. The potential was started from -0.75V O.C.P and held at 0.75 V.*

The frequency of the QCM started to decrease slightly at the initial scan rate (- 0.75 V). When the potential reached - 0.235 V the rate of frequency increased and the mass started to decrease.
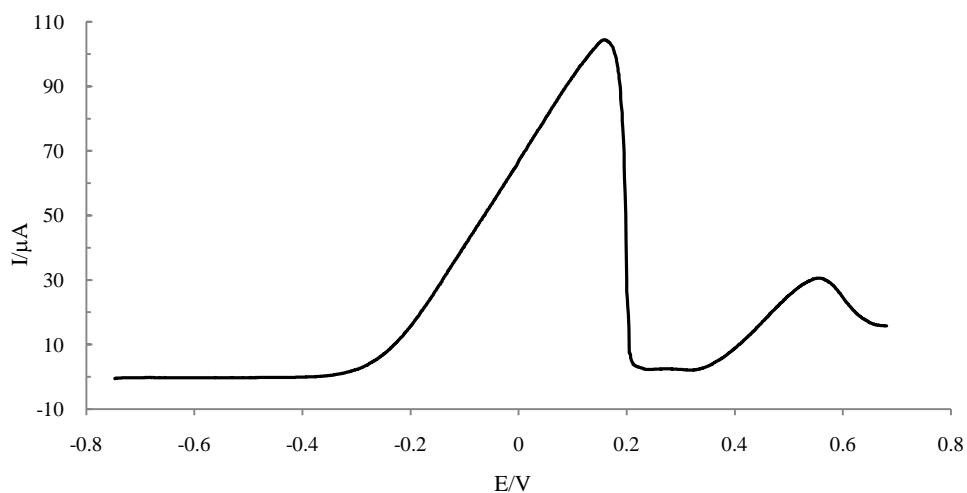


***Figure 5.21*** *Cyclic voltamogram for copper dissolution using unpolished gold crystal after coated by 0.5 mol dm$^{-3}$ copper using QCM at scan rate 0.5 mVs$^{-1}$. The potential was started from - 0.75V O.C.P and held at 0.75 V.*
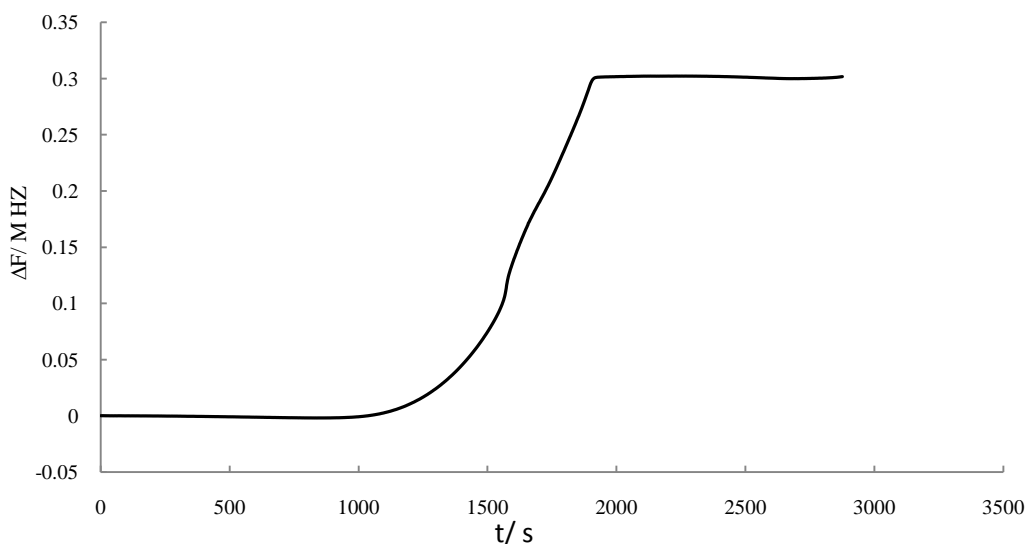
*Figure 5.22* *Frequency versus time for copper dissolution using unpolished gold crystal after being coated by 0.5 mol dm$^{-3}$ copper using QCM at scan rate 0.5 mV s$^{-1}$. The potential was started from - 0.75V O.C.P and held at 0.75 V.*

The increase in the QCM frequency (mass loss) had the highest rate when the potential of the anodic peak was reached at around + 0.159 V, as shown in **Figure 5.21**. From this data we can plot the charge versus mass for the dissolution of copper at - 0.235 V, as shown in **Figure 5.20**

The change of frequency ($\Delta F$) readings during a typical Cu dissolution experiment is illustrated in **Figure 5.22**. As the anodic scan of the potential started at - 0.75 V, the frequency changed. One can see a small initial decrease of the QCM frequency which corresponds to the mass increase until - 0.235 V, then the dissolution of copper to cupric ions started, as shown in **Figure 5.20**. The change of frequency shows a straight line until it began to increase at 1040 s, and then increased further as the solute dissolved into the solution. This increase in frequency is directly proportional to the decrease of the mass of solute loaded onto the quartz crystal. The change in frequency is very stable at the beginning of the experiment due to a high driving force favouring rapid dissolution. The change of frequency continues to increase but at a fast rate until stopped, and finally the frequency stabilizes. This shows a good agreement with the anodic dissolution data illustrated in **Figure 5.20**.

In order to calculate the dissolution, the change of frequency shifted was used in the equation to determine the mass of Cu dissolved in Ethaline ionic liquid.[20] The dissolution of Cu is presented in **Figure 5.20** as a plot of the change of mass with charge. The SEM image, as shown in **Figure 5.23,** is related to the dissolution of Cu after deposited into the gold crystal.

136
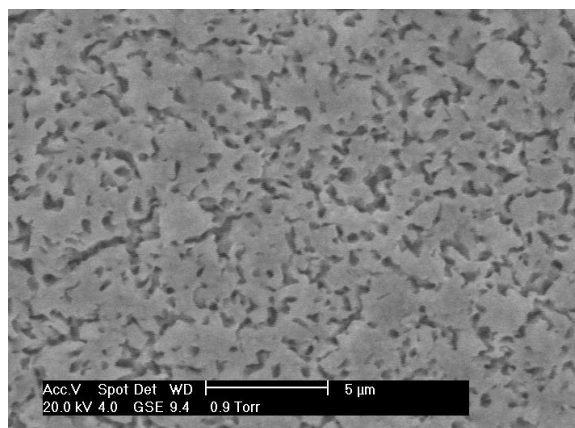
*Figure 5.23Representative scanning electron micrographs of Cu dissolution from Ethaline after depositing onto gold crystal using QCM. The potential was started from -0.75V O.C.P and held at 0.75 V.*

**Figures 5.24** and **5.25** show the surface formation of Cu dissolution from Ethaline by comparing between the cyclic voltammetry and SEM images at different stages. The experiment carried out to study the influence of the anodic potential was performed with the 5 mV s$^{-1}$ scanning rate after a steady voltammogram had been achieved.
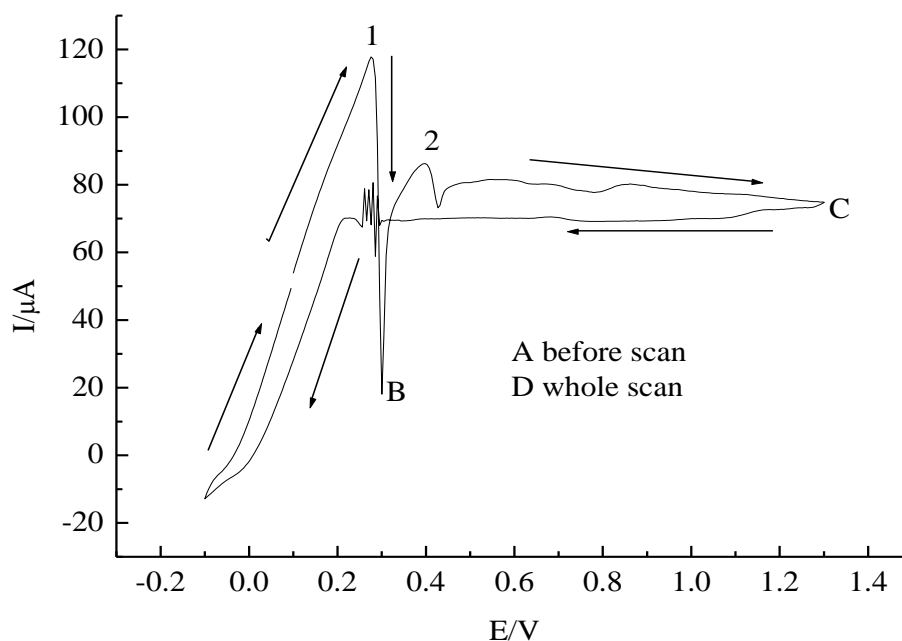


*Figure 5.24 Anodic peak for the electro-dissolution of freshly polished copper after each step in Ethaline at different potential starts A) before starting scan B) at 0.1 to 0.3 V C) at 0.1 to 1.3 V D) at whole scan the scan rate at 5mVs$^{-1}$.*

Also the scan was reversed at a value between - 0.1 to 1.5 V. As has been seen in **Figure 5.24**, the two peaks 1 and 2 were observed.

In order to investigate the formation of the passivating film more clearly, the morphology of the Cu electrode was observed by SEM after multiple different stages CV scan sweep in the Ethaline as shown in **Figure 5.25**. In addition, the morphology of a copper Cu electrode before use (**Figure 5.25 A**) was also taken as a reference. As shown in **Figure 5.25B, C and D**, some pits were observed on the surface of the Cu electrode, indicating that the dissolution of the Cu took place in Ethaline, which led to the rise of anodic current during the potential swept to about 1.5 V.
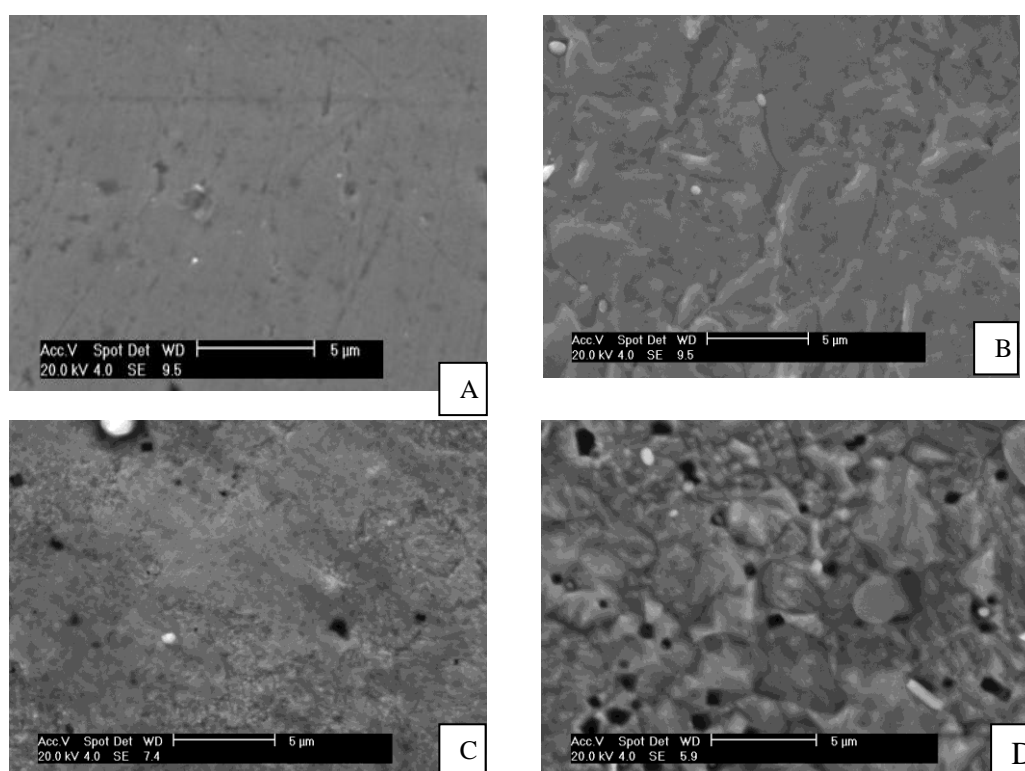


*Figure 5.25* SEM images of copper freshly polished electrode surface after the potential scanning from -0.1 to 1.3 V in Ethaline at 5mVs$^{-1}$ scan rate, at different step as seen in Figure 5.24.

## 5.9 Conclusions

This is the first time the deposition of copper-phosphorus alloy has been studied from an ionic liquid. It was shown that thin sheets of Cu and Cu-P alloys deposited from Ethaline, which allowed their mechanical properties to be determined. It was shown that the copper phosphorous alloys have increased strength and improved ductility compared to the pure copper films.

Electrochemical quartz crystal microbalance experiments were also used to obtain the mass–charge plots for copper-phosphorus deposition with several metal composition in the ionic liquids. The mechanism of copper-phosphorus nucleation is studied using chronoamperometry and it has shown very poor fit for the theoretical values but very close to instantaneous with addition of 1% $(CH_3)_3N.BH_3$.

The anodic dissolution process of copper from Ethaline was successfully studied by electrochemical methods and a variety of surface analysis techniques. The effects of ultrasound and rotation on the rate of copper dissolution were also studied. It is shows that, in the anodic scan, anodic peak potential for the dissolution of copper is increased by 3-fold under rotation (1200 rpm) when compared to silent conditions.

## 5.10 References

1.  R. Zauter and D.V. Kudashov, in *Electrical Contacts*, Proceedings of The 23rd International Conference on Electrical Contacts, Sendai, Japan, 2006, pp. 257-261.

2.  *Equilibrium Diagrams,CDA Publication No 94, 1992, www.cda.org.uk*.

3.  T. Noda, K. Oikawa, S. Itoh, M. Hino and T. Nagasaka, *Calphad*, 2009, **33**, 557-560.

4.  M. Bayes, I. Sinitskaya, K. Schell and R. House, *Transactions of the Institute of Metal Finishing*, 1991, **69**, 140-144.

5.  D. Baudrand and J. Bengston, *Metal Finishing*, 1995, **93**, 55-57.

6.  N. Dadvand, G. J. Kipouros and W. F. Caley, *Canadian Metallurgical Quarterly*, 2003, **42**, 349-363.

7.  Y. Wu, Y. Xiang, W. Hu, C. Zhao and W. Ding, *Transactions of the Institute of Metal Finishing*, 2005, **83**, 91-94.

8.  I. N. A. Oguocha, R. Taheri, S. Yannacopoulos, W. A. Uju, R. Sammynaiken, S. Wettig and Y. F. Hu, *Thin Solid Films*, 2010, **518**, 2045-2049.

9.  T. Mahalingam, M. Raja, S. Thanikaikarasan, C. Sanjeeviraja, S. Velumani, H. Moon and Y. D. Kim, *Materials Characterization*, 2007, **58**, 800-804.

10. K. N. Srinivasan and S. John, *Journal of Alloys and Compounds*, 2009, **486**, 447-450.

11. K. M. Shartal and G. J. Kipouros, *Metallurgical and Materials Transactions B-Process Metallurgy and Materials Processing Science*, 2009, **40**, 208-222.

12. M. M. Younan and S. A. A. El-Enine, *Galvanotechnik*, 2004, **95**, 2876-2881+iv.

13. J. Crousier, L. Pardessus and J. P. Crousier, *Electrochimica Acta*, 1988, **33**, 1039-1042.

14. C. X. Peng, L. Yang, S. H. Fang, J. X. Wang, Z. X. Zhang, K. Tachibana, Y. Yang and S. Y. Zhao, *Journal of Applied Electrochemistry*, 2010, **40**, 653-662.

15. A. P. Abbott, G. Capper, K. J. McKenzie and K. S. Ryder, *Electrochimica Acta*, 2006, **51**, 4420-4425.

16. B. Scharifker and G. Hills, *Electrochimica Acta*, 1983, **28**, 879-889.

17. J. C. Barron, PhD, University of Leicester, 24- Mar-2010.

18. M. Hommel and O. Kraft, *Acta Materialia*, 2001, **49**, 3935-3947.

19. D. T. Read, Y. W. Cheng and R. Geiss, *Microelectron. Eng.*, 2004, **75**, 63-70.

20. G. Sauerbrey, *Z. Physik* 1959, **155**, 206.

## 6.1 Summary

6.1.1 The electrodeposition of copper-silver alloys

6.1.2 The electrodeposition of copper-tin alloys

6.1.3 The electrodeposition of copper-phosphorus

## 6.2 Future directions

## 6.1 Summary

The key results obtained in this work show that a range of copper alloys can be electrodeposited using Deep Eutectic Solvents. This study underpins other similar investigations in a range of ionic liquids which shows that ionic media allow increased control of alloy morphology and composition when compared with aqueous solutions.

## 6.1.1 The electrodeposition of copper-silver alloys

The co-deposition of Cu-Ag alloys was studied using a combination of cyclic voltammetry, chronoamperommetry, chronocoulommetry, ESEM, AFM, EQCM and EDAX. The novelty associated with this approach was the use of EQCM for monitoring co-deposit formation in real time. It was shown that the EQCM data correlated well with EDAX data. It was shown that EQCM can be used for this purpose as long as the deposition is 100 % current efficient and the deposit is relatively smooth. For the copper-silver system both of these conditions were met except when the silver content was high and dendritic deposits were obtained. EQCM allows surface roughness to be characterised and these data correlated well with the images obtained using ESEM. The Cu-Ag alloy is a simple eutectic solid solution and the voltammetric response is relatively similar to the sum of the voltammograms for the two individual metals.

It was shown that the rate of deposition of copper on silver and silver on copper were both slower than the respective metal on the same substrate. This clearly accounts for the variability of the alloy composition as the relative solution composition and surface reactivity will change during the deposition process. It was shown that the composition of the alloy was similar to the composition of ions in solution for high copper and equimolar solutions. This agrees with the recent studies in our laboratory of Zn alloys in the same DESs which showed that the alloy composition was similar to the relative proportions of metals in solution. It was shown that high copper alloys tended to be more amorphous whereas the higher silver alloys were more crystalline.

## 6.1.2 The electrodeposition of copper-tin alloys

Unlike the results in the previous chapter the copper tin system forms a variety of discrete alloy phases. The voltammetry of solutions containing copper and tin was considerably more complex than the corresponding copper silver system. It was envisaged that it would be possible to identify specific voltammetric peaks and correlate them to the major phases formed. The overlap of the copper and tin signals made this impossible. The nucleation of the copper-tin alloys was neither like that for copper nor that for tin. This suggested that the formation of the alloy phases is slow compared to the deposition of the pure metals.

The alloy composition could once again be determined using EQCM despite the fact that the two metals had the same charge. In the high copper system the composition of the alloy remained approximately the same as the solution composition throughout the deposition process. In the equimolar solution the composition varied slightly more but was relatively similar to that of the solution. In the high tin solution the results vary significantly throughout the deposition process which may be due to surface roughening or just the change in phase formation as the tin concentration in solution changes. It would appear that the technique of EQCM for monitoring alloy composition is best applied to metals or alloys which form nanocrystalline or amorphous deposits.

Hull cell tests were carried out and it was found that alloy composition and surface morphology was very dependent upon current density. At high current density pure copper was favoured in all systems suggesting that this is the fastest metal to nucleate and grow. The pure tin phase was only observed at low current density showing that it is kinetic factors which control growth given that the thermodynamics of reduction of the two metals was the same in both liquids.

This chapter also investigated the use of brighteners in alloy systems. Classical aqueous systems were studied and these were found to cause a brightening effect by reducing the grain size of the deposits. It was, however shown that these suppress the deposition of tin in the alloy.

### 6.1.3 The electrodeposition of copper-phosphorus alloys

In this chapter, copper-phosphorus (Cu–P) deposits were electroplated from the ionic liquids containing sodium hypophosphate as the phosphorous source. Experimental results show that phosphorus could be included in relatively high concentrations. The incorporation of phosphorus is shown to improve the metal ductility compared to a pure copper film, however, the results were less than those expected for pure copper and are probably not accurate due to the uncertainty in the material thickness.

In this chapter, the Cu dissolution from the ChCl based ionic liquids was studied to investigate the limitations of using soluble copper anodes. In the case of copper dissolution, the nature of the Cu species dissolved in solution is still a topic of debate, depending on the potentials applied. EQCM was used to study the anodic process in real time. As the potential is swept in a positive direction, the anodic current increases to a maximum and then drops as the solution becomes super-saturated. It was seen that diffusion of $Cl^-$ to the electrode surface was rate determining.

### 6.2 Future directions

This thesis has been concentrated on the electrodeposition processes in deep eutectic solvents. It is clear that the electrodeposition mechanism is strongly dependent on the solvent used and the alloy composition concentration. Additionally it has been shown that the growth mechanism is dependent on the metal concentration in these alloy systems.

Preliminary results have highlighted some additives that function as brighteners. One area of further study that should be carried out is the choice of organic hydrogen bond donor to these systems and their effect as brighteners. It has previously been shown that additives such as ethylene diamine function as effective brighteners in zinc based systems. This was thought to be due to double layer changes preventing the specific adsorption of $Cl^-$. It would be useful to investigate the speciation of copper which can be observed using either visible spectroscopy or EXAFS. Recently it has been shown in the group that the redox potential of copper ions can be significantly shifted using either different anions or different hydrogen bond donors. This has the ability to shift the reactivity of copper with respect to silver or tin.

Recent developments in our laboratory have used digital holographic microscopy (DHM) to study the nucleation of silver in DESs. This technique uses confocal laser beams to construct a hologram of the electrode surface. It has the advantages that it has nm resolution in the Z-

direction while retaining low resolution in the X and Y direction, which is ideal for nucleation studies. While it is possible to get similar resolution using AFM, DHM has millisecond time resolution and allows real-time study of nucleation on electrode surfaces. It could be used to investigate the mechanism of alloy deposition and determine why they do not follow either classical instantaneous or progressive nucleation mechanisms.

The study of electroforming copper phosphorous alloys has significant application for the formation of strong copper rollers. It would be interesting to try the protocols developed in Chapter 6 using the pilot plant facilities in the laboratory. To apply this to large rollers it may be interesting to investigate a rolling cathode system which would decrease the amount of ionic liquid needed in a full plating system.

**Chapter 7: Appendices**
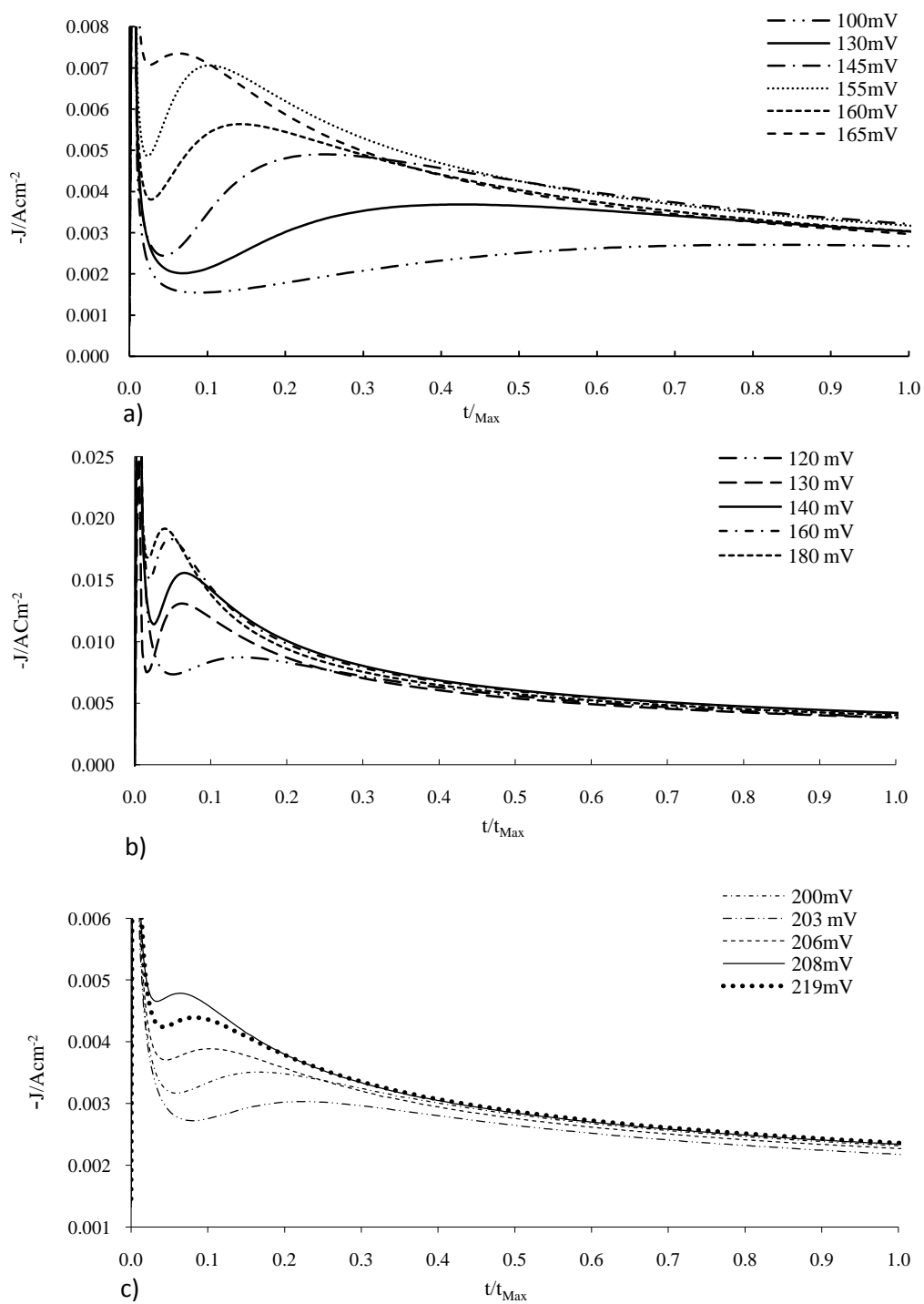
***Figure 7.1*** *Set of current time transients measured at different potentials of a) 1:1 Cu: Ag, b)  1:3 Cu: Ag and c) 3: 1 Cu: Ag from Ethaline See Chapter 3 for details. Applied potentials all in negative.*
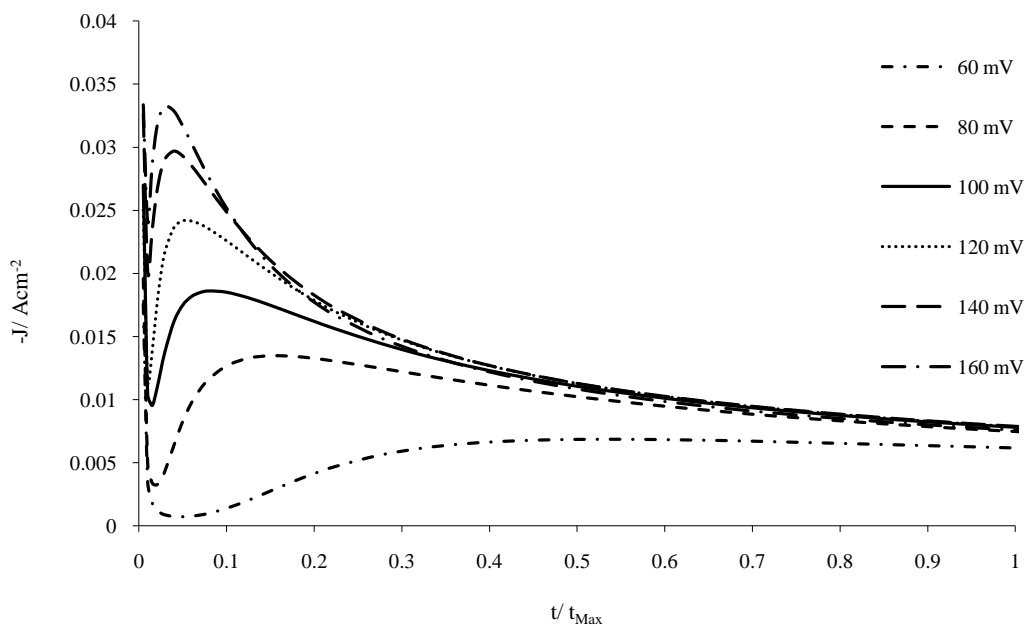
***Figure 7.2*** *Set of current time transients measured at different potentials of 0.1 mol dm$^{-3}$ AgNO$_3$ from Ethaline. Applied potentials all in negative.*
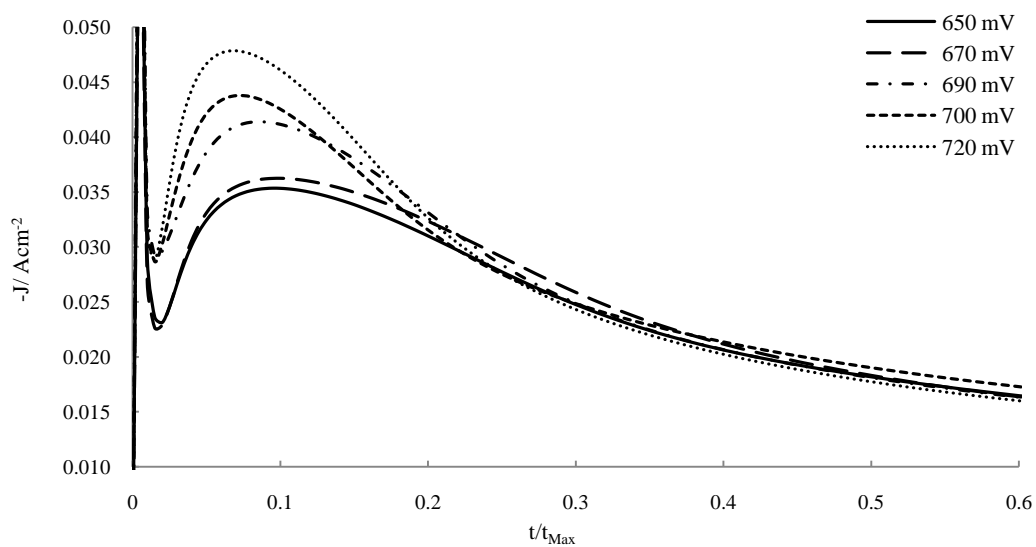


***Figure 7.3*** *Set of current time transients measured at different potentials of 0.1 mole dm$^{-3}$ SnCl$_2$·2H$_2$O from Ethaline. Applied potentials all in negative.*
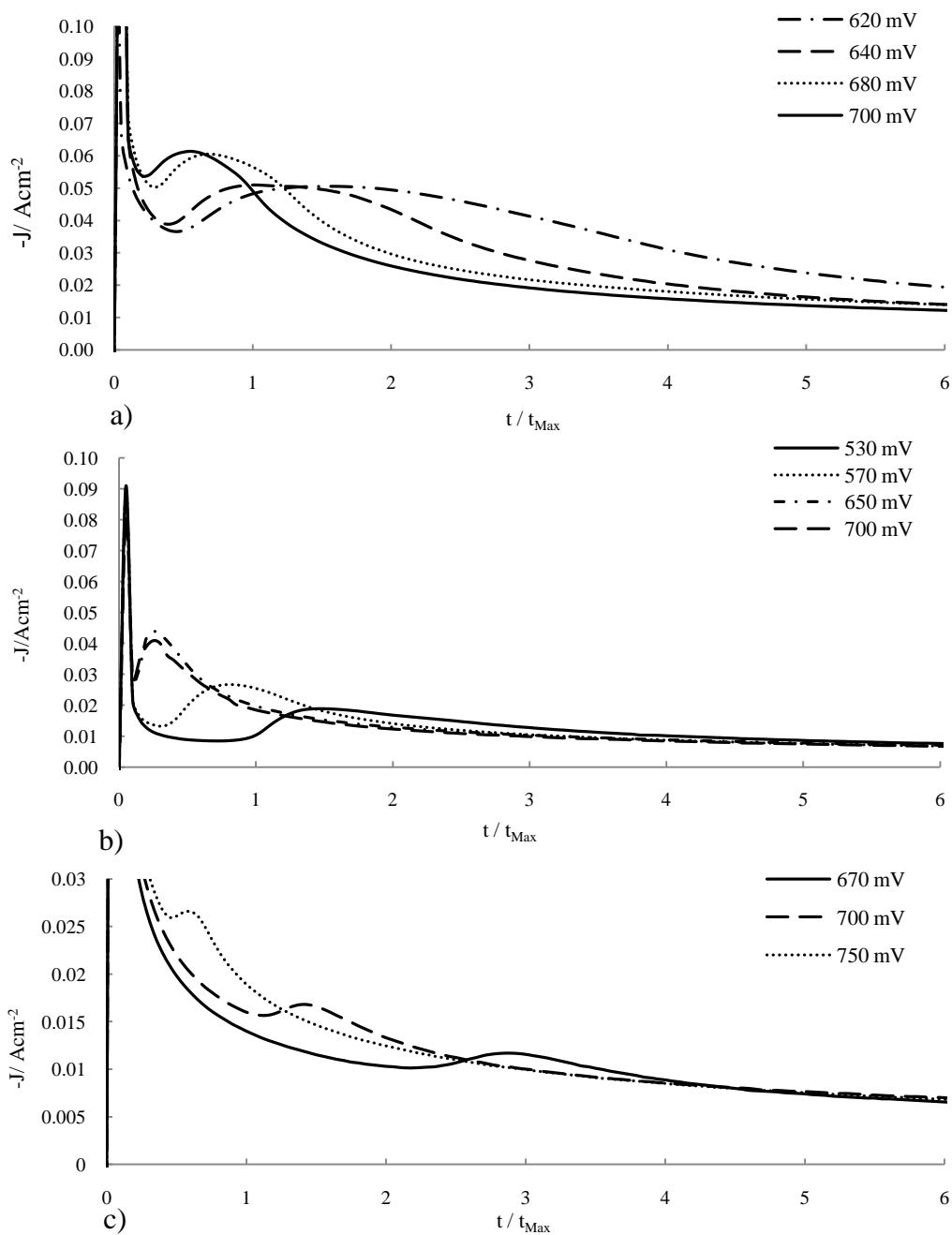
***Figure 7.4*** *Set of current time transients measured at different potentials for **a)** equimolar 1CuCl$_2$.2H$_2$O: 1 SnCl$_2$2H$_2$O, **b)** 0.3 CuCl$_2$.2H$_2$O: 1 SnCl$_2$2H$_2$O and **c)** 1 CuCl$_2$.2H$_2$O: 0.3 SnCl$_2$.2H$_2$O from Ethaline. Applied potentials all in negative.*
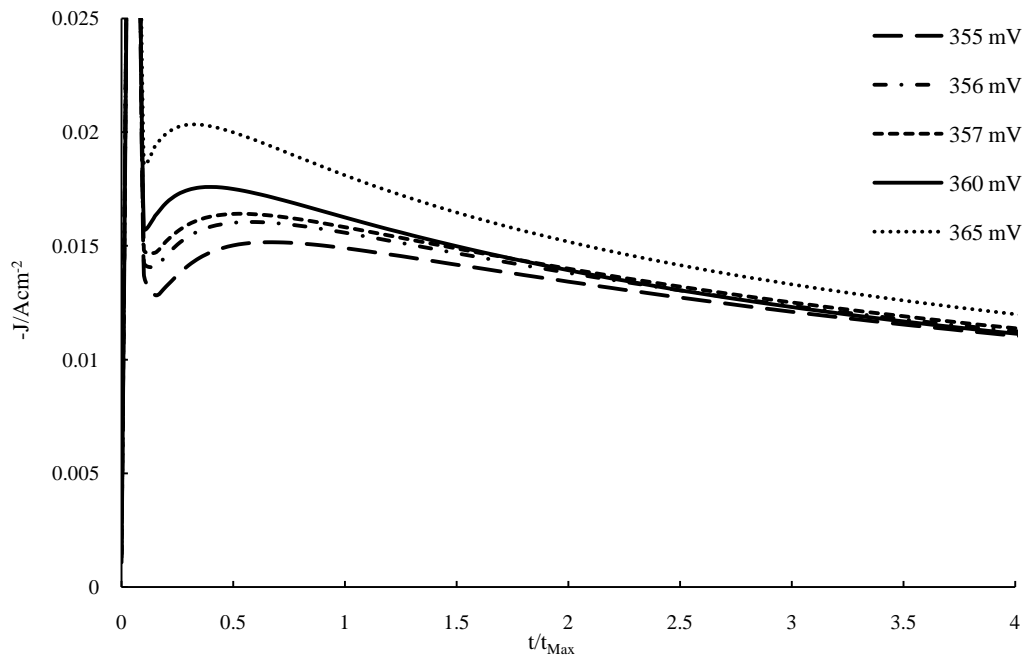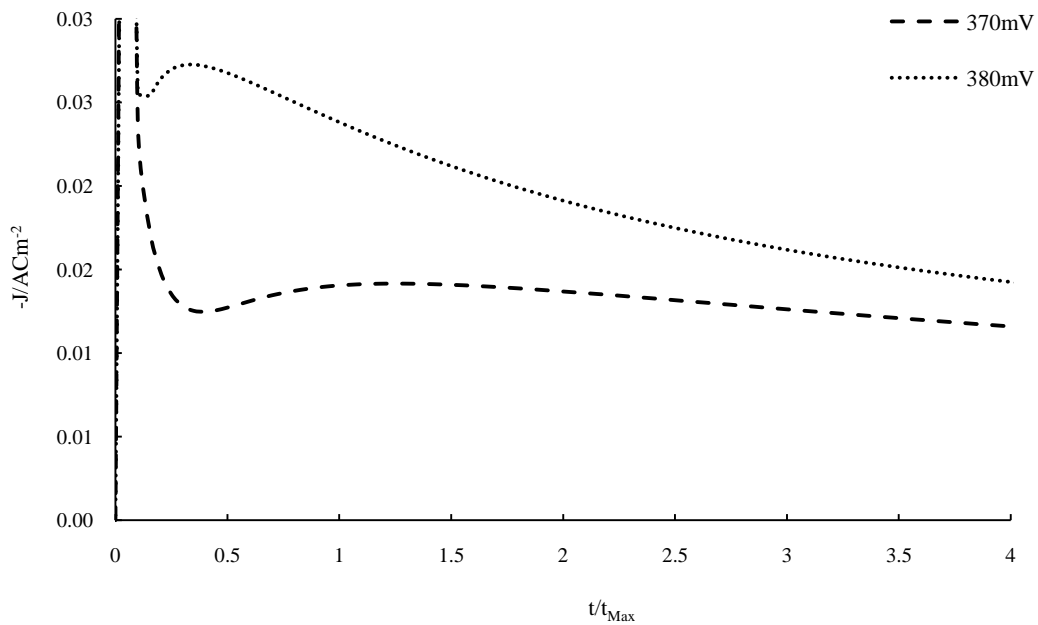
**Figure 7.5** *Set of current time transients measured at different potential for a) 3:1 Cu:P alloy without 1% boron trimethylamine complexes and b) 3:1 Cu:P alloy with 1% boron trimethylamine complexes. Applied potentials all in negative.*